Advances in High Energy Physics

Non-Minimal Coupling, Generalized Entropy, and Deformed Statistics in Gravitation

Lead Guest Editor: Hooman Moradpour
Guest Editors: Amir Hadi Ziaie, M. Kord Zangeneh, and Everton M. C. Abreu

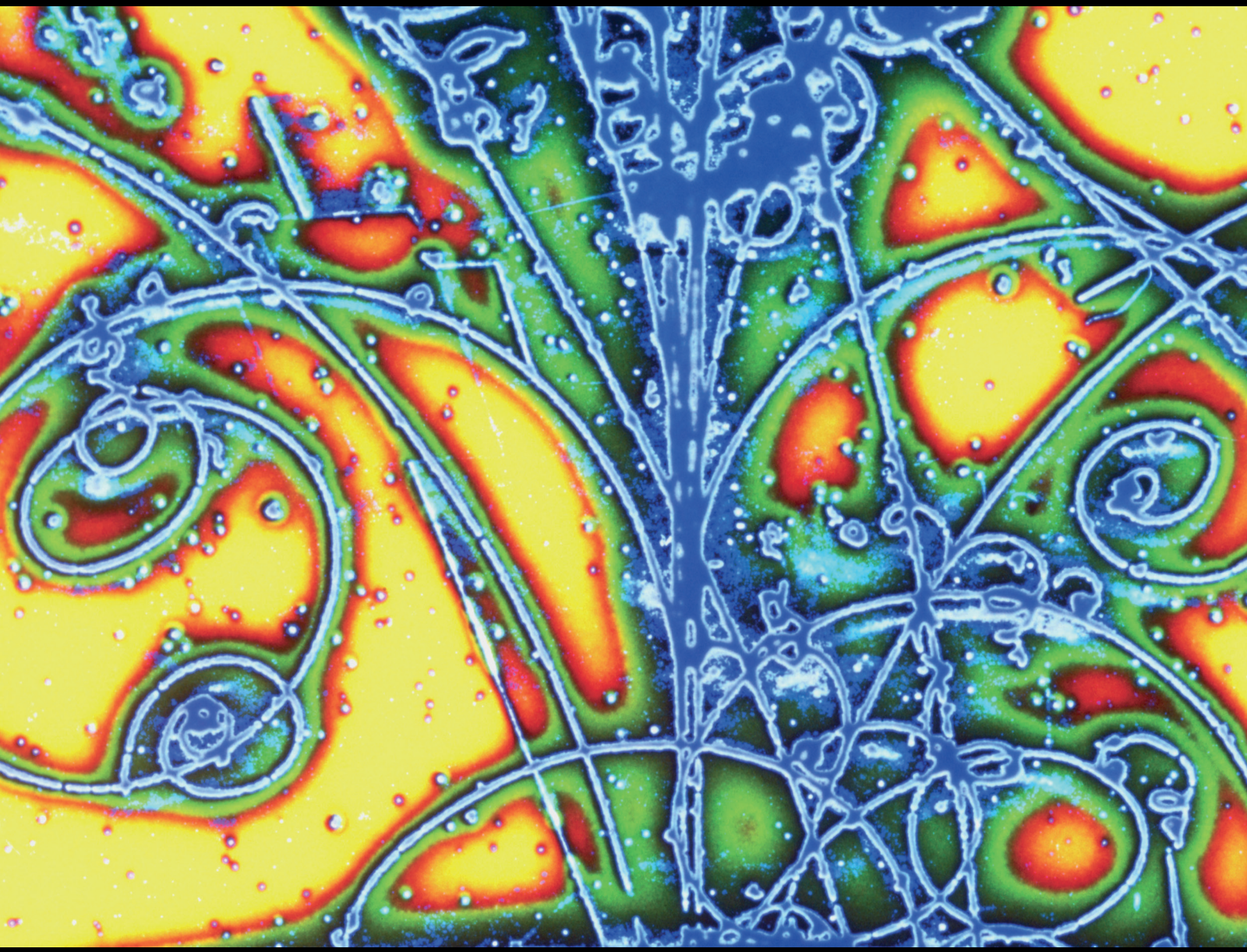

Non-Minimal Coupling, Generalized Entropy, and Deformed Statistics in Gravitation

Advances in High Energy Physics

Non-Minimal Coupling, Generalized Entropy, and Deformed Statistics in Gravitation

Lead Guest Editor: Hooman Moradpour
Guest Editors: Amir Hadi Ziaie, M. Kord Zangeneh, and Everton M. C. Abreu

Contents

Hindawi
Advances in High Energy Physics
Volume 2021, Article ID 5519028, 12 pages
https://doi.org/10.1155/2021/5519028

Research Article

Cosmic Consequences of Kaniadakis and Generalized Tsallis Holographic Dark Energy Models in the Fractal Universe

Abdul Jawad[1] **and Abdul Malik Sultan**[1,2]

[1]*Department of Mathematics, COMSATS University Islamabad, Lahore Campus 54000, Pakistan*
[2]*Department of Mathematics, University of Okara, Okara 56130, Pakistan*

Correspondence should be addressed to Abdul Jawad; jawadab181@yahoo.com

Received 2 February 2021; Revised 24 March 2021; Accepted 3 April 2021; Published 20 April 2021

Academic Editor: Hooman Moradpour

We investigate the recently proposed holographic dark energy models with the apparent horizon as the IR cutoff by assuming Kaniadakis and generalized Tsallis entropies in the fractal universe. The implications of these models are discussed for both the interacting ($\Gamma = 3Hb^2\rho_m$) and noninteracting ($b^2 = 0$) cases through different cosmological parameters. Accelerated expansion of the universe is justified for both models through deceleration parameter q. In this way, the equation of state parameter ω_d describes the phantom and quintessence phases of the universe. However, the coincidence parameter $\tilde{r} = \Omega_m/\Omega_d$ shows the dark energy- and dark matter-dominated eras for different values of parameters. It is also mentioned here that the squared speed of sound gives the stability of the model except for the interacting case of the generalized Tsallis holographic dark energy model. It is mentioned here that the current dark energy models at the apparent horizon give consistent results with recent observations.

1. Introduction

To acquire a unified understanding of various entropy measures and how they connect to each other in a generalized form, it is required to recall characteristics of "classical" entropies. In information theory, information can be collected through the probability distribution of some events that belong to the sample space of all possible events which are called entropies. Gibbs was the first who stated a hypothesis [1] which was the source of inspiration for people to define numerous entropies [2–4]. We hear and read frequently as it is claimed due to Gibbs that the black hole (BH) entropy is proportional to the area of the BH boundary in spite of having proportionality to the volume of BH. In recent times, these entropies have been the source for the modeling of cosmic evolution in different setups [5–7]. It is a matter of fact that to retrieve thermodynamical extensivity for nonstandard systems, the entropies generalizing that of Boltzman-Gibbs (BG) become necessary. For the study of BH, generalized entropies have been employed [8–11], also for the construction of new holographic dark energy (HDE) models [12, 13]. Besides this, it has been revealed that such kind of entropies can affect the Jeans mass [14], can provide a theoretical basis for the modified Newtonian dynamics (MOND) theory [15], may be inspired by the quantum features of gravity [16], and even may illustrate inflation without assuming inflation [17]. The foundation stone of primary HDE [18] is a holographic principle, and it is proposed on Bakenstein entropy [19–21]. It is observed that the Hubble horizon is a proper casual boundary for the universe meeting thermodynamics and conservation laws [22–25]. However, HDE suffers from some problems when the Hubble horizon is considered the IR cutoff [18, 26]. Some other HDE models based on generalized entropy can give a considerable description of accelerated expansion of the universe even when the apparent horizon is used as the IR cutoff [12, 13, 27]. Consequently, more suitable models of HDE may be found using generalized entropies.

The Tsallis entropy is a generalized form of BG entropy which was presented in 1988 by Constantino Tsallis [28] as

a fundamental to generalize the standard statistical mechanics. In the literature, there is a wide debate regarding the physical relevance of Tsallis entropy [29, 30]. However, at the start of the 21st century, there is an identified increasing wide spectrum of an artificial, natural, and social complex system which certifies the consequences and predictions that resulted from this nonadditive entropy (i.e., nonextensive statistical mechanics). In this regard, one of the most precise investigated frameworks is developed by Kaniadakis which is the Tsallis nonextensive statistical mechanics and the generalized power law statistics [28].

A lot of work has been done by Dubey et al. [31], Sharma et al. [32–34], Srivastava et al. [35], and Ghaffari et al. [17, 36] on cosmic expansion in various theories of gravity by using recently obtained DE models such as new Tsallis HDE (NTHDE), Réyni HDE (RHDE), and Barrow HDE (BHDE). They have made versatile studies on accelerated expansion of the universe through various cosmological parameters and planes and found consistent results with recent Planck's data [37]. In recent times, the Kaniadakis statistics have been studied as generalized entropy measures [2, 4] with some gravitational and cosmological consequences [7, 38]. In view of these generalized entropies, HDE models have been developed by Moradpour et al. [11]. They have examined the deceleration parameter, EoS parameter, and coincidence parameter for these models and found consistent results with recent Planck's data. It is suggested that generalized entropies must obey fundamental laws of thermodynamics such as the zeroth law [39–43]. The above arguments and work done are the sources of motivation due to which we are going to examine BH entropy in the different well-known generalized entropy formalisms and study their capability in representing the current accelerated expansion of the universe by formulating their corresponding HDE models.

In the next section, Tsallis entropy of BH will be calculated using the relation of Boltzmann and Tsallis entropies. Additionally, Kaniadakis entropy of BH will be computed using the relationship of Kaniadakis statistics with Tsallis entropy. Moreover, Sharma-Mittal and Rényi entropies of BH will also be discussed by applying their relation with Tsallis entropy. In Section 3, the Kaniadakis holographic dark energy (KHDE) will be discussed along with some of its cosmological consequences such as deceleration parameter q, EoS parameter ω_d^K, and the dimensionless ratio called coincidence parameter $\tilde{r} = \Omega_m/\Omega_d^K$ for both the interacting and noninteracting cases. The stability of the achieved model for both the interacting and noninteracting cases is also analyzed by the squared speed of sound C_s^2. In Section 4, the NTHDE of BH will be discussed. We will find some cosmological parameters using this model for both the noninteracting and interacting cases such as deceleration parameter q, EoS parameter ω_d^T, and the dimensionless ratio called coincidence parameter $\tilde{r} = \Omega_m/\Omega_d^T$. The squared speed of sound C_s^2 will also be evaluated to investigate the stability of the model taking both the interacting and noninteracting cases into account. In Section 5, achieved results are compared with the observational data and some concluding remarks about our work have been discussed.

2. Tsallis and Kaniadakis Entropies of BH

Both the Gibbs [1] and Shannon [44] entropies of distribution with W states working in the unit $k_B = 1$ leads to the relation explicitly dealt in [11]:

$$S = -\sum_{i=1}^{W} P_i \ln (P_i), \tag{1}$$

where P_i represents the probability of occupying the ith state for the classical system. The so-called von Neumann entropy which is a quantum mechanical form of this entropy is represented as

$$S = -Tr[\rho \ln (\rho)]. \tag{2}$$

The utilization of Equation (2) for the classical system goes back to the proposal of Boltzmann, where ρ represents the state density in the phase space [45]. One can obtain the so-called Bekenstein entropy ($S_{\mathrm{BH}} = A/4$) by applying Equation (2) to a purely gravitational system [19]. Since degrees of freedom are disseminated on the horizon without any preference w.r.t. one another, one may consider that P_i is equal for all of them [20, 21] permitting us to write $P_i = 1/W$. In such manner, Equations (1) and (2) lead to the Boltzmann entropy ($S = \ln (W)$), and thus, we have [7]

$$S_{\mathrm{BH}} = \frac{A}{4} = \ln (W) \Rightarrow W = \exp\left(\frac{A}{4}\right), \tag{3}$$

for horizon entropy and accordingly $W(A)$. As a unique free parameter generalized entropy, the Tsallis entropy is defined as [4]

$$S_Q^T = \frac{1}{1-Q}\sum_{i=1}^{W}\left(P_i^Q - P_i\right), \tag{4}$$

where Q is an unknown free parameter named as the nonextensive or Tsallis parameter ($S_Q^T \to S$ for $Q \to 1$). When the probability distribution meets the conditions $P_i = 1/W$, Equation (4) yields

$$S_Q^T = \frac{W^{1-Q} - 1}{1-Q}. \tag{5}$$

The quantum features of gravity [7, 46] are also a source for the existence of Q parameter. Now, taking $\delta = 1 - Q$ and utilizing Equation (3) with Equation (5), one can find easily

$$S_Q^T = \frac{1}{1-Q}\left[\exp\left((1-Q)S_{\mathrm{BH}}\right) - 1\right] = \frac{2\exp\left(\delta S_{\mathrm{BH}}/2\right)}{\delta}\sinh\left(\frac{\delta S_{\mathrm{BH}}}{2}\right). \tag{6}$$

In the scenario of loop quantum gravity, it is acquired by applying the Tsallis entropy definition to BH [11, 47] that

$$S_Q^T = \frac{1}{1-Q}\left[\exp\left(\frac{(1-Q)\ln(2)}{\pi\beta\sqrt{3}}S_{\mathrm{BH}}\right)-1\right], \quad (7)$$

satisfying $S_Q^T \to S$ whenever $Q \to 1$ and $\beta = \ln(2)/\pi\sqrt{3}$ [11, 47]. Furthermore, Equation (6) and (7) become accordingly the same when we consider $\beta = \ln(2)/\pi\sqrt{3}$.

Another single-free parameter generalized entropy is Kaniadakis entropy (K-entropy) [2, 3, 11], defined as

$$S_K = -\sum_{i=1}^{W}\frac{P_i^{1+K}-P_i^{1-K}}{2K} = \frac{1}{2}\left(\frac{\Sigma_{i=1}^{W}\left(P_i^{1-K}-P_i\right)}{K}+\frac{\Sigma_{i=1}^{W}\left(P_i^{1+K}-P_i\right)}{-K}\right), \quad (8)$$

where K represents an unknown parameter, and the limit $K \to 0$ is a way to obtain Boltzmann-Gibbs entropy [2, 3]. Comparing Equation (8) with (4) and (5), it can easily obtain

$$S_K = \frac{S_{1+K}^T + S_{1-K}^T}{2}. \quad (9)$$

Furthermore, by taking $P_i = 1/W$, Equation (8) assists in getting [2, 3, 11]

$$S_K = \frac{W^K - W^{-K}}{2K}. \quad (10)$$

Combining Equation (10) with Equation (3) yields

$$S_K = \frac{1}{K}\sinh(KS_{\mathrm{BH}}). \quad (11)$$

It is observed that Sharma-Mittal and Rényi entropies can be obtained as a function of Tsallis entropy as [13, 48]

$$S_{\mathrm{SM}} = \frac{1}{R}\left(\left(1+(1-Q)S_T\right)^{R/1-Q}-1\right), \qquad \mathcal{S} = \frac{1}{1-Q}\ln\left(1+(1-Q)S_T\right), \quad (12)$$

which leads to

$$S_{\mathrm{SM}} = \frac{1}{R}\left[\exp(RS_{\mathrm{BH}})-1\right], \quad \mathcal{S} = S_{\mathrm{BH}}, \quad (13)$$

where R is an unknown parameter. It is suggested that $\beta = \ln(2)/\pi\sqrt{3}$; otherwise, $(\ln(2)/\beta\pi\sqrt{3})S_{\mathrm{BH}}$ would occur in mathematical results rather than S_{BH}.

3. Kaniadakis Holographic Dark Energy

As it was claimed by the HDE hypothesis that if the current accelerated universe is driven by vacuum energy, then its total amount stored in a packet with size L^3 should not go beyond the energy of BH having the same size as it [18]. By keeping in mind this, one can generate the following relation in view of Kaniadakis entropy (11) as

$$\Lambda^4 = \rho_d^K \propto \frac{S_K}{L^4}, \quad (14)$$

for the vacuum energy ρ_d^K. Now, taking the Hubble horizon of the cosmos as the IR cutoff (i.e., $L = 1/H \Rightarrow A = 4\pi/H^2$), we obtain

$$\rho_d^K = \frac{3c^2H^4}{8\pi\kappa}\sinh\left(\frac{\pi\kappa}{H^2}\right), \quad (15)$$

where the constant c^2 is unknown [18], κ belongs to a set of real numbers [3], and $H = \dot{a}/a$ is the Hubble parameter. Now, it is clear that we have $\rho_d^K \to 3c^2H^2/8$ (the well-known Bekenstein entropy-based HDE) when $k \to 0$ [18]. Considering the pressureless fluid (with energy density ρ_m) and the dark energy candidate (with pressure p_d and density ρ_d^K), the energy-momentum conservation laws for the fractal universe take the form

$$\dot{\rho}_m + \left(3H + \frac{\dot{\upsilon}}{\upsilon}\right)\rho_m = \Gamma, \quad (16)$$

$$\dot{\rho}_d + \left(3H + \frac{\dot{\upsilon}}{\upsilon}\right)(\rho_d + p_d) = -\Gamma, \quad (17)$$

where the "dot" represents the derivative w.r.t. cosmic time t, and the phenomenal term Γ represents the interaction between dark matter and DE (it also gives the flow of energy between the two fluids) and has different mathematical values for both the linear and nonlinear cases, among which some linear cases are $\Gamma_1 = 3Hb^2(\rho_m + \rho_d)$, $\Gamma_2 = 3Hb^2\rho_m$, and $\Gamma_3 = 3Hb^2\rho_d$ [49–54] while some nonlinear cases are $\Gamma_4 = 3Hb^2((\rho_m^2/(\rho_m+\rho_d)) + \rho_m)$, $\Gamma_5 = 3Hb^2((\rho_d^2/(\rho_m+\rho_d)) + \rho_d)$, $\Gamma_6 = 3Hb^2((\rho_d^2/(\rho_m+\rho_d)) + \rho_d + \rho_m)$, and $\Gamma_7 = 3Hb^2((\rho_m^2/(\rho_m+\rho_d)) + \rho_d + \rho_m)$ [53, 54] with b^2 being the coupling constant. We have chosen $\Gamma = 3Hb^2\rho_m$ [49] as it is simple and leads to precise results. The fractal profile is either timelike or spacelike. We have chosen the timelike fractal profile in the power law form as $\upsilon = a^{-\gamma}$ [36, 55] with a being the scale factor depending upon cosmic time t and γ being a positive constant. In the fractal universe, the Friedmann equations can be obtained as

$$H^2 + H\frac{\dot{\upsilon}}{\upsilon} - \frac{\omega}{6}\dot{\upsilon}^2 = \frac{1}{3}(\rho_m + \rho_d), \quad (18)$$

$$\dot{H} + H^2 - H\frac{\dot{\upsilon}}{\upsilon} + \frac{\omega}{3}\upsilon^2 - \frac{\Box\upsilon}{2\upsilon} = -\frac{1}{6}(\rho + 3p), \quad (19)$$

where $\Box\upsilon = (1/\sqrt{-g})\partial^\mu(\sqrt{-g}\partial_\mu\upsilon)$ with simplified relation as $\Box\upsilon = -[\ddot{\upsilon} + 3H\dot{\upsilon}]$. From simplification of (16), one can find

$$\rho_m = \frac{3\Omega_{m_o}H_o^2}{8\pi}(1+z)^{\Delta}, \quad (20)$$

where $\Delta = 3 - \gamma - 3b^2$, z represents the redshift parameter, H_o is the value of the Hubble parameter at $t = 0$, and $\Omega_{m_o} = 8\pi\rho_{m_o}/3H_o^2$ with ρ_{m_o} being a constant of integration.

The scope and importance of cosmological parameters is increasing day by day as they are favorable tools to analyze and track the history and evaluation of the universe. The parameter q is one which decides whether the universe is facing accelerated expansion or not (i.e., $q < 0$ gives the accelerated expansion of the universe while $q > 0$ when the universe has decelerating expansion behavior) [56, 57]. The equation of state (EoS) parameter ω_d is one which decides the phases of the cosmos (i.e., $\omega_d < -1$ represents the phantom phase of the universe, and $-1 < \omega_d < -1/3$ describes the quintessence phase while $\omega_d > -1/3$ gives the vacuum phase of the universe) [58, 59]. The squared speed of sound C_s^2 is another important cosmological parameter which decides whether the model is stable or not (i.e., $C_s^2 > 0$ describes the stable model while $C_s^2 < 0$ only when the model is unstable) [57, 58, 60]. The ratio of $\Omega_m = \rho_m/\rho_c$ and $\Omega_d = \rho_d/\rho_c$ called the coincidence parameter given by $\tilde{r} = \Omega_m/\Omega_d = \rho_m/\rho_d$ decides the dark energy- and dark matter-dominated eras of the universe (i.e., $0 < \Omega_m/\Omega_d < 1$ describes the dark energy-dominated era, and $\Omega_m/\Omega_d > 1$ gives the dark matter-dominated era) [61]. In the upcoming, we will discuss these cosmological parameters.

Differentiating (18) with respect to cosmic time t and substituting all necessary values in it, one can get

$$\dot{H} = \frac{-3\kappa\Omega_{m_o}H_o^2\Delta a^{-\Delta} - 8\pi\kappa\omega H^2\gamma^3 a^{-2\gamma}}{48\pi\kappa - 48\pi\kappa\gamma - 8\pi\kappa\omega\gamma^2 a^{-2\gamma} - 12c^2H^2\sinh\left(\pi\kappa/H^2\right) + 6\pi\kappa c^2\cosh\left(\pi\kappa/H^2\right)}. \tag{21}$$

Using the transformation $d/dt = -(1+z)H(d/dz)$ from cosmic time t to the redshift parameter z, simplification of (21) gives the relation for H in terms of the redshift parameter as

$$H' = \frac{8\pi\kappa\omega H^2\gamma^3(1+z)^{2\gamma-1} + 3\kappa\Omega_{m_o}H_o^2\Delta(1+z)^{\Delta-1}}{H\left[48\pi\kappa - 48\pi\kappa\gamma - 8\pi\kappa\omega\gamma^2(1+z)^{2\gamma} - 12c^2H^2\sinh\left(\pi\kappa/H^2\right) + 6\pi\kappa c^2\cosh\left(\pi\kappa/H^2\right)\right]}, \tag{22}$$

where the "prime" denotes the derivative with respect to redshift parameter z. The deceleration parameter q which is of great importance to decide the accelerated expansion of the universe can be found as

$$q = -1 - \frac{\dot{H}}{H^2} = -1 + \frac{8\pi\kappa\omega H^2\gamma^3(1+z)^{2\gamma} + 3\kappa\Omega_{m_o}H_o^2\Delta(1+z)^{\Delta}}{H^2\left[48\pi\kappa - 48\pi\kappa\gamma - 8\pi\kappa\omega\gamma^2(1+z)^{2\gamma} - 12c^2H^2\sinh\left(\pi\kappa/H^2\right) + 6\pi\kappa c^2\cosh\left(\pi\kappa/H^2\right)\right]}. \tag{23}$$

Substituting the corresponding values and simplifying (17), we obtain

$$\begin{aligned} p_d^K = \frac{3}{8\pi\kappa(\gamma-3)}\Bigg[&\left(2\pi\kappa c^2H(1+z)\cosh\left(\frac{\pi\kappa}{H^2}\right) - 4c^2H^3\right.\\ &\left.\cdot(1+z)\sinh\left(\frac{\pi\kappa}{H^2}\right)\right)H' - c^2H^4(\gamma-3)\sinh\left(\frac{\pi\kappa}{H^2}\right)\\ &+ 3\kappa b^2\Omega_{m_o}H_o^2(1+z)^{\Delta}\Bigg]. \end{aligned} \tag{24}$$

The mathematical formalism for the EoS parameter is $\omega_d^K = p_d^K/\rho_d^K$, and the relation for ω_d^K can be obtained by using (15) and (24) in this formula as

$$\begin{aligned} \omega_d^K = -1 + &\left(\frac{2\pi\kappa(1+z)\coth\left(\pi\kappa/H^2\right)}{H^3(\gamma-3)} - \frac{4(1+z)}{H(\gamma-3)}\right)H'\\ &+ \frac{3\kappa b^2\Omega_{m_o}H_o^2(1+z)^{\Delta}}{c^2H^4(\gamma-3)\sinh\left(\pi\kappa/H^2\right)}. \end{aligned} \tag{25}$$

Some other important mathematical formulas of cosmological consequences which we will use later on are

$$\begin{aligned} \Omega_m &= \frac{\rho_m}{\rho_c},\\ \Omega_d &= \frac{\rho_d}{\rho_c},\\ \frac{\Omega_m}{\Omega_d} &= \frac{\rho_m}{\rho_d},\\ \rho_c &= \frac{3H^2}{8\pi}. \end{aligned} \tag{26}$$

The ratio Ω_m/Ω_d^K which is of great importance to decide about the dark energy- and dark matter-dominated eras of the universe for the Kaniadakis entropy content of BH is given by

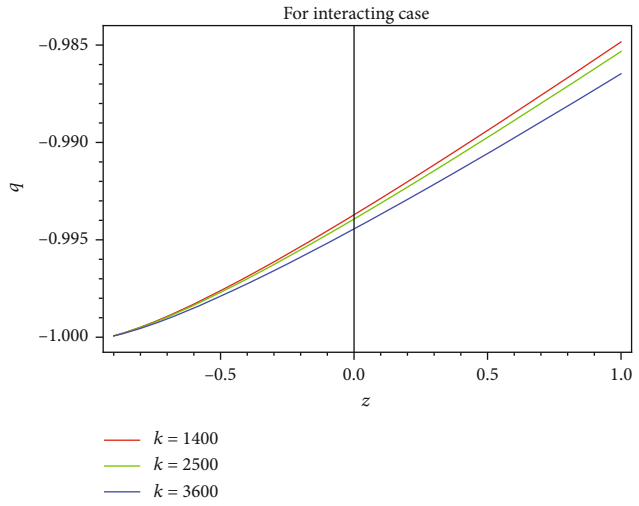

FIGURE 1: Behavior of deceleration parameter q against redshift parameter z considering different values of κ when $\Omega_{m_o} = 0.315$, $b^2 = 0.5$, $H_o = 67.9$, $\omega = -0.3$, $c^2 = 0.313$, and $\gamma = 0.127$.

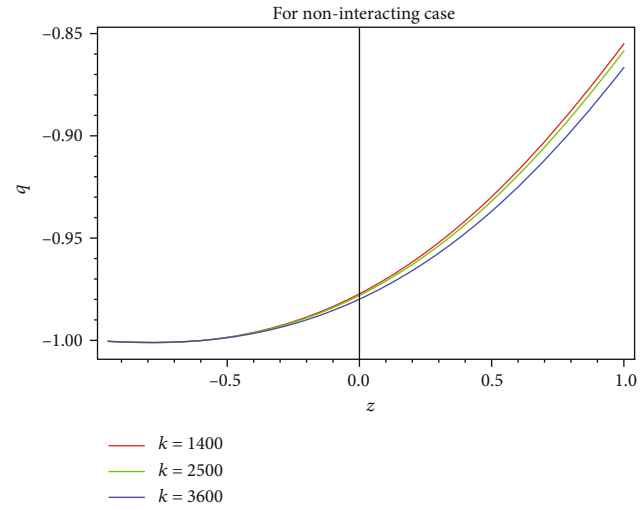

FIGURE 2: Behavior of q against z.

$$\frac{\Omega_m}{\Omega_d^K} = \frac{\kappa\Omega_{m_o}H_o^2(1+z)^{\Delta}}{c^2H^4\sinh\left(\pi\kappa/H^2\right)}. \tag{27}$$

The stability of the system is examined by a perturbed parameter called the squared speed of sound (C_s^2). The mathematical formalism for this parameter is given by

$$C_s^2 = \frac{\partial p_{\text{eff}}}{\partial \rho_{\text{eff}}}, \tag{28}$$

where $\rho_{\text{eff}} = \rho_m + \rho_d^K$ and $p_{\text{eff}} = p_d^K$. Differentiating these relations with respect to the redshift parameter leads to the following mathematical result:

$$\begin{aligned} C_s^2 = {} & \frac{1}{(\gamma-3)\left[\kappa\Omega_{m_o}H_o^2\Delta(1+z)^{\Delta-1} + c^2\left[4H^3H'\sinh\left(\pi\kappa/H^2\right) - 2\pi\kappa HH'\cosh\left(\pi\kappa/H^2\right)\right]\right]} \\ & \cdot\left[2\pi\kappa c^2(1+z)\cosh\left(\frac{\pi\kappa}{H^2}\right)\left(H'^2 + HH'\times(1+z)^{-1} + HH'' + 2\pi\kappa H^{-2}H'^2\tanh\left(\frac{\pi\kappa}{H^2}\right)\right)\right. \\ & - 4(1+z)\sinh\left(\frac{\pi\kappa}{H^2}\right)c^2\left(3H^2H'^2 + H^3H'(1+z)^{-1} + H^3H'' - 2\pi\kappa\times H'^2\coth\left(\frac{\pi\kappa}{H^2}\right)\right) \\ & \left. + 3\kappa b^2\Omega_{m_o}H_o^2\Delta(1+z)^{\Delta-1} - c^2(\gamma-3)HH'\left(4H^2\sinh\left(\frac{\pi\kappa}{H^2}\right) - 2\pi\kappa\cosh\left(\frac{\pi\kappa}{H^2}\right)\right)\right]. \end{aligned} \tag{29}$$

Variation of q against z has been plotted for interacting (Figure 1) and noninteracting (Figure 2) cases, respectively. By considering $\kappa = 1400,2500,3600$ with fixed values of other parameters as $\Omega_{m_o} = 0.315$, $b^2 = 0.5$, $H_o = 67.9$, $\omega = -0.3$, $c^2 = 0.313$, and $\gamma = 0.127$, we obtain the cosmic acceleration phase in both cases. Also, the values of the deceleration parameter lie in the range $[-1, 0)$ which is a compatible range with observational data. In Figure 3, EoS parameter ω_d^K for the KHDE model is plotted versus deceleration parameter q for the interacting case while in Figure 4, the same is plotted for the noninteracting case. The evolved constant parameters are taken, the same as in Figures 1 and 2. The phantom phase of the universe is observed for the interacting case. For the noninteracting case, the quintessence phase is achieved for $\kappa = 1400, 2500$ and the phantom phase for $\kappa = 3600$. Moreover, the EoS parameter $\omega_d^K \to -1$ as $z \to -1$ which coincides with the ΛCDM model. In Figures 5 and 6, the coincidence parameter $\tilde{r} = \Omega_m/\Omega_d^K$ is plotted against q for interacting and noninteracting cases, respectively. The dark energy-dominated era is recovered for the interacting case while for the noninteracting case, when $\kappa = 1400$, the interval $-0.95 < z < 0.65$ gives the energy-dominated era while $z > 0.65$ results in the matter-dominated era; for $\kappa = 2500$, the matter-dominated era is obtained when $z > 0.83$, and for $\kappa = 3600$, the matter-dominated era is achieved when $z > 1.1$. The squared speed of sound C_s^2 which decides the stability of the model is examined for both cases (interacting and noninteracting) in Figures 7 and 8, respectively. For the

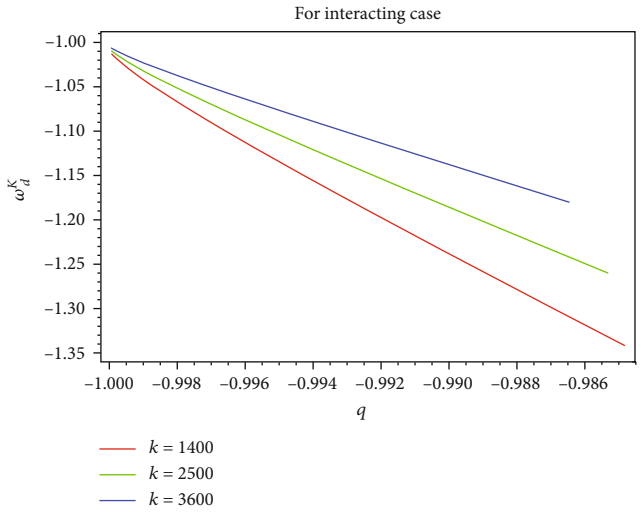

FIGURE 3: Graph of EoS ω_d^K versus deceleration parameter q.

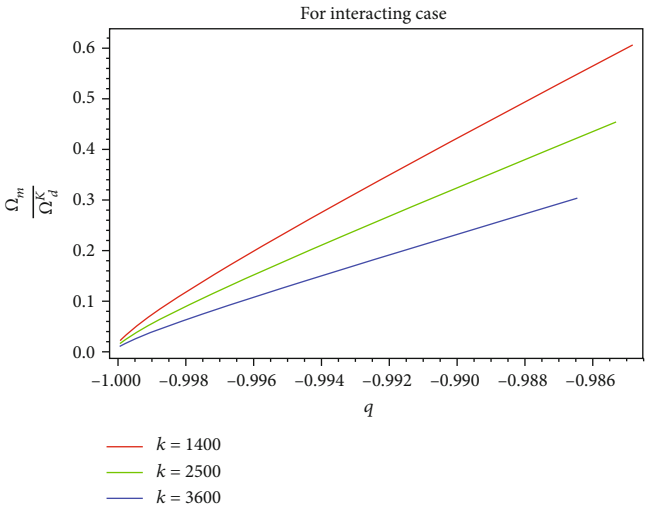

FIGURE 5: Plot of coincidence parameter $\tilde{r} = \Omega_m/\Omega_d^K$ against deceleration parameter q.

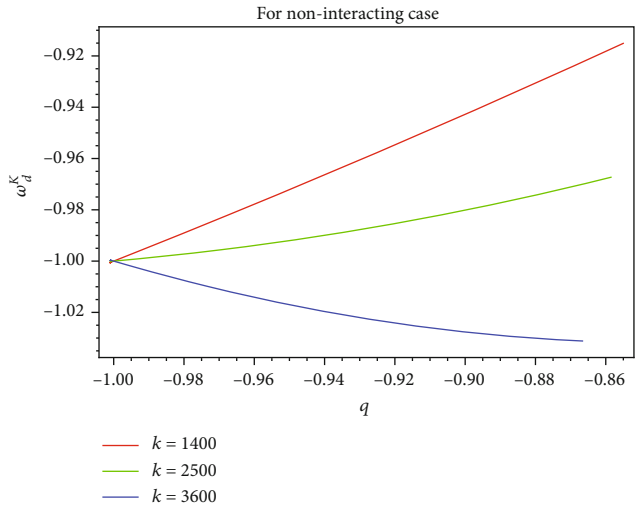

FIGURE 4: Variation of EoS parameter ω_d^K versus deceleration parameter q.

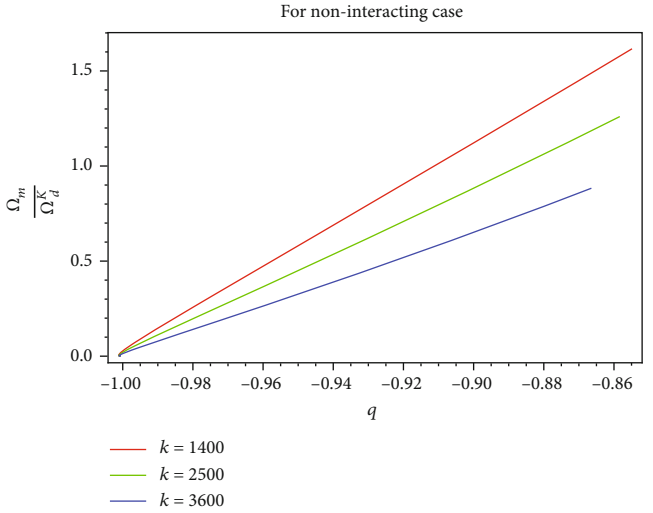

FIGURE 6: Plot of $\tilde{r} = \Omega_m/\Omega_d^K$ against q.

interacting case, $C_s^2 > 0$ in the interval $-0.95 < z < 0.63$ which leads to the stable model in this interval. The noninteracting case model is stable when $z < -0.18$ while it becomes unstable when $z > -0.18$.

4. New Tsallis Holographic Dark Energy

Considering the pattern of (14) and (15) and taking Tsallis entropy (6) into account, it is easy to have NTHDE as

$$\rho_d^T \propto \frac{S_Q^T}{L^4} \Rightarrow \rho_d^T = \left(\frac{3T^2}{8\pi}\right)\frac{S_Q^T}{L^4}, \tag{30}$$

where T^2 is an unknown real number [18]. Taking $D^2 = \pi T^2$ and the apparent horizon as the IR cutoff ($H = 1/L$), we have

$$\rho_d^T = \frac{2D^2\rho_c}{X}\exp\left(\frac{X}{2}\right)\sinh\left(\frac{X}{2}\right), \tag{31}$$

in which $X = \delta\pi/H^2$, where δ belongs to a set of real numbers [11]. Substituting all required assumed and obtained values in (29), we get

$$\rho_d^T = \frac{3H^4D^2}{4\pi^2\delta}\lambda, \tag{32}$$

where $\lambda = \exp(\pi\delta/2H^2)\sinh(\pi\delta/2H^2)$. Considering all assumptions, differentiating (18) w.r.t. cosmic time t, and putting necessary values in it, we reach the following result:

$$H' = \frac{16\pi^2\delta H\gamma^3\omega(1+z)^{2\gamma-1} + 6\pi\delta\Omega_{m_o}H_o^2\Delta(1+z)^{\Delta-1}H^{-1}}{16\pi^2\delta\left(6-6\gamma-\omega\gamma^2(1+z)^{2\gamma}\right) - 9D^2\lambda\left(16H^2 - \pi\delta\left(\coth\left(\pi\gamma/2H^2\right)+1\right)\right)}. \tag{33}$$

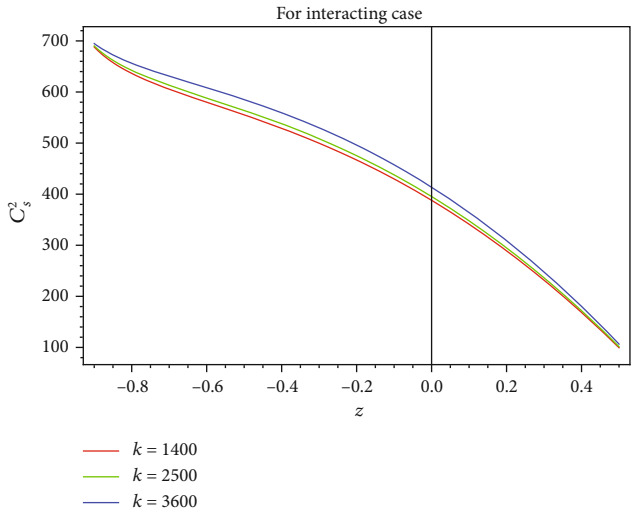

Figure 7: Variation of squared speed of sound C_s^2 versus redshift parameter z.

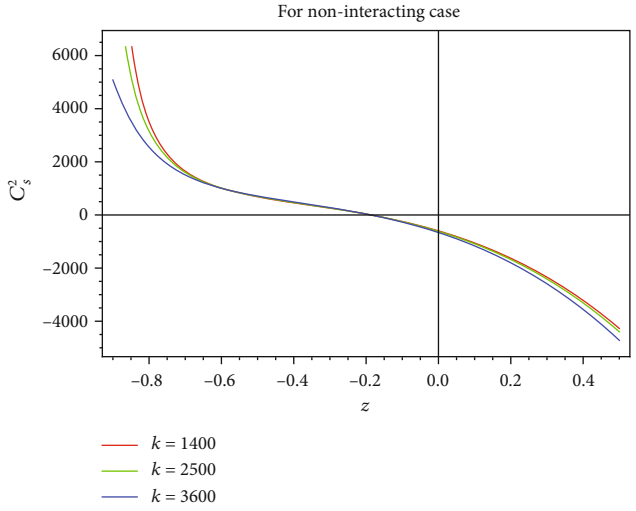

Figure 8: Variation of squared speed of sound C_s^2 versus redshift parameter z.

The deceleration parameter q for the NTHDE model is obtained as

$$q = -1 - \frac{\dot{H}}{H^2} = -1 + \frac{16\pi^2\delta\gamma^3\omega(1+z)^{2\gamma} + 6\pi\delta\Omega_{m_o}H_o^2H^{-2}\Delta(1+z)^{\Delta}}{96\pi^2\delta(1-\gamma) - 16\pi^2\delta\omega\gamma^2(1+z)^{2\gamma} - 9D^2\lambda\left[16H^2 - \pi\delta\left(\coth\left(\pi\gamma/2H^2\right)+1\right)\right]}. \tag{34}$$

Substituting the concern values from the NTHDE model and simplifying Equation (17) yield

$$p_d^T = \frac{9b^2\Omega_{m_o}H_o^2(1+z)^{\Delta}}{8\pi(\gamma-3)} - \frac{3D^2H^4H'\lambda}{4\pi^2\delta} + \frac{3D^2H(1+z)\lambda H'}{4\pi(\gamma-3)} \cdot \left[\coth\left(\frac{\pi\delta}{2H^2}\right) + 1 - \frac{4H^2}{\pi\delta}\right]. \tag{35}$$

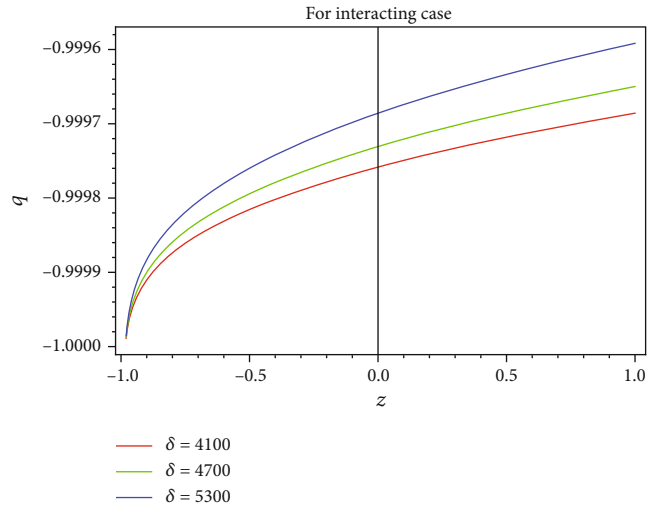

Figure 9: Variation of deceleration parameter q against redshift parameter z considering different values of δ when $\Omega_{m_o} = 0.315$, $b^2 = 0.5$, $\omega = -0.3$, $H_o = 67.9$, $D^2 = 0.3136$, and $\gamma = 0.127$.

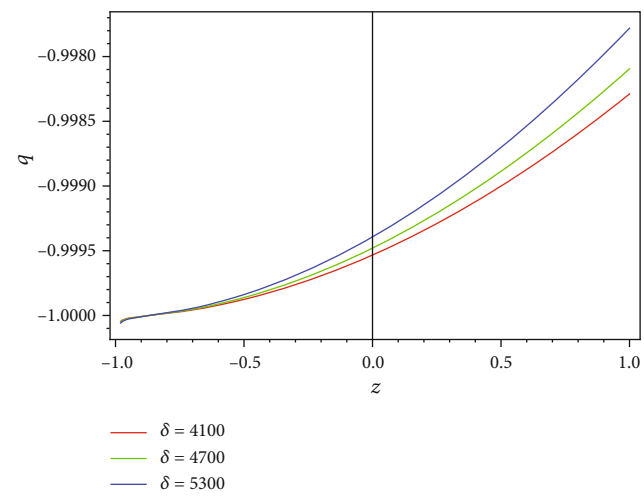

Figure 10: Graph of q against z.

The relation for EoS parameter ω_d^T is obtainable after simplifications of Equations (32) and (35) as

$$\omega_d^T = \frac{p_d^T}{\rho_d^T} = \frac{\pi\delta b^2\Omega_{m_o}H_o^2(1+z)^{\Delta}}{2H^4D^2(\gamma-3)\lambda} - 1 + \frac{1+z}{\gamma-3} \cdot \left[\frac{\pi\delta}{4H^3}\coth\left(\frac{\pi\delta}{2H^2}\right) + \frac{\pi\delta}{4H^3} - \frac{4}{H}\right]H'. \tag{36}$$

The coincidence parameter for the obtained model is

$$\tilde{r} = \frac{\Omega_m}{\Omega_d^K} = \frac{\pi\delta\Omega_{m_o}H_o^2(1+z)^{\Delta}}{2D^2H^4\lambda}. \tag{37}$$

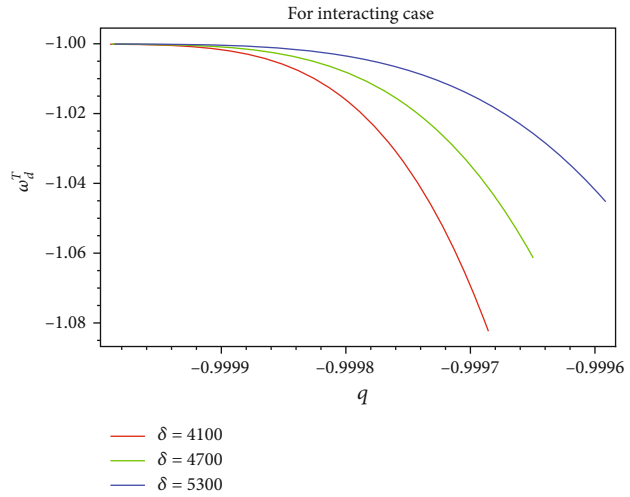

FIGURE 11: Plot of EoS parameter ω_d^T versus deceleration parameter q.

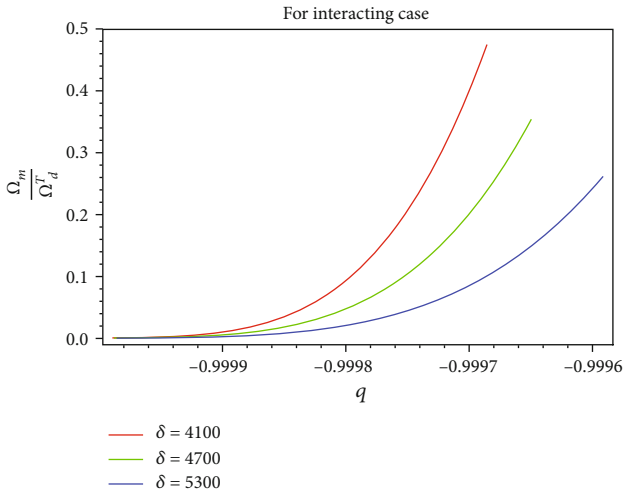

FIGURE 13: Behavior of coincidence parameter $\tilde{r} = \Omega_m/\Omega_d^T$ against deceleration parameter q.

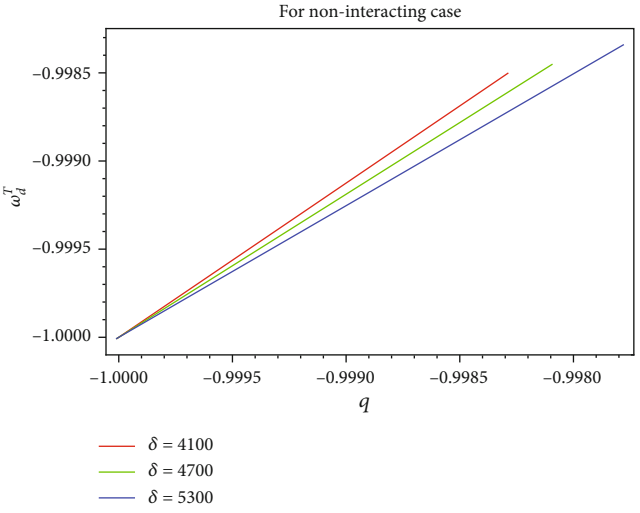

FIGURE 12: Plot of EoS parameter ω_d^T versus deceleration parameter q.

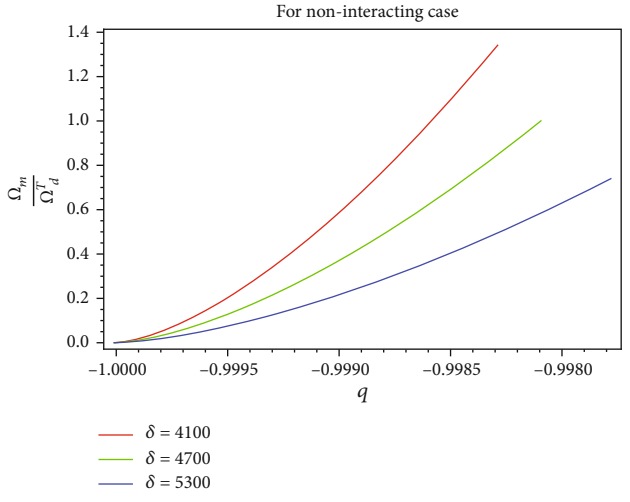

FIGURE 14: Behavior of coincidence parameter $\tilde{r} = \Omega_m/\Omega_d^T$ against q.

The relation for a perturbed parameter called the squared speed of sound which is given in (28) is obtainable as

$$C_s^2 = \frac{1}{(\gamma-3)\left[3\pi\delta\Omega_{m_o}H_o^2\Delta(1+z)^{\Delta-1} + 6D^2HH'\lambda\left[4H^2 - \pi\delta - \pi\delta\coth\left(\pi\delta/2H^2\right)\right]\right]}$$
$$\cdot\left[9\pi\delta b^2\Omega_{m_o}H_o^2\Delta(1+z)^{\Delta-1} + 6D^2\times(\gamma-3)HH'\lambda\right.$$
$$\cdot\left(\pi\delta\coth\left(\frac{\pi\delta}{2H^2}\right) - 4H^2 + \pi\delta\right) + 6D^2\pi\delta\beta(1+z)$$
$$\cdot\left(H'^2 + HH'(1+z)^{-1} + HH'' - \pi\delta H^{-2}H'^2 + \pi\delta\times H^{-2}H'^2\tanh\left(\frac{\pi\delta}{2H^2}\right)\right)$$
$$+ 6D^2\pi\delta(1+z)\lambda\left(H'^2 + HH'(1+z)^{-1} + HH'' - \pi\delta H^{-2}H'^2\right.$$
$$\left.\left.- \pi\delta H^{-2}H'^2\coth\left(\frac{\pi\delta}{2H^2}\right)\right) - 24D^2(1+z)\lambda\left(3H^2H'^2 + H^3H'(1+z)^{-1}\right.\right.$$
$$\left.\left.+ H^3H'' - \pi\delta H'^2 - \pi\delta H'^2\coth\left(\frac{\pi\delta}{2H^2}\right)\right)\right], \tag{38}$$

where $\beta = \exp(\pi\delta/2H^2)\cosh(\pi\delta/2H^2)$.

The graph of deceleration parameter q against redshift parameter z is plotted in Figures 9 and 10 for interacting and noninteracting cases, respectively. Constant parameters are $\delta = 4100,4700,5300$, $\Omega_{m_o} = 0.315$, $b^2 = 0.5$, $H_o = 67.9$, $\omega = -0.3$, $D^2 = 0.313$, and $\gamma = 0.127$. Required results (accelerated expansion) of the universe are achieved in both cases. EoS parameter ω_d^T for the NTHDE model is plotted versus deceleration parameter q for interacting and noninteracting cases in Figures 11 and 12, respectively. The involved parameters are taken, the same as in Figures 9 and 10. The phantom phase of the universe is observed for the interacting case, and the quintessence phase is achieved for the noninteracting case. In Figures 13 and 14, the coincidence parameter $\tilde{r} = \Omega_m/\Omega_d^T$ is plotted against q for interacting and noninteracting cases, respectively. The dark energy-dominated era is recovered for the interacting case whereas for the noninteracting case, when $\delta = 4100$, the interval $-0.95 < z < 0.8$ gives the energy-dominated era while $z > 0.8$ results in the matter-

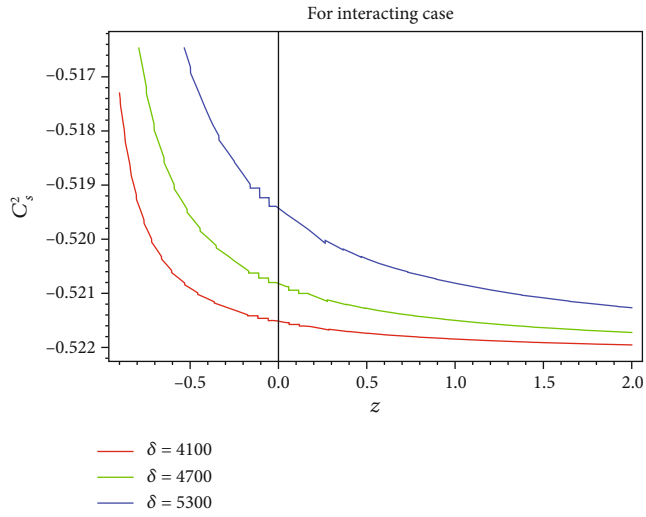

Figure 15: Plot of squared speed of sound C_s^2 versus redshift parameter z.

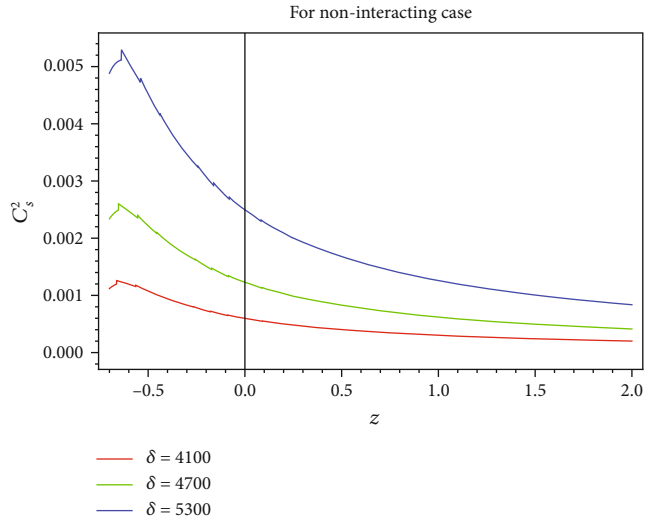

Figure 16: Graph of C_s^2 against z.

Table 1

q	Observational schemes
$-0.644^{+0.223}_{-0.223}$	BAO+TDSL+Masers+Pantheon
$-0.6401^{+0.187}_{-0.187}$	BAO+TDSL+Masers+Pantheon+H_o
$-0.930^{+0.218}_{-0.218}$	BAO+TDSL+Masers+Pantheon+H_z
$-1.2037^{+0.175}_{-0.175}$	BAO+TDSL+Masers+Pantheon+H_o+H_z

dominated era; for $\delta = 4700$, the matter-dominated era is obtained when $z > 1$, and for $\delta = 5300$, the matter-dominated era is achieved when $z > 1.23$. In Figures 15 and 16, the squared speed of sound C_s^2 has been plotted to examine the stability of the model for both the interacting and noninteracting cases, respectively. For the interacting case, $C_s^2 < 0$ while for the noninteracting case, it leads to positive values which describes the stable model.

Table 2

ω_d	Observational schemes
$-1.56^{+0.60}_{-0.48}$	Planck+lowE+TT
$-1.58^{+0.52}_{-0.41}$	Planck+lowE+TT, TE, EE
$-1.57^{+0.50}_{-0.40}$	Planck+lowE+lensing+TT, TE, EE
$-1.40^{+0.10}_{-0.10}$	Planck+lowE+lensing+BAO+TT, TE, EE

5. Conclusions

We have investigated the interacting and noninteracting behaviors of KHDE and NTHDE with the apparent horizon and extracted various cosmological parameters by varying the value of κ for KHDE and δ for NTHDE and keeping all other parameters fixed as $\Omega_{m_o} = 0.315$, $b^2 = 0.5$, $H_o = 67.9$, $\omega = -0.3$, $c^2 = 0.313$, $D^2 = 0.313$, and $\gamma = 0.127$. The cosmological consequences resulted as follows.

5.1. Deceleration Parameter. For the KHDE model, the deceleration parameter q provides the accelerated universe in both the interacting and noninteracting cases. The results obtained in both cases for q are compared with Planck's observational data [62] presented in Table 1. It has been found that the results of the KHDE model are consistent with the observational data at the present epoch in both the interacting and noninteracting cases. At $z = 0$, for the interacting case, we have achieved $(\kappa, q) = (1400, -0.9937), (2500, -0.9939), (3600, -0.9944)$, and for the noninteracting case, we obtained $(\kappa, q) = (1400, -0.9773), (2500, -0.9781), (3600, -0.9800)$. The deceleration parameter q has given that NTHDE can model the accelerated universe in both the interacting and noninteracting cases. The results obtained in both cases for q are compared with Planck's observational data [62] presented in Table 1. It has been found that the results of the NTHDE model are consistent with the observational data at the present epoch in both the interacting and noninteracting cases. At $z = 0$, for the interacting case, we achieve $(\delta, q) = (4100, -0.99976), (4700, -0.99973), (5300, -0.99968)$, and for the noninteracting case, we obtain $(\delta, q) = (4100, -0.99954), (4700, -0.99948), (5300, -0.99939)$.

5.2. EoS Parameter. For the KHDE model, the EoS parameter ω_d^K has illustrated the phantom phase of the universe at different values of κ for the interacting case. However, it shows the quintessence phase of the universe for $\kappa = 1400, 2500$ and the phantom phase for $\kappa = 3600$ when the noninteracting case is under consideration. Moreover, we compared these results with Planck's observational data [62] presented in Table 2. The comparison shows that results obtained by the KHDE model have consistency with the observational data at $z = 0$ in both cases. For the interacting case, we found the values of (κ, ω_d^K) at the present epoch as $(1400, -1.16), (2500, -1.12), (3600, -1.08)$ while for the noninteracting case, we achieve $(\kappa, \omega_d^K) = (1400, -0.988), (2500, -0.997), (3600, -1.007)$. For the NTHDE model, the EoS parameter ω_d^T tells about the phantom phase of the universe at different values of δ for the interacting case while it shows the quintessence

phase of the universe for the noninteracting case. Moreover, we compared these results obtained with Planck's observational data [62] presented in Table 2. The comparison shows that results obtained by the NTHDE model have consistency with the observational data at $z = 0$ in both cases. For the interacting case, we found the values of (δ, ω_d^T) at the present epoch as $(4100,-1.032), (4700,-1.023), (5300,-1.017)$, and for the noninteracting case, we achieve $(\delta, \omega_d^T) = (4100,-0.99959), (4700,-0.99958), (5300,-0.99955)$.

5.3. Coincidence Parameter. For the KHDE model, the coincidence parameter $\tilde{r} = \Omega_m/\Omega_d^K$ is achieved for both the interacting and noninteracting cases. For the interacting case, we obtain the dark energy-dominated era for $-0.95 < z < 1$. For the noninteracting case, when $\kappa = 1400$, the interval $-0.95 < z < 0.65$ gives the energy-dominated era while $z > 0.65$ results in the matter-dominated era; for $\kappa = 2500$, the matter-dominated era is obtained when $z > 0.83$, and for $\kappa = 3600$, the matter-dominated era is achieved when $z > 1.1$. The coincidence parameter for the NTHDE model $\tilde{r} = \Omega_m/\Omega_d^K$ has been examined for both the interacting and noninteracting cases. For the interacting case, we got the dark energy-dominated era in the interval $-0.95 < z < 1$. For the noninteracting case, when $\delta = 4100$, the interval $-0.95 < z < 0.8$ gives the energy-dominated era while $z > 0.8$ results in the matter-dominated era; for $\delta = 4700$, the matter-dominated era is obtained when $z > 1$, and for $\delta = 5300$, the matter-dominated era is achieved when $z > 1.23$.

5.4. Squared Speed of Sound. The squared speed of sound C_s^2 which decides the stability of the model is examined for both the interacting and noninteracting cases. For the interacting case, $C_s^2 > 0$ in the interval $-0.95 < z < 0.63$ which is a justification for the stable model in this interval while the KHDE model is unstable when $z > 0.63$. For the noninteracting case model, behavior is stable when $z < -0.1873$ while it becomes unstable when $z > -0.1873$. For the NTHDE model, the squared speed of sound C_s^2 is examined for both the interacting and noninteracting cases. For the interacting case, $C_s^2 < 0$ which gives that the achieved model is unstable for the interacting case but it has given positive values of C_s^2 for the noninteracting case in the interval $-0.95 < z < 2$, which is a justification for the stable model.

Ghaffari et al. investigated the cosmological consequences of the interacting THDE model with the apparent radius in the fractal universe [36]. They constructed various cosmological parameters such as the EoS parameter, the deceleration parameter, and the evolution equation. They suggested that THDE described the transition that took place from the deceleration phase of the universe to the accelerated phase, eventually in both the noninteracting and interacting scenarios. Also, it is checked that the free parameters of the models are compatible with the latest observational results by using the Pantheon supernovae data, 6df, eBOSS, BOSS DR12, CMB Planck 2015, and Gamma-Ray Burst. They also found unstable behavior of the THDE model in both scenarios. However, in our case, KHDE and NTHDE with the apparent horizon in the fractal universe have provided consistent results with recent Planck's data [37] (as mentioned in Tables 1 and 2). It is also found that at the present epoch, the KHDE model is stable for the interacting case but unstable for the noninteracting case. The NTHDE model shows unstable behavior for the interacting case while stable behavior for the noninteracting case.

Data Availability

I have mentioned all the results in the manuscript and references therein.

Conflicts of Interest

The authors declare that they have no conflicts of interest.

References

[1] J. W. Gibbs, *Elementry Priciples in Statistical Mechanics*, Charles Scribner's Sons, New York, 1902.

[2] G. Kaniadakis, "Non-linear kinetics underlying generalized statistics," *Physica A: Statistical Mechanics and its Applications*, vol. 296, no. 3-4, pp. 405–425, 2001.

[3] G. Kaniadakis, "Statistical mechanics in the context of special relativity," *Physical Review E*, vol. 66, no. 5, 2002.

[4] M. Masi, "A step beyond Tsallis and Renyi entropies," *Physics Letters A*, vol. 338, no. 3-5, pp. 217–224, 2005.

[5] N. Komatsu, "Cosmological model from the holographic equipartition law with a modified Rényi entropy," *The European Physical Journal C*, vol. 77, no. 4, 2017.

[6] H. Moradpour, A. Bonilla, E. M. . C. Abreu, and J. A. Neto, "Accelerated cosmos in a nonextensive setup," *Physical Review D*, vol. 96, no. 12, 2017.

[7] E. M. C. Abreu, J. A. Neto, A. C. R. Mendes, A. Bonilla, and R. M. de Paula, "Tsallis' entropy, modified Newtonian accelerations and the Tully-Fisher relation," *EPL (Europhysics Letters)*, vol. 124, no. 3, p. 30005, 2018.

[8] A. Bialas and W. Czyz, "Renyi entropies of a black hole from Hawking radiation," *EPL (Europhysics Letters)*, vol. 83, no. 6, p. 60009, 2008.

[9] V. G. Czinner and H. Iguchi, "Thermodynamics, stability and Hawking–Page transition of Kerr black holes from Rényi statistics," *The European Physical Journal C*, vol. 77, no. 12, 2017.

[10] J. Sadeghi, M. Rostami, and M. R. Alipour, "Investigation of phase transition of BTZ black hole with Sharma–Mittal entropy approaches," *International Journal of Modern Physics A*, vol. 34, no. 30, p. 1950182, 2019.

[11] H. Moradpour, A. H. Ziaie, and M. K. Zangeneh, "Generalized entropies and corresponding holographic dark energy models," *The European Physical Journal C*, vol. 80, no. 8, 2020.

[12] M. Tavayef, A. Sheykhi, K. Bamba, and H. Moradpour, "Tsallis holographic dark energy," *Physics Letters B*, vol. 781, pp. 195–200, 2018.

[13] H. Moradpour, S. A. Moosavi, I. P. Lobo, J. P. M. Graça, A. Jawad, and I. G. Salako, "Thermodynamic approach to holographic dark energy and the Rényi entropy," *The European Physical Journal C*, vol. 78, no. 10, 2018.

[14] H. Moradpour, A. H. Ziaie, S. Ghaffari, and F. Feleppa, "The generalized and extended uncertainty principles and their implications on the Jeans mass," *Monthly Notices of the Royal Astronomical Society*, vol. 488, no. 1, pp. L69–L74, 2019.

[15] H. Moradpour, A. Sheykhi, C. Corda, and I. G. Salako, "Implications of the generalized entropy formalisms on the Newtonian gravity and dynamics," *Physics Letters B*, vol. 783, pp. 82–85, 2018.

[16] J. D. Barrow, "The area of a rough black hole," *Physics Letters B*, vol. 808, no. 135643, article 135643, 2020.

[17] S. Ghaffari, A. H. Ziaie, V. B. Bezerra, and H. Moradpour, "Inflation in the Rényi cosmology," *Modern Physics Letters A*, vol. 35, no. 1, article 1950341, 2020.

[18] M. Li, "A model of holographic dark energy," *Physics Letters B*, vol. 603, no. 1-2, pp. 1–5, 2004.

[19] M. Srednicki, "Entropy and area," *Physical Review Letters*, vol. 71, no. 5, pp. 666–669, 1993.

[20] S. Das and S. Shankaranarayanan, "Where are the black-hole entropy degrees of freedom?," *Classical and Quantum Gravity*, vol. 24, no. 20, pp. 5299–5306, 2007.

[21] D. Pavon, "On the degrees of freedom of a black hole," 2020, https://arxiv.org/abs/2001.05716.

[22] S. A. Hayward, "Unified first law of black-hole dynamics and relativistic thermodynamics," *Classical and Quantum Gravity*, vol. 15, no. 10, pp. 3147–3162, 1998.

[23] D. Bak and S.-J. Rey, "Cosmic holography+," *Classical and Quantum Gravity*, vol. 17, no. 15, pp. L83–L89, 2000.

[24] R.-G. Cai and S. P. Kim, "First law of thermodynamics and Friedmann equations of Friedmann–Robertson–Walker universe," *Journal of High Energy Physics*, vol. 2005, no. 2, pp. 50–50, 2005.

[25] M. Akbar and R.-G. Cai, "Thermodynamic behavior of the Friedmann equation at the apparent horizon of the FRW universe," *Physical Review D*, vol. 75, no. 8, 2007.

[26] Y. S. Myung, "Instability of holographic dark energy models," *Physics Letters B*, vol. 652, no. 5-6, pp. 223–227, 2007.

[27] Q. Huang, H. Huang, J. Chen, L. Zhang, and F. Tu, "Stability analysis of a Tsallis holographic dark energy model," *Classical and Quantum Gravity*, vol. 36, no. 17, p. 175001, 2019.

[28] C. Tsallis, "Possible generalization of Boltzmann-Gibbs statistics," *Journal of Statistical Physics*, vol. 52, no. 1-2, pp. 479–487, 1988.

[29] A. Cho, "Statistical physics: a fresh take on disorder, or disorderly science," *Science*, vol. 297, no. 5585, pp. 1268-1269, 2002.

[30] S. Pressé, K. Ghosh, J. Lee, and K. A. Dill, "Nonadditive entropies yield probability distributions with biases not warranted by the data," *Physical Review Letters*, vol. 111, no. 18, p. 180604, 2013.

[31] V. C. Dubey, U. K. Sharma, and A. Beesham, "Tsallis holographic model of dark energy: cosmic behavior, statefinder analysis and $\omega_D - \omega_D'$ pair in the nonflat universe," *International Journal of Modern Physics D*, vol. 28, no. 15, p. 1950164, 2019.

[32] U. K. Sharma and V. C. Dubey, "Rényi holographic dark energy in the Brans–Dicke cosmology," *Modern Physics Letters A*, vol. 35, no. 34, p. 2050281, 2020.

[33] U. K. Sharma and S. Srivastava, "The cosmological behavior and the statefinder diagnosis for the new Tsallis agegraphic dark energy," *Modern Physics Letters A*, vol. 35, no. 38, p. 2050318, 2020.

[34] U. K. Sharma and V. Srivastava, "Tsallis HDE with an IR cutoff as Ricci horizon in a flat FLRW universe," *New Astronomy*, vol. 84, p. 101519, 2021.

[35] S. Srivastava and U. K. Sharma, "Barrow holographic dark energy with Hubble horizon as IR cutoff," *International Journal of Geometric Methods in Modern Physics*, vol. 18, no. 1, p. 2150014, 2021.

[36] S. Ghaffari, E. Sadri, and A. H. Ziaie, "Tsallis holographic dark energy in fractal universe," *Modern Physics Letters A*, vol. 35, no. 14, p. 2050107, 2020.

[37] P. A. Ade, N. Aghanim, M. Arnaud et al., "Planck 2015 results-XVIII. Background geometry and topology of the universe," *Astronomy & Astrophysics*, vol. 594, p. A13, 2016.

[38] R. C. Nunes, E. M. B. Jr, E. M. C. Abreu, and J. A. Neto, "Probing the cosmological viability of non-Gaussian statistics," *Journal of Cosmology and Astroparticle Physics*, vol. 2016, no. 8, pp. 51–51, 2016.

[39] M. Nauenberg, "Critique of q-entropy for thermal statistics," *Physical Review E*, vol. 67, no. 3, 2003.

[40] G. A. Tsekouras, A. Provata, and C. Tsallis, "Nonextensivity of the cyclic lattice Lotka-Volterra model," *Physical Review E*, vol. 69, no. 1, 2004.

[41] W. Li, Q. A. Wang, L. Nivanen, and A. le Méhauté, "On different q-systems in nonextensive thermostatistics," *The European Physical Journal B*, vol. 48, no. 1, pp. 95–100, 2005.

[42] S. Abe, "Temperature of nonextensive systems: Tsallis entropy as Clausius entropy," *Physica A: Statistical Mechanics and its Applications*, vol. 368, no. 2, pp. 430–434, 2006.

[43] T. S. Biro and P. Van, "Publisher's note: zeroth law compatibility of nonadditive thermodynamics," *Physical Review E*, vol. 84, no. 1, 2011.

[44] N. Farvardin and F. Y. Lin, "Performance of entropy-constrained block transform quantizers," *IEEE Transactions on Information Theory*, vol. 37, no. 5, pp. 1433–1439, 1991.

[45] E. T. Jaynes, "Gibbs vs Boltzmann entropies," *American Journal of Physics*, vol. 33, no. 5, pp. 391–398, 1965.

[46] H. Moradpour, C. Corda, A. H. Ziaie, and S. Ghaffari, "The extended uncertainty principle inspires the Rényi entropy," *EPL (Europhysics Letters)*, vol. 127, no. 6, p. 60006, 2019.

[47] K. Mejrhit and S.-E. Ennadifi, "Thermodynamics, stability and Hawking-Page transition of black holes from non- extensive statistical mechanics in quantum geometry," *Physics Letters B*, vol. 794, pp. 45–49, 2019.

[48] A. Sayahian Jahromi, S. A. Moosavi, H. Moradpour et al., "Generalized entropy formalism and a new holographic dark energy model," *Physics Letters B*, vol. 780, pp. 21–24, 2018.

[49] L. Amendola, "Scaling solutions in general nonminimal coupling theories," *Physical Review D*, vol. 60, no. 4, 1999.

[50] L. Amendola, "Coupled quintessence," *Physical Review D*, vol. 62, no. 4, 2000.

[51] B. Wang, Y. Gong, and E. Abdalla, "Transition of the dark energy equation of state in an interacting holographic dark energy model," *Physics Letters B*, vol. 624, no. 3-4, pp. 141–146, 2005.

[52] Z. K. Guo, N. Ohta, and S. Tsujikawa, "Probing the coupling between dark components of the universe," *Physical Review D*, vol. 76, p. 023508, 2007.

[53] M. Khurshudyan and R. Myrzakulov, "Phase space analysis of some interacting Chaplygin gas models," *European Physical Journal C: Particles and Fields*, vol. 77, no. 2, p. 65, 2017.

[54] E. Sadri, M. Khurshudyan, and D. F. Zeng, "Scrutinizing various phenomenological interactions in the context of holographic Ricci dark energy models," *European Physical Journal C: Particles and Fields*, vol. 80, no. 5, p. 393, 2020.

[55] A. Jawad, S. Butt, S. Rani, and K. Asif, "Cosmological aspects of sound speed parameterizations in fractal universe," *The European Physical Journal C*, vol. 79, no. 11, p. 926, 2019.

[56] V. K. Oikonomou, 2020, https://arxiv.org/abs/2012.000586v1.

[57] S. Ali, S. Khan, and S. Sattar, 2020, https://arxiv.org/abs/2011.10046v1.

[58] A. A. Mamon, A. H. Ziaie, and K. Bamba, "A generalized interacting Tsallis holographic dark energy model and its thermodynamic implications," *European Physical Journal C: Particles and Fields*, vol. 80, no. 10, p. 974, 2020.

[59] A. Jawad, Z. Khan, and S. Rani, "Cosmological and thermodynamics analysis in Weyl gravity," *The European Physical Journal C*, vol. 80, no. 1, p. 71, 2020.

[60] U. Debnath, "Constructions of $f(R, G, \mathcal{T})$ gravity from some expansions of the universe," *International Journal of Modern Physics A*, vol. 35, no. 31, p. 2050203, 2020.

[61] A. Jawad, S. Rani, S. Saleem, K. Bamba, and R. Jabeen, "Cosmological consequences of a parametrized equation of state," *Symmetry*, vol. 11, no. 8, p. 1009, 2019.

[62] N. Aghanim, Y. Akrami, M. Ashdown et al., "Planck 2018 results-VI. Cosmological parameters," *Astronomy and Astrophysics*, vol. 641, p. A6, 2020.

Hindawi
Advances in High Energy Physics
Volume 2021, Article ID 6643546, 7 pages
https://doi.org/10.1155/2021/6643546

Research Article

Multiscale Entropy Analysis of Gravitational Waves

Mohsen Javaherian [1] **and Saeid Mollaei** [2]

[1]*Research Institute for Astronomy and Astrophysics of Maragha (RIAAM), University of Maragheh, P.O. Box: 55136-553, Maragheh, Iran*
[2]*Department of Physics, University of Zanjan, P.O. Box: 45196-313, Zanjan, Iran*

Correspondence should be addressed to Mohsen Javaherian; m_javaherian@znu.ac.ir

Received 4 December 2020; Revised 17 January 2021; Accepted 22 February 2021; Published 8 March 2021

Academic Editor: Enrico Lunghi

The first gravitational-wave (GW) signal was detected in the year 2015 indicating tiny distortions of spacetime caused by accelerated masses. We focused on the GW signals consisting of a peak GW strain of 1.0×10^{-21} that shows merging pairs of large masses. We applied the generalized entropy known as multiscale entropy to the GW interval time series recorded by different observatories (H1, L1, and V1). This enables us to investigate the behavior of entropies on different scales as a method of studying complexity and organization. We found that the entropies of GW interval data with similar physical properties make the identical manner in different scales. Moreover, the results reveal that the signals collected by each observatory have approximately a similar trend in the multiscale analysis results. According to our findings, although different signals have different values for short-range correlations, the long-range correlations are not noticeable in most of them.

1. Introduction

Gravitational-wave (GW) signals, firstly predicted by Albert Einstein in 1916, are known as transverse waves of spatial strain with very small amplitudes which travel at the speed of light [1, 2]. After linearizing weak-field equations, Sitzungsber found a solution for the field equations [3], and then, Kerr generalized the solution for the rotating black holes [4]. Lots of theoretical works in the purification of analytical studies of relativistic two-body dynamics were done [5, 6]. Moreover, since the signals of GW merger are accompanied with electromagnetic emission as a gamma-ray burst [7–9], the field of numerical-relativity simulations progressed, and in the later step, it led to advances in GW modeling of two massive binary mergers (e.g., see [10–14]).

In the last decade, the GW signals are detected by the networks of the Virgo [15] and LIGO [16] interferometers. The first observation of GWs, which was appeared as a transient GW signal, indicated a binary black hole merger [17]. For other detections of GW mergers, the reader can refer to [18, 19] and references therein. Since the GW sources can be categorized in one of the three classes of transient and bursts, periodic or continuous wave, and stochastic, the type of method for analyzing GW data seems to be important [20]. GWs are very weak signals of order 10^{-21} or even less that travel in spacetime containing noises of order 10^{-18}. So, it is not possible to study this kind of signal using methods that are prevalent in statistics.

Using the Hurst exponent is one of the proposed ways to discriminate stochastic (irregular) time series and signals with long-range interaction within system components (self-affinity) which was firstly proposed by Hurst in 1951 [21, 22]. In this approach, for a time series $[y_t]$, a self-affinity of different parts of a signal can be explained by $y_{\alpha t} = \alpha^{-H} y_t$, wherein α and H are a positive coefficient and the Hurst exponent, respectively (e.g., see [23]). The range of (0.5,1) for the Hurst exponent determines that there would be long-term memory in the system of interest. Among lots of methods for estimation of the Hurst exponent such as the analyses of detrended fluctuation [24], rescale range (e.g., [25]), and wavelet method [26], using the concept of entropy enables us to issue solid results about the complexity of a system and give a quantitative interpretation of long-term memory in the system [27]. The multiscale entropy

Table 1: The list of GW data.

Name	Version	Mass 1 ($M_\odot$)	Mass 2 ($M_\odot$)	Network SNR	Distance (Mpc)	Strains
GW150914	v3	$35.6^{+4.7}_{-3.1}$	$30.6^{+3.0}_{-4.4}$	24.4	440^{+150}_{-170}	H1 & L1
GW151012	v3	$23.2^{+14.9}_{-5.5}$	$13.6^{+4.1}_{-4.8}$	10.0	1080^{+550}_{-490}	H1 & L1
GW151226	v2	$13.7^{+8.8}_{-3.2}$	$7.7^{+2.2}_{-2.5}$	13.1	450^{+180}_{-190}	H1 & L1
GW170104	v2	$30.8^{+7.3}_{-5.6}$	$20.0^{+4.9}_{-4.6}$	13	990^{+440}_{-430}	H1 & L1
GW170608	v3	$11.0^{+5.5}_{-1.7}$	$7.6^{+1.4}_{-2.2}$	14.9	320^{+120}_{-110}	H1 & L1
GW170729	v1	$50.2^{+16.2}_{-10.2}$	$34.0^{+9.1}_{-10.1}$	10.2	2840^{+1400}_{-1360}	H1, L1 & V1
GW170809	v1	$35.0^{+8.3}_{-5.9}$	$23.8^{+5.1}_{-5.2}$	12.4	1030^{+320}_{-390}	H1, L1 & V1
GW170814	v3	$30.6^{+5.6}_{-3.0}$	$25.2^{+2.8}_{-4.0}$	15.9	600^{+150}_{-220}	H1, L1 & V1
GW170817	v3	$1.46^{+0.12}_{-0.10}$	$1.27^{+0.09}_{-0.09}$	33	40^{+7}_{-15}	H1, L1 & V1
GW170818	v1	$35.4^{+7.5}_{-4.7}$	$26.7^{+4.3}_{-5.2}$	11.3	1060^{+420}_{-380}	H1, L1 & V1
GW170823	v1	$39.5^{+11.2}_{-6.7}$	$29.0^{+6.7}_{-7.8}$	11.5	1940^{+970}_{-900}	H1 & L1
GW190412	v2	$30.1^{+4.6}_{-5.3}$	$8.3^{+1.6}_{-0.9}$	$19.0^{+0.2}_{-0.3}$	740^{+130}_{-160}	H1, L1 & V1
GW190425	v1	$1.74^{+0.17}_{-0.09}$	$1.56^{+0.08}_{-0.14}$	$12.46^{+0.29}_{-0.43}$	159^{+69}_{-72}	L1 & V1
GW190521	v2	85^{+21}_{-14}	66^{+17}_{-18}	$14.6^{+0.4}_{-0.4}$	5300^{+2400}_{-2600}	H1, L1 & V1
GW190814	v1	$23.2^{+1.1}_{-1.0}$	$2.59^{+0.08}_{-0.09}$	$25.0^{+0.1}_{-0.2}$	241^{+41}_{-45}	H1, L1 & V1

(MSE) is firstly introduced in a paper for analyzing the complexity of physiologic time series [28], and then, it was broadly used in biological signals such as characterizing the complexity of human heartbeat [29, 30]. For a review of other improvements about the MSE estimation, the reader can refer to [31].

Here, we applied the MSE to GW binary mergers to investigate the entropy level of signals in different scales. To do this, we employed the GW signals of events detected by different observatories. It may help to characterize the GW signals. This paper is organized as follows: the employed data sets are described in Section 2. Section 3 is devoted to briefly explaining the method. The results are discussed in Section 4. The concluding remarks are given in Section 5.

Table 2: The list of GWTC-1-marginal data.

Name	Version	Mass 1 ($M_\odot$)	Mass 2 ($M_\odot$)	Network SNR	Distance (Mpc)	Strains
170208	v1	–	–	10.0	–	H1 & L1
170219	v1	–	–	9.6	–	H1 & L1
170405	v1	–	–	9.3	–	H1 & L1
170412	v1	–	–	9.7	–	H1 & L1
170423	v1	–	–	8.9	–	H1 & L1

2. Description of Data Sets

The networks of the Virgo interferometers in Cascina, Italy, [15] and the Laser Interferometer Gravitational-wave Observatory [LIGO: [16] including two branches in Hanford, Washington, USA (LHO), and Livingstone, Louisiana, USA (LLO), with the arms of 4 km record the received GW signals]. Recorded data are strains ($\Delta L/L$) of the arms, caused by gravitational waves; so, they are dimensionless. The data published by the Virgo observatory is labeled "V1," and the two branches of LIGO detectors are known as "H1" and "L1," respectively. We employed the GW time series (https://www.gw-openscience.org/data/) with the sampling rate of 16 KHz during the period of 32 seconds (the time of recording data). The employed data sets are categorized into two groups. In the first group, the physical properties of triggered events such as masses and distances of binaries have been found. We selected all confirmed GW data consisting of 15 time series of compact binary mergers recorded by different observatories. The second group is marginal triggers observed by LIGO and Virgo discovered by the advanced interferometric GW detector network. This network can detect frequencies in the range of 15 Hz up to a few kilohertz belonging to inspiral, merger, and ringdown GW signals of compact binary mergers (for more information about this type of data set and some technical details, the reader can refer to [32]). They are listed in the GW transient catalog and are known as "GWTC-1-marginal." We selected 5 times series of this type of GW data. Details of the first and the second groups of the GW data are given in Tables 1 and 2, respectively (also, the extended reviews about the Advanced LIGO and Advanced Virgo data sets are given in [33]). Both groups of data sets are named by the date of observations with a difference that the names of the first group have the

prefix "GW." For instance, the series "GW190425" belongs to the first group and was recorded on 25 April 2019.

For a given data set $B_H(t)$ (a time series with a Hurst exponent of H), we can produce a data set from its increments as $G_H(t) = \Delta B_H(t) = B_H(t + \Delta t) - B_H(t)$, which is known as interval data set. Our measurements show that the $G_H(t)$ constructed from GW time series (listed in Tables 1 and 2) has Gaussian distribution. Also, their Hurst exponents are ranged from 0.61 to 0.89 (extracted by the R/S method) led to categorize GW interval signals in the class of the fractional Gaussian noises. We apply multiscale entropy to GW interval data sets as explained in Section 3.

3. Multiscale Entropy Analysis

The time series of a system can be influenced by noises rooted in the interaction between the system and its environment. Inducing noise can accumulate short-range correlations in time series that may lead to a nonoriginal long-range effect. So, reducing the effect of undesirable noises and short-range correlations from time series seems to be essential. This task is accomplished by using the coarse-graining procedure. To do this, the time series of length N with data points y_1, $y_2, \cdots, y_N$ is partitioned into nonoverlapping windows with the same length λ. Averaging on data points over each window provides the coarse-grained signal as the following form

$$y_p^{(\lambda)} = \frac{1}{\lambda} \Sigma_{q=1}^{\lambda} y_{(p-1)\lambda+q}. \tag{1}$$

The new sequence with data points $(y_1^{(\lambda)}, \cdots, y_{N/\lambda}^{(\lambda)})$ is obtained, wherein λ is known as scale factor. The late signal can be determined by the m-dimensional vectors as follows:

$$Y_m^{(\lambda)}(p) = \left(y_p^{\lambda}, \cdots, y_{p+m-1}^{\lambda}\right). \tag{2}$$

In this step, the number of vector pairs with distances less than r is counted. This set of pairs is denoted by $n_m(r, \lambda)$. The task of finding the pairs set is repeated for the $(m+1)$ -dimensional vector pairs $n_{m+1}(r, \lambda)$. The sample entropy is given by

$$S_E(m, r, \lambda) = -\log\left(\frac{n_{m+1}(r, \lambda)}{n_m(r, \lambda)}\right). \tag{3}$$

Since $n_{m+1}(r, \lambda) \leq n_m(r, \lambda)$, then $S_E \geq 0$. The diagram of sample entropy versus scale factor can be representative of the range of correlations. The whole process is named the multiscale entropy (MSE) analysis [27].

4. Results and Discussions

We plotted the sample entropy of GW interval data for different scale factors. To do this, 15 GW signals received from binary mergers with some discovered physical properties and 5 marginal triggers (GWTC-1-marginal data) with indeterminate parameters of sources were chosen to generate interval data. The results of MSE analysis for binary mergers

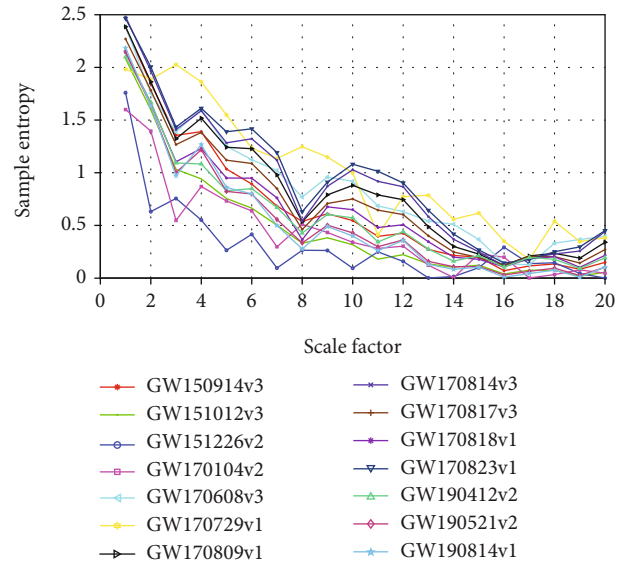

Figure 1: MSE analysis of the GW interval data recorded by H1 observatory.

recorded by observatories H1, L1, and V1 are shown in Figures 1–3, respectively.

As we see in Figure 1, approximately all graphs have analogous trends, and despite consecutive peaks and valleys, they all exhibit a decrement of sample entropy toward values below 0.5. In scale 8, a valley can be seen for most of the graphs except for four of them. Also, there is a progressing convergence reaching its maximum value in the range [16, 17] which is the other noticeable case in Figure 1. In Figure 2, the decreasing trend is repeated with a less obvious convergence between graphs. One can see that the MSE analysis for the last six recorded data has very close and similar trends. There is a valley in scale 16 for all graphs, and then, the first four recorded data begin to show a divergent manner gradually. In Figure 3, alongside the decrement of all trends toward zero, a duality can be seen among the graphs. Both groups of the graphs show consecutive peaks and valleys, but it is obvious that the entropy behavior of the last four recorded data is different from the others' trend, and the trends of the two groups of graphs follow the decline trends completely out of phase after scale 11.

In the same manner, as explained above, the results for interval data generated from marginal triggers recorded by observatories H1 and L1 are displayed in Figures 4 and 5, respectively. For the two last interval data generated from GWTC-1-marginal H1 data discovered in April 2017, it is seen that the sample entropies show the same behavior while the others' trends exhibit gradual declines through all scales. The results for GWTC-1-marginal L1 data (except for the signal taken on 8 February 2017 that is the first recoded data) show similar falling trends in MSE graphs with fewer peaks and valleys in comparing with the results of GWTC-1-marginal H1. For all the graphs of 15 GW signals and 5 marginal triggers that monotonically decrease, the best model can be obtained by fitting a q-exponential function, $f(x) = A[1 - B(q-1)x]^{1/1-q}$, wherein A, B, and q are constant values.

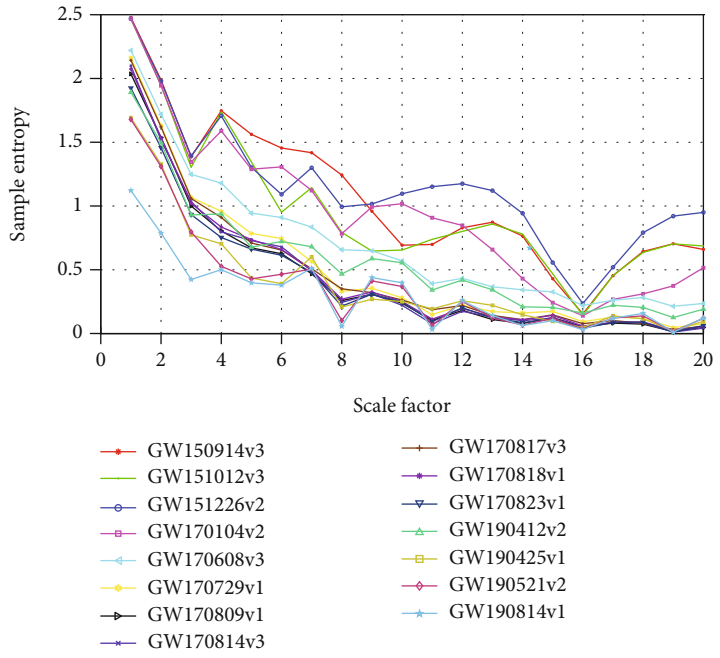

Figure 2: MSE analysis of the GW interval data recorded by L1 observatory.

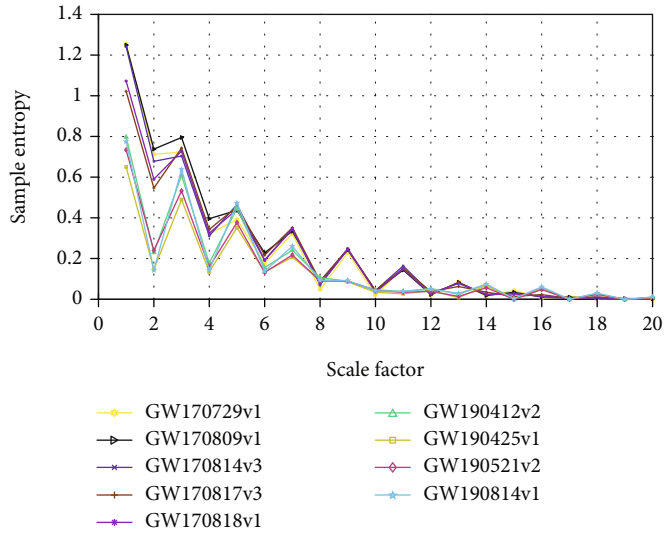

Figure 3: MSE analysis of the GW interval data recorded by V1 observatory.

To know whether there is any relation between the physical parameters of GW data and behavior of sample entropy for their corresponding interval data in different scales, we focused on masses, distances, and network SNR of binary mergers. First of all, we compared the entropies of two GW interval data with comparable characteristics in different scales. As we see in Table 1, both the GW170809 (with mass 1 $\approx$35.0 $M_\odot$, mass 2 $\approx$23.8 $M_\odot$, distance $\approx$1030 Mpc, and network SNR $\approx$12.4) and the GW170818 (with mass 1 $\approx$35.4 $M_\odot$, mass 2 $\approx$26.7 $M_\odot$, distance $\approx$1060 Mpc, and network SNR $\approx$11.3) have approximately the analogous properties. Their entropy trends are very similar in different scales recorded by H1 (Figure 1), L1 (Figure 2), and V1 (Figure 3). Then, we focused on two GW time series with different physical properties. As it is seen in Table 1, the mergers of GW190521 data are more massive (mass 1 $\approx$85 $M_\odot$ and mass 2 66 $M_\odot$) than the others, and also, the distance of the mergers from detectors is significant ($\approx$5300 Mpc). On the other hand, the GW170817 mergers have the lowest masses (mass 1 $\approx$1.46 $M_\odot$ and mass 2 $\approx$1.27 $M_\odot$) and are placed in a shorter distance than the other mergers ($\approx$40 Mpc). Let us make a comparison between the entropy diagrams of mergers of the GW190521 with SNR $\approx$14.6 and the GW170817 with SNR $\approx$33. A closer look at results extracted from data recorded by H1 (Figure 1) shows that both approximately have similar trends with in an in-phase manner. However, the values of sample entropy for GW170817 are higher than that of GW190521 in all scales. In Figure 2, we

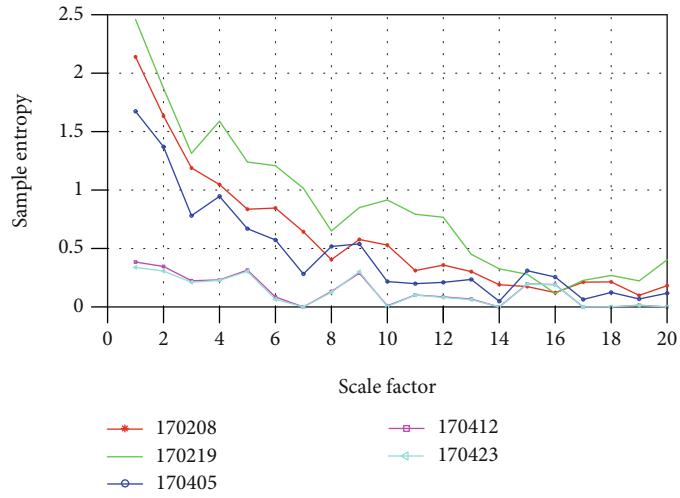

Figure 4: MSE analysis of the GWTC-1-marginal interval data recorded by H1 observatory.

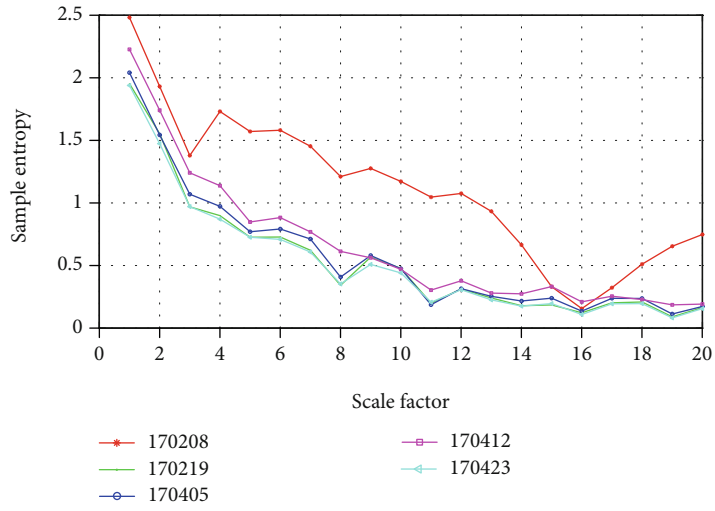

Figure 5: MSE analysis of the GWTC-1-marginal interval data recorded by L1 observatory.

see the same trends for both data. The MSE diagram of GW190521 has more fluctuations than that of obtained for GW170817, and it takes the greater values at some scales. We see in Figure 3 that rises and falls of both data are very similar up to scale 10; after that, although both approximately have the analogous slopes, the fluctuation of GW190521 data is more. In the GWTC-1-marginal data set, the only recorded property is network SNR that is approximately comparable for 170219 (network SNR ≈9.6) and 170412 (network SNR ≈9.7) signals. The MSE diagrams of the 170219 and 170412 interval data sets recorded by H1 show that their entropy behaviors are completely different. The sample entropy of 170412 data takes the value zero in some scales, while the minimum value of 170219 data (≈0.21) is in the scale 16. On the other hand, for the data recorded by L1, the entropy behaviors are similar. Hence, we can say that the network SNR does not play a key role in determining the entropy behaviors of the GW signals.

5. Conclusions

In this study, we first generated interval data sets from GW data and measured their Hurst exponent using R/S analysis. Our measurements show that the interval data have the Hurst exponents ranged from 0.61 to 0.89. We applied MSE analysis as a method of investigating complexity and organization in time series, on two groups of interval data generated from GW data recorded by different observatories (Virgo and LIGO). We found that the GW interval signals with similar sources represent analogous behaviors in different scales. Focusing on entropy diagrams of GWTC-1-marginal interval data with about the same network SNR demonstrates that the entropy behaviors of the GW interval time series cannot relate to the network SNRs of observatories. Moreover, the entropy-scale diagrams show that the entropy behaviors of the GW interval data are analogous for each observatory which may return to the characteristics

of each observatory depended on input noises, noise reduction methods, and/or the orientation of the received GW signals. All of the multiscale entropy analysis results for corresponding interval data recorded by H1, L1, and V1 show a decreasing trend with some degrees of convergence. The diversity of the entropy in small scales implies that the signals have different values of short-range correlations. By increasing the scale factor, the effects of short-range correlations are excluded from signals. The declining trend of entropy indicates that the long-term correlations cannot have an effective influence on the system. The observed convergence in the MSE graphs, especially during the last scale factors, can be interpreted as the existence of similarity between all the GW interval time series in lack of long-range correlations. It suggests that this type of GW signal should be categorized in the class of systems with a low level of complexity.

Data Availability

We employed the GW time series with a sampling rate of 16 KHz during the period of 32 seconds (the time of recording data). The link of used data sets is as follows: https://www.gw-openscience.org/data/.

Conflicts of Interest

The authors declare that they have no conflicts of interest.

Acknowledgments

This research has made use of data, software, and/or web tools obtained from the Gravitational Wave Open Science Center (https://www.gw-openscience.org/), a service of LIGO Laboratory, the LIGO Scientific Collaboration, and the Virgo Collaboration. LIGO Laboratory and Advanced LIGO are funded by the United States National Science Foundation (NSF) as well as the Science and Technology Facilities Council (STFC) of the United Kingdom, the Max-Planck-Society (MPS), and the State of Niedersachsen/Germany for support of the construction of Advanced LIGO and construction and operation of the GEO600 detector. Additional support for Advanced LIGO was provided by the Australian Research Council. Virgo is funded, through the European Gravitational Observatory (EGO), by the French Centre National de Recherche Scientifique (CNRS), the Italian Istituto Nazionale di Fisica Nucleare (INFN), and the Dutch Nikhef, with contributions by institutions from Belgium, Germany, Greece, Hungary, Ireland, Japan, Monaco, Poland, Portugal, and Spain. Also, the authors thank K. Derakhshani and Professor Amir H. Darooneh for helpful discussions.

References

[1] A. Einstein, "Erklarung der perihelionbewegung der Merkur aus der allgemeinen relativitatstheorie," *Sitzungsberichte der Königlich Preussischen Akademie der Wissenschaften*, vol. 47, pp. 831–839, 1915.

[2] A. Einstein, "Über gravitationswellen," *Sitzungsberichte der Königlich Preussischen Akademie der Wissenschaften*, vol. 1, p. 154, 1918.

[3] K. Schwarzschild, "Über das Gravitationsfeld eines Massenpunktes nach der Einsteinschen Theorie," *Sitzungsberichte der Königlich Preussischen Akademie der Wissenschaften*, vol. 1, p. 189, 1916.

[4] R. P. Kerr, "Gravitational field of a spinning mass as an example of algebraically special metrics," *Physical Review Letters*, vol. 11, no. 5, pp. 237-238, 1963.

[5] A. Buonanno and T. Damour, "Effective one-body approach to general relativistic two-body dynamics," *Physical Review D*, vol. 59, no. 8, article 084006, 1999.

[6] L. Blanchet, "Gravitational radiation from post-Newtonian sources and inspiralling compact binaries," *Living Reviews in Relativity*, vol. 17, no. 1, p. 2, 2014.

[7] R. Narayan, B. Paczynski, and T. Piran, "Gamma-ray bursts as the death throes of massive binary stars," *The Astrophysical Journal Letters*, vol. 395, p. L83, 1992.

[8] A. Goldstein, P. Veres, E. Burns et al., "An ordinary short gamma-ray burst with extraordinary implications: Fermi-GBM detection of GRB 170817a," *The Astrophysical Journal*, vol. 848, no. 2, p. L14, 2017.

[9] B. P. Abbott, R. Abbott, T. D. Abbott et al., "Gravitational waves and gamma-rays from a binary neutron star merger: GW170817 and GRB 170817a," *The Astrophysical Journal*, vol. 848, no. 2, p. L13, 2017.

[10] F. Pretorius, "Evolution of binary black-hole spacetimes," *Physical Review Letters*, vol. 95, no. 12, p. 121101, 2005.

[11] M. A. Aloy, H. T. Janka, and E. Müller, "Relativistic outflows from remnants of compact object mergers and their viability for short gamma-ray bursts," *Astronomy & Astrophysics*, vol. 436, no. 1, pp. 273–311, 2005.

[12] M. Campanelli, C. O. Lousto, P. Marronetti, and Y. Zlochower, "Accurate evolutions of orbiting black-hole binaries without excision," *Physical Review Letters*, vol. 96, no. 11, p. 111101, 2006.

[13] J. G. Baker, J. Centrella, D.-I. Choi, M. Koppitz, and J. van Meter, "Gravitational-wave extraction from an inspiraling configuration of merging black holes," *Physical Review Letters*, vol. 96, no. 11, p. 111102, 2006.

[14] K. Kiuchi, Y. Sekiguchi, K. Kyutoku, M. Shibata, K. Taniguchi, and T. Wada, "High resolution magnetohydrodynamic simulation of black hole-neutron star merger: mass ejection and short gamma ray bursts," *Physical Review D*, vol. 92, no. 6, article 064034, 2015.

[15] F. Acernese, M. Agathos, K. Agatsuma et al., "Advanced Virgo: a second-generation interferometric gravitational wave detector," *Classical and Quantum Gravity*, vol. 32, no. 2, p. 024001, 2015.

[16] The LIGO Scientific Collaboration, J. Aasi, B. P. Abbott et al., "Advanced LIGO," *Classical and Quantum Gravity*, vol. 32, no. 7, article 074001, 2015.

[17] B. P. Abbott, R. Abbott, T. D. Abbott et al., "Observation of gravitational waves from a binary black hole merger," *Physical Review Letters*, vol. 116, no. 6, article 061102, 2016.

[18] R. Abbott, T. D. Abbott, S. Abraham et al., "Gw190412: observation of a binary-black-hole coalescence with asymmetric masses," *Physical Review D*, vol. 102, no. 4, article 043015, 2020.

[19] R. Abbott, T. D. Abbott, S. Abraham et al., "Gw190521: a binary black hole merger with a total mass of150 M⊙," *Physical Review Letters*, vol. 125, no. 10, p. 101102, 2020.

[20] S. V. Dhurandhar, "Data analysis techniques for gravitational wave observations," *Pramana*, vol. 63, no. 4, pp. 717–730, 2004.

[21] H. E. Hurst, "Long-term storage of reservoirs: an experimental study," *Transactions of the American Society of Civil Engineers*, vol. 116, pp. 770–799, 1951.

[22] H. E. Hurst, R. P. Black, and Y. M. Simaika, *Long-term storage: an experimental study*, H. E. Hurst, R. P. Black, and Y. M. Simaika, Eds., Constable London, 1965.

[23] M. Javaherian, H. Safari, N. Dadashi, and M. J. Aschwanden, "Statistical properties of photospheric magnetic elements observed by the helioseismic and magnetic imager onboard the Solar Dynamics Observatory," *Solar Physics*, vol. 292, no. 11, p. 164, 2017.

[24] C.-K. Peng, S. V. Buldyrev, S. Havlin, M. Simons, H. E. Stanley, and A. L. Goldberger, "Mosaic organization of DNA nucleotides," *Physical Review E*, vol. 49, no. 2, pp. 1685–1689, 1994.

[25] W. D. Pesnell, "Solar cycle predictions (invited review)," *Solar Physics*, vol. 281, no. 1, pp. 507–532, 2012.

[26] C. L. Jones, G. T. Lonergan, and D. E. Mainwaring, "Wavelet packet computation of the hurst exponent," *Journal of Physics A: Mathematical and General*, vol. 29, no. 10, pp. 2509–2527, 1996.

[27] S. Mollaei, A. H. Darooneh, and S. Karimi, "Multi-scale entropy analysis and Hurst exponent," *Physica A: Statistical Mechanics and its Applications*, vol. 528, p. 121292, 2019.

[28] M. Costa, A. L. Goldberger, and C.-K. Peng, "Multiscale entropy analysis of complex physiologic time series," *Physical Review Letters*, vol. 89, no. 6, article 068102, 2002.

[29] M. Costa, A. L. Goldberger, and C.-K. Peng, "Multiscale entropy analysis of biological signals," *Physical Review E*, vol. 71, no. 2, article 021906, 2005.

[30] M. Costa and A. Goldberger, "Generalized multiscale entropy analysis: application to quantifying the complex volatility of human heartbeat time series," *Entropy*, vol. 17, no. 3, pp. 1197–1203, 2015.

[31] A. Humeau-Heurtier, "The multiscale entropy algorithm and its variants: a review," *Entropy*, vol. 17, no. 5, pp. 3110–3123, 2015.

[32] B. P. Abbott, R. Abbott, T. D. Abbott et al., "Gwtc-1: a gravitational-wave transient catalog of compact binary mergers observed by LIGO and Virgo during the first and second observing runs," *Physical Review X*, vol. 9, no. 3, article 031040, 2019.

[33] R. Abbott, T. Abbott, S. Abraham et al., "Open data from the first and second observing runs of Advanced LIGO and Advanced Virgo," *SoftwareX*, vol. 13, article 100658, 2021.

Hindawi
Advances in High Energy Physics
Volume 2021, Article ID 6658862, 17 pages
https://doi.org/10.1155/2021/6658862

Research Article

Interacting Rényi Holographic Dark Energy in the Brans-Dicke Theory

Vipin Chandra Dubey,[1] **Umesh Kumar Sharma**,[1] **and Abdulla Al Mamon**[2]

[1]*Department of Mathematics, Institute of Applied Sciences and Humanities, GLA University, Mathura, 281 406 Uttar Pradesh, India*
[2]*Department of Physics, Vivekananda Satavarshiki Mahavidyalaya (Affiliated to the Vidyasagar University), Manikpara, 721513 West Bengal, India*

Correspondence should be addressed to Umesh Kumar Sharma; sharma.umesh@gla.ac.in

Received 29 November 2020; Revised 31 January 2021; Accepted 11 February 2021; Published 3 March 2021

Academic Editor: Hooman Moradpour

In this work, we construct an interacting model of the Rényi holographic dark energy in the Brans-Dicke theory of gravity using Rényi entropy in a spatially flat Friedmann-Lemaître-Robertson-Walker Universe considering the infrared cut-off as the Hubble horizon. In this setup, we then study the evolutionary history of some important cosmological parameters, in particular, deceleration parameter, Hubble parameter, equation of state parameter, and Rényi holographic dark energy density parameter in both nonflat Universe and flat Universe scenarios and also observe satisfactory behaviors of these parameters in the model. We find that during the evolution, the present model can give rise to a late-time accelerated expansion phase for the Universe preceded by a decelerated expansion phase for both flat and nonflat cases. Moreover, we obtain $\omega_D \to -1$ as $z \to -1$, which indicates that this model behaves like the cosmological constant at the future. The stability analysis for the distinct estimations of the Rényi parameter δ and coupling coefficient b^2 has been analyzed. The results indicate that the model is stable at the late time.

1. Introduction

The Virial theorem (1930s) which provided the Coma galaxy cluster mass [1, 2], accompanied by the galaxy rotation curve study (1970) [3] and the two different research groups' observational results in the 1990s [4, 5], has uncovered one of the most interesting issues of cosmology at present: the dark sector. It is suggested by the researchers that the five percent of the present energy content of the cosmos is composed of the radiation and the ordinary matter (baryons); the remaining ninety-five percent is dominated by this dark component to clarify the late accelerated expansion of the Universe. It is believed that this dark sector of the Universe mainly includes two constituents: *dark energy* (DE) and *dark matter* (DM). Both are important and significant to understand the phenomena of scales and nature. The significance of DM lies primarily in the structure formation, for instance, to permit baryonic structures to become nonlinear in the wake of decoupling from the photons. Interestingly, dark energy is the subject of study to answer the late-time accelerated expansion for the observable Universe [6]. Also, the DM is narrated as *cold dark matter* (CDM), and dark energy is portrayed by the *cosmological constant* (Λ) in the standard cosmological scenario. The dark component of the Universe with radiation and baryons combined the ΛCDM model. Also, despite the fact that the ΛCDM model appreciates an impressive observational achievement [7–9], there are still a number of hypothetical and observational focuses that have the right to be completely researched [10]. The greatest test lies in understanding the crucial idea of these dark sectors from the theoretical perspective [6]. In 2004, Li [11] proposed the idea of *holographic dark energy* (HDE) which is also used to explain the DE scenario to explain the late-time accelerated expansion of the Universe inspired by the holographic principle [12–18]. Right after a paper by Li, the most complete generalization which includes all known HDE models were suggested [19]. Furthermore, it is shown that the Nojiri-Odintsov HDE describes also covariant theories unlike Li's HDE [20].

Recently, inspired by the holographic principle and using the Rényi entropy [21], a new dark energy model has been proposed by Moradpour et al. [22] named the *Rényi holographic dark energy* (RHDE) model for the cosmological and gravitational investigations. Generalizing one of the entropy or gravity, as entropy-area connection relies on the gravity hypothesis, will change the corresponding one. It is proposed that by using the Rényi entropy, the modified Friedmann equations can be obtained [23–25]. Ghaffari et al. [26] proposed that inflation may be found in the Rényi formalism. The RHDE models have been explored with IR cut-off as the particle and future event horizons [27]. The spatially homogeneous and anisotropic Bianchi VI_0 Universe filled with RHDE with Granda-Oliveros and Hubble horizons as the IR cut-off has been investigated in general relativity [28]. Recently, Sharma et al. [29, 30] discriminated the RHDE model from the ΛCDM model by using different diagnostic tools such as statefinder diagnostic and statefinder hierarchy in ample details. Also, the RHDE model has been compared with the holographic and Tsallis holographic dark energy through the statefinder diagnostic tool [31].

Indeed, all the above attempts claim that, at least mathematically, the DE density profile introduced under the shadow of the RHDE hypothesis has considerable potential for modelling the DE behavior, and thus, more studies on this density profile are motivated. Further, at large scales, the models presenting interaction fare well when confronted with observational outcomes from the CMB [32] and matter distribution [33]. Therefore, the interaction between DE and DM must be handled seriously. Then again, there exist limits for the quality of this association for different setups [34–48]. This newly proposed Rényi HDE has also been examined by many researchers by considering the interaction between DE and DM to explain the accelerated expansion of the Universe with different IR cut-offs in general relativity, braneworld, loop quantum cosmology, and modified gravity [49–52]. Sharma and Dubey [53] investigated the Rényi HDE model in the Friedmann-Lemaître-Robertson-Walker (FLRW) Universe considering different parametrizations of the interaction between the DM and DE.

On the other side, the modified gravity theories have been broadly applied in cosmology [54–56]. The modified theories of gravity are not new and have a long history. A well-known modified gravity theory, the Brans-Dicke gravity [57], is also a choice to general relativity to explain the accelerated expansion of the cosmos [58] and also can pass the experimental tests from the solar system [59]. Theoretically, the value of the Brans-Dicke coupling parameter has a smaller value than observed by the observational data, which encouraged physicists to suggest various DE scenarios to describe the present cosmos in the Brans-Dicke formalism [58–60]. Using the holographic principle, Gong [61] investigated the holographic bound in the Jordan and Einstein frames to the Brans-Dicke gravity, and for larger ω, the similar results were proposed as those in general relativity. The similar problem was studied in [62], by considering Bianchi identity as a consistency condition. For the IR cut-off as a future event horizon, the importance of Brans-Dicke gravity for the dust matter and the HDE has been explored in [63]. It is proposed that with the Hubble radius as infrared cut-off, the standard HDE may not produce the accelerated expansion Universe in the Brans-Dicke gravity, but the suitable description of the Universe can be obtained by taking the IR cut-off as a future event horizon [64]. Therefore, many other works proposed that the Brans-Dicke gravity is suitable for the examination in the holographic dark energy scenario [65–71]. Observational constraints also have been proposed for a sign-changeable interaction among the Universe sectors [72–74]. Considering different IR cut-offs, the noninteracting and interacting Tsallis HDE and their cosmological consequences are explored in the Brans-Dicke theory [75–77].

Very recently, the authors constructed the noninteracting RHDE model in the Brans-Dicke theory taking the Hubble horizon as the IR cut-off [78]. While in this work, we propose the interacting RHDE model in the framework of the Brans-Dicke theory in both flat and nonflat Universes. The paper is organized as follows: we explored the interacting RHDE model and physical parameters in the Brans-Dicke theory in Section 2. We study the stability of the RHDE model in Section 3. The conclusion is given in the last section.

Throughout the text, an "overdot" represents a derivative with respect to cosmic time.

2. Interacting Rényi Holographic Dark Energy in the Brans-Dicke Theory

We consider a homogeneous and isotropic FLRW Universe which is described by the line element

$$ds^2 = dt^2 - a^2(t)\left(\frac{dr^2}{1-kr^2} + r^2 d\theta^2 + r^2 \sin^2\theta d\phi^2\right), \quad (1)$$

where $a(t)$ is the scale factor of the Universe, t is the cosmic time, and the curvature constant $k = +1, 0, -1$ corresponds to closed, flat, and open Universes, respectively. The coordinates r, θ, and ϕ are known as *comoving* coordinates.

In BD theory, the action is given by [57, 79]

$$S = \frac{1}{16\pi G}\int \sqrt{-g}\left[\phi R - \omega\frac{\phi_{,\alpha}\phi^{,\alpha}}{\phi} + L_m\right] d^4x, \quad (2)$$

where ϕ is the BD scalar field, R is the Ricci scalar, ω is the BD parameter, and L_m is the Lagrangian matter. Here, the gravitational constant (G) takes the place of the time-dependent scalar field ϕ, which is inversely proportional to G, i.e., $\phi(t) = 1/8\pi G$. If we assume the matter field to consist of a perfect fluid, then the BD field equations from the variation of action (2) and for the FLRW space-time are obtained as [79]

$$\frac{3}{4w}\phi^2\left(\frac{k}{a^2} + H^2\right) + \frac{3H\phi\dot{\phi}}{2w} - \frac{\dot{\phi}^2}{2} = \rho_D + \rho_m, \quad (3)$$

$$\frac{-\phi^2}{4w}\left(\frac{k}{a^2} + \frac{2\ddot{a}}{a} + H^2\right) - \frac{H\phi\dot{\phi}}{w} - \frac{\phi\ddot{\phi}}{2w} - \frac{1}{2}\left(\frac{1}{w} + 1\right)\dot{\phi}^2 = p_D, \quad (4)$$

where $H = \dot{a}/a$ is the Hubble parameter, ρ_m is the matter energy density, ρ_D is the RHDE density, and p_D is the RHDE pressure. The BD scalar field evolution equation is

$$\ddot{\phi} + 3H\dot{\phi} - \phi\frac{3}{2w}\left(H^2 + \frac{k}{a^2} + \frac{\ddot{a}}{a}\right) = 0. \tag{5}$$

2.1. Rényi Entropy and HDE. It is important to mention here that it seems there is a deep connection between quantum gravity and generalized entropy scenarios, and indeed, quantum aspects of gravity may also be considered as another motivation for considering generalized entropies [22, 80]. Tsallis entropy is one of the generalized entropy measures which lead to acceptable results in the gravitational and different cosmological setups [23, 25, 43, 81–89]. Usually, Tsallis entropy is defined as [86]

$$S_{\mathrm{TE}} = \frac{1}{1-N}\sum_{i=1}^{W}\left(P_i^N - P_i\right), \tag{6}$$

for a system consisting of W discrete states. In the above equation, P_i is the ordinary probability of accessing state i, and N is a real parameter which may be originated from the nonextensive features of the system such as the long-range nature of gravity [22, 83, 86]. In fact, the concept of nonextensivity is more complex than that of nonadditivity [87]. For example, the well-known Bekenstein entropy is nonadditive and nonextensive simultaneously (for details, see Refs. [84, 85]). It is proposed recently that the Bekenstein entropy ($S = A/4$, where $A = 4\pi L^2$ and L is the IR cut-off) is actually a Tsallis entropy leading to

$$S = \frac{1}{\delta}\log\left(\frac{\delta}{4}A + 1\right) = \frac{1}{\delta}\log\left(\pi\delta L^2 + 1\right), \tag{7}$$

for the Rényi entropy content of the system [21, 22]. Here, δ is a free parameter and known in the current literature as the real nonextensive parameter that quantifies the degree of nonextensibility [22, 86, 87]. It is proposed in [90] that the δ parameter affects the energy balance of the Universe. When $\delta < 1$, the gravitational field is strong enough in such a way that we need only a small quantity of DE and DM to construct the observable Universe. On the other hand, when $\delta > 1$, the gravitational field is weak in such a way that we need, contrarily to the $\delta < 1$ case, a larger quantity of DE and DM. To sum up, $\delta < 1$ implies less DE and $\delta > 1$ implies more DE than we would have if we consider the standard Boltzmann-Gibbs scenario [90, 91]. In [22], the authors used the value of δ from −1400 to −900. There are wide ranges for δ which can produce desired results, while we have taken the values of δ from −1600 to −1400. Authors investigated late-time acceleration for a spatially flat dust filled Universe in the Brans-Dicke theory in the presence of a positive cosmological constant Λ, where the value for the Brans-Dicke-coupling constant w is taken as 40,000 [92]. Authors have studied the Tsallis holographic dark energy in the Brans-Dicke framework using $b^2 = 0.05, 0.10, 0.15$ and $n = 0.001, 0.005, 0.05$ [77]. The primary focus is in [93] on the FLRW Universe specified by WMAP data. The role of dark energy is played by the vacuum energy density in this model, that is, one had $\Lambda^4 \sim \rho_\Lambda \equiv \rho_D$. With the assumption $\rho_d \propto TdS$ [22] and $L = 1/H$ (i.e., Hubble horizon) and using Equation (7), we obtained energy density for the RHDE as

$$\rho_D = \frac{3c^2H^2}{\left(\pi\delta/H^2 + 1\right)8\pi}, \tag{8}$$

where c^2 is a numeric constant. We used $T = H/2\pi$ and $A = 4\pi/H = 4\pi(3V/4\pi)^{2/3}$; relations to get this equation corroborated in a flat FLRW Universe [94]. One can get $\rho_D = 3c^2H^2/8\pi$ without δ, which is in complete agreement with the standard HDE [14–18]. It deserves mention here that the apparent horizon is a proper causal boundary for the cosmos in agreement with the thermodynamics laws. Besides, in a flat FLRW Universe, Friedmann equations indicate that whenever DE is dominant in the cosmos, its energy density will scale with H^2 (for details, see [22, 94]). Therefore, from a thermodynamic point of view, a HDE model in the flat FLRW Universe, for which the radii of the apparent horizon and the Hubble horizon $(1/H)$ are the same, will be more compatible with the thermodynamics laws, if it can provide a proper description for the Universe by using the Hubble horizon as its IR cut-off. Following [68], we assume that $\phi \propto a^n$, i.e., the power law of scale factor in this case to the BD scalar field ϕ. One can now easily obtain

$$\dot{\phi} = n\phi\frac{\dot{a}}{a}, \tag{9}$$

and hence,

$$\ddot{\phi} = H^2n^2\phi + \phi n\dot{H}. \tag{10}$$

The Rényi HDE density with the Hubble horizon as the IR cut-off is given as

$$\rho_D = \frac{3c^2H^2\phi^{2\delta}}{8\pi\left(\pi\delta/H^2 + 1\right)}. \tag{11}$$

Here, the holographic principle [17] is used, and the effective gravitational constant G_{eff} is given by $G_{\mathrm{eff}} = w/2\pi\phi^2$. The gravitational constant G may be found from G_{eff} as a limit. The RHDE energy density can be recovered in the fundamental cosmology [22]. The Holographic DE can also be found in the Brans-Dicke gravity for the case $\delta = 1$ [64]. The dimensionless density parameters are defined as

$$\Omega_m = \frac{4w\rho_m}{3\phi^2H^2}, \Omega_D = \frac{c^2H^2w\phi^{2\delta-2}}{2\pi\left(\pi\delta + H^2\right)}, \Omega_k = \frac{k}{a^2H^2}, \Omega_\phi = 2n\left(\frac{nw}{3} - 1\right). \tag{12}$$

Our main goal of this work is to build a cosmological model of late acceleration based on the BD theory of

gravity and on the assumption that the RHDE and the pressureless dark matter do not conserve separately. Therefore, we assume that both components—the RHDE and the pressureless matter—interact with each other, i.e., one component may grow at the expense of the other. Hence, the energy conservation equations for them are given as follows:

$$\dot{\rho}_D + 3\rho_D(1+\omega_D) = -Q, \tag{13}$$

and

$$\dot{\rho}_m + 3H\rho_m = Q, \tag{14}$$

where $\omega_D = p_D/\rho_D$ represents the Rényi HDE equation of state (EoS) parameter and Q denotes the interaction term. Clearly, for $Q<0$ $(Q>0)$, there is an energy flow from pressureless matter (RHDE) to RHDE (pressureless matter). We assume the form of interaction as$Q = 3b^2Hq(\rho_D+\rho_m)$ [41, 42, 74], in which b^2 is the coupling constant and q denotes the deceleration parameter. Here, the main ingredient is the deceleration parameter q $(\equiv -\ddot{a}/aH^2)$ in the interaction term Q, and hence, Q can change its sign when the expansion of our Universe changes from the early decelerated $(q>0)$ phase to the late-time accelerated $(q<0)$ phase. So, the above interacting term deserves further investigation in the present context. Now, taking derivatives with respect to time of Equation (11), we get

$$\dot{\rho}_D = 2H\rho_D\left(\delta n + \left(\frac{\pi\delta}{\pi\delta+H^2}+1\right)\frac{\dot{H}}{H^2}\right), \tag{15}$$

combined with relation $\Omega_D{}' = \dot{\Omega}_D/H$ to obtain

$$\Omega_D{}' = 2\Omega_D\left(n(\delta-1) + \left(\frac{\pi\delta}{\pi\delta+H^2}\right)\frac{\dot{H}}{H^2}\right), \tag{16}$$

where the prime denotes derivative with $x = \log a$. Now, taking the derivative with respect to time of Equation (3) and substituting the value of $\dot{\phi}$, $\ddot{\phi}$, $\dot{\rho}_m$, and $\dot{\rho}_D$ from Equations (9), (10), (14), and (15), respectively, we get

$$\frac{\dot{H}}{H^2} = -\frac{\left(\pi\delta+H^2\right)\left(3\left(3b^2-2n+5\right)\Omega_k - 9b^2 + \Omega_D(6\delta n+9) + 2n(2n(nw-3)-3)-9\right)}{H^2\left(-9b^2+6\Omega_D+4n(nw-3)-6\right)+\pi\delta\left(-9b^2+12\Omega_D+4n(nw-3)-6\right)+9b^2\left(\pi\delta+H^2\right)\Omega_k}. \tag{17}$$

Defining, as usual, the deceleration parameter as

$$q = -\frac{\ddot{a}}{aH^2} = -1 - \frac{\dot{H}}{H^2}, \tag{18}$$

and using Equation (17), we obtain

$$q = -1 + \frac{\left(\pi\delta+H^2\right)\left(3\left(3b^2-2n+5\right)\Omega_k - 9b^2 + \Omega_D(6\delta n+9) + 2n(2n(nw-3)-3)-9\right)}{H^2\left(-9b^2+6\Omega_D+4n(nw-3)-6\right)+\pi\delta\left(-9b^2+12\Omega_D+4n(nw-3)-6\right)+9b^2\left(\pi\delta+H^2\right)\Omega_k}. \tag{19}$$

The evolutionary behavior of the deceleration parameter is plotted for the interacting Rényi HDE model versus redshift z by finding its numerical solution using the initial values $\Omega_{D0} = 0.70$ and $H_0 = 72.30$, for both flat Universe $\Omega_k = 0$ and nonflat Universe $\Omega_k = 0.012$. It is proposed by different observations that the Universe is in an accelerated expansion phase, and the value of the deceleration parameter lies in the range $-1 \le q < 0$. Also, we have used $n = 0.0005$ [77] for all plots. All the physical parameters are examined through δ and coupling coefficient b^2 because they play a crucial role in the evolution of dynamical parameters of the RHDE. From Figure 1, we see the evolutionary behavior of q for interacting RHDE in BD gravity, for distinct estimations of b^2 and δ in the nonflat Universe (lower two panels) and flat Universe (upper two panels). We can observe from Figure 1 that the RHDE model shows the transition from an early decelerated stage to a current accelerated stage for both cases for distinct estimations of b^2 and parameter δ. In this context, it is worthwhile mentioning that the standard HDE in the framework of BD theory can explain the accelerated expansion if the event horizon is taken as the role of the IR cut-off [64]. Such a scenario also predicts no acceleration if the Hubble horizon is considered as the IR cut-off. Therefore, the novelty of the present work is that it can explain the current accelerated phase of the Universe if we choose the IR cut-off to be the Hubble horizon.

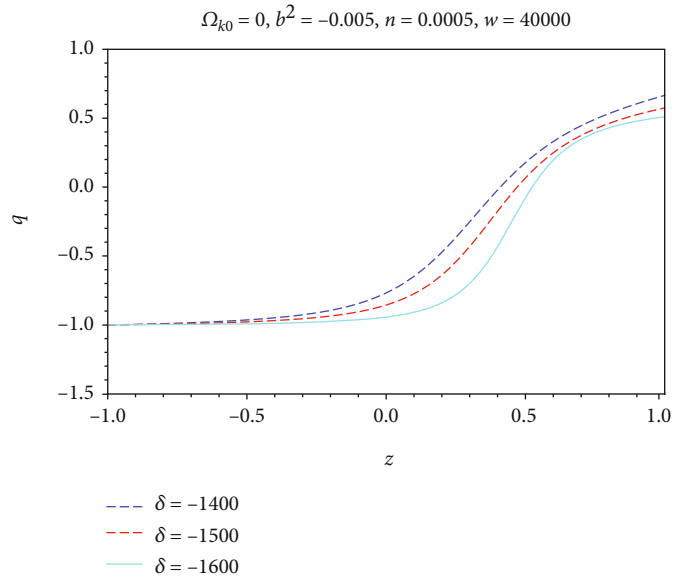

(a)

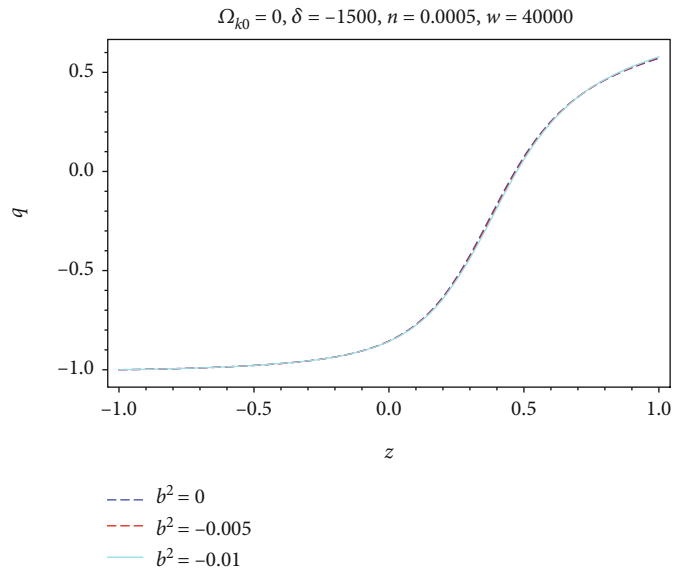

(b)

Figure 1: Continued.

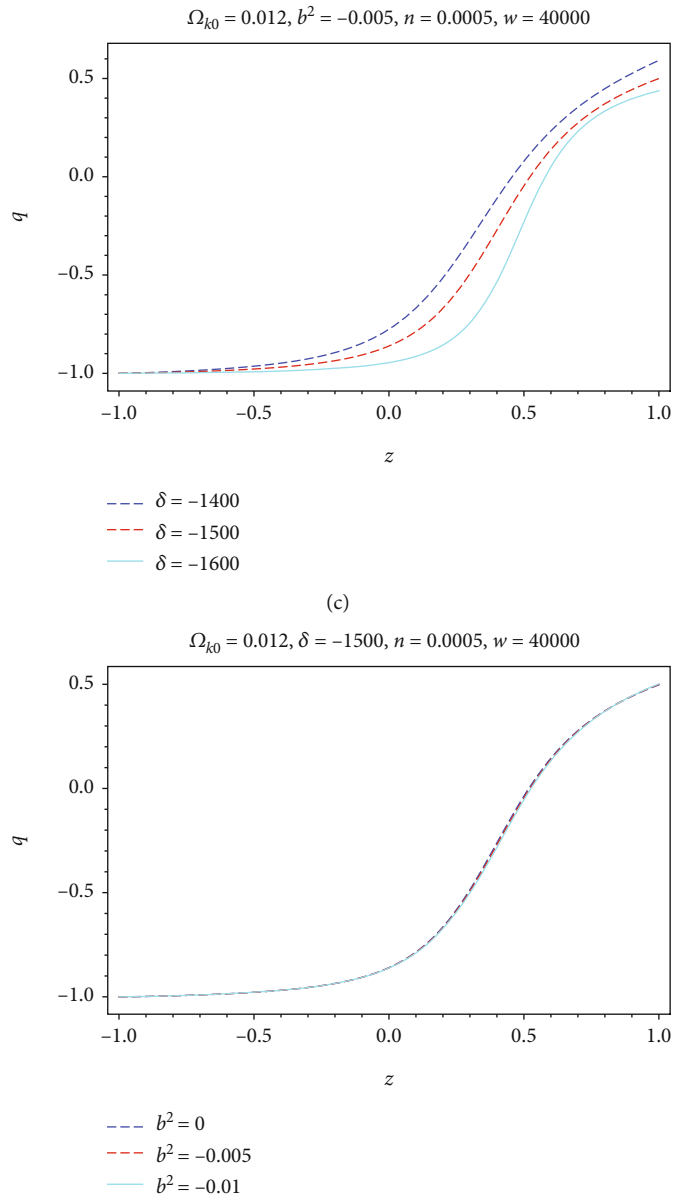

FIGURE 1: The deceleration parameter (q) evolutionary behavior versus redshift for nonflat Universe (c, d) and flat Universe (a, b) for distinct values of δ and b^2. Here, $H_0 = 72.30$ and $\Omega_{D0} = 0.704$.

Combining Equations (13), (15), and (17) with each other, the EoS parameter is obtained as

$$\begin{aligned}\omega_D = {} & \left[3\Omega_D\left(H^2\left(-9b^2 + 6\Omega_D + 4n(nw-3) - 6\right)\right.\right. \\ & \left. + \pi\delta\left(-9b^2 + 12\Omega_D + 4n(nw-3) - 6\right) + 9b^2\left(\pi\delta + H^2\right)\Omega_k\right)\Big]^{-1} \\ & \times \Big[\left(H^2\left(2\Omega_D\left(-4(\delta-1)n^3w - 6n^2(-2\delta + w + 2)\right.\right.\right. \\ & \left. + 6(\delta+2)n + 3(5-2n)\Omega_k\right) - 3b^2(\Omega_k - 1)(3(2n-5)\Omega_k \\ & + 2n(2n(-nw + w + 3) - 3) + 3)) + \pi\delta\left(-3b^2(\Omega_k - 1)(3(2n-5)\Omega_k\right. \\ & + 2n(2n(-nw + w + 3) - 3) + 3) - 2\Omega_D\left(6(2n-5)\Omega_k + 4(\delta-2)n^3w\right. \\ & \left.\left.\left. + 6n^2(-2\delta + w + 4) - 6(\delta+1)n + 9\right)\right)\Big].\end{aligned} \tag{20}$$

We have graphed the behavior of EoS parameter ω_D of our derived interacting RHDE model for both $\Omega_k = 0$ (two upper panels) and $\Omega_k = 0.012$ (two lower panels) cases, in Figure 2 for distinct values of parameter δ and coupling coefficient b^2. According to this figure, it can be seen that ω_D of the RHDE model varies from quintessence to the phantom region ($\omega_D < -1$). Moreover, we can observe that the EoS parameter approaches ΛCDM model ($\omega_D = -1$) for all values of δ and b^2 in the future, which is in agreement with cosmological observations. We also noted that the evolution of the EoS parameter at an early time in both flat and nonflat Universes is more distinct for different values of δ in comparison to coupling coefficient b^2.

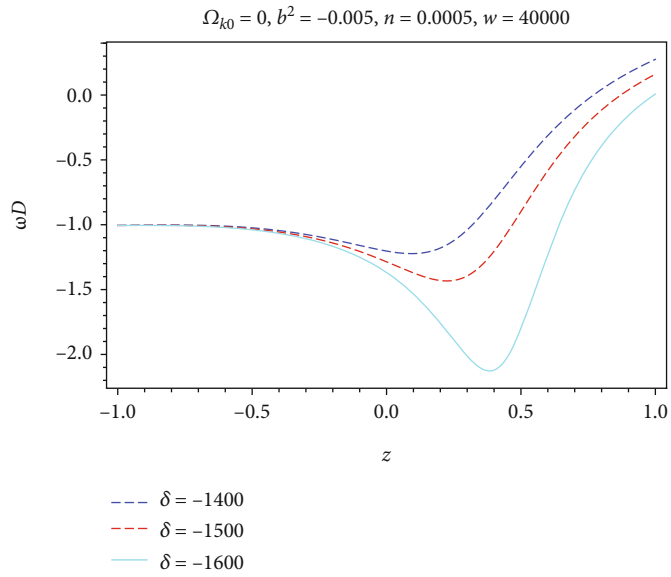

(a)

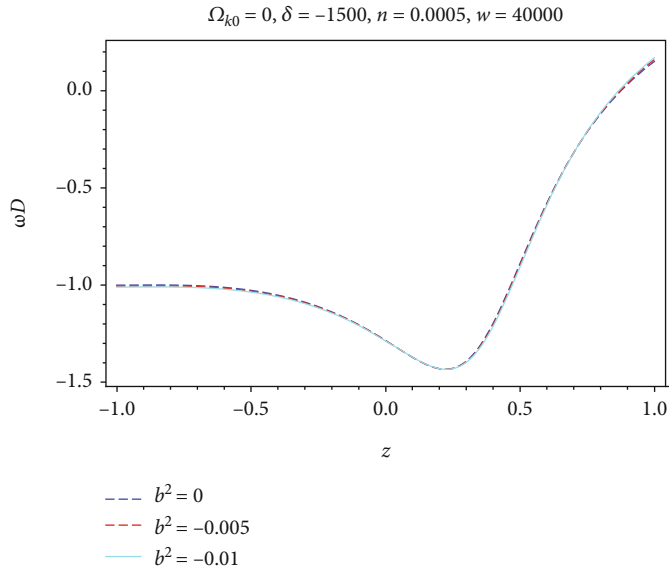

(b)

Figure 2: Continued.

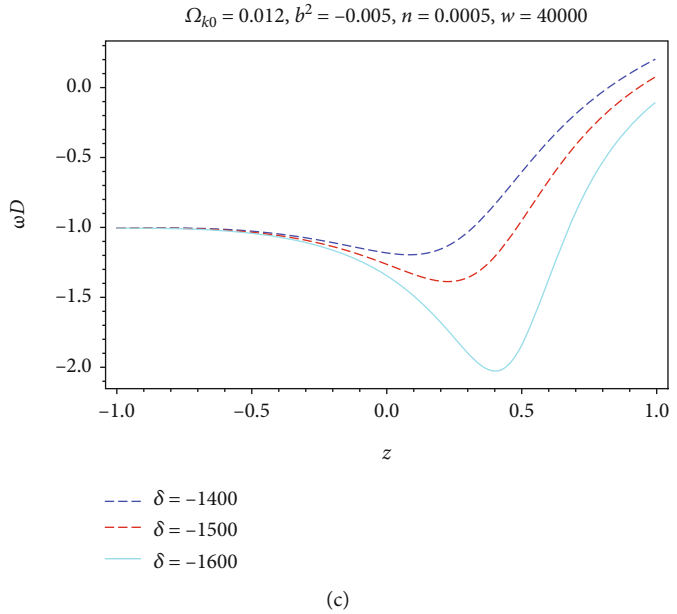

(c)

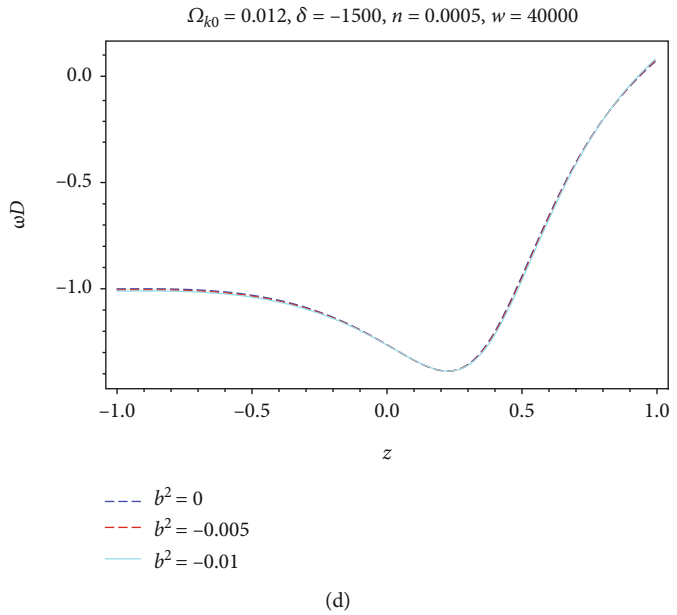

(d)

FIGURE 2: Evolutionary behavior of the EoS parameter ω_D against redshift for interacting RHDE for nonflat Universe (c, d) and flat Universe (a, b) for distinct values of δ and b^2. Here, $\Omega_{D0} = 0.704$ and $H_0 = 72.30$.

By putting Equation (17) in Equation (16), we also obtain the evolution of dimensionless RHDE density parameter as

$$\Omega_D{}' = \left[(\delta - 1)n + 2\Omega_D \times \frac{\pi\delta\left(-3\left(3b^2 - 2n + 5\right)\Omega_k + 9b^2 - 3\Omega_D(2\delta n + 3) + 2n\left(-2n^2w + 6n + 3\right) + 9\right)}{H^2\left(-9b^2 + 6\Omega_D + 4n(nw - 3) - 6\right) + \pi\delta\left(-9b^2 + 12\Omega_D + 4n(nw - 3) - 6\right) + 9b^2\left(\pi\delta + H^2\right)\Omega_k}\right]. \tag{21}$$

We have shown the behavior of interacting RHDE density parameter Ω_D in Figure 3 for both $\Omega_k = 0$ (two upper panels) and $\Omega_k = 0.012$, (two lower panels) cases, for distinct values of coupling coefficient b^2 and δ. The thermal history of

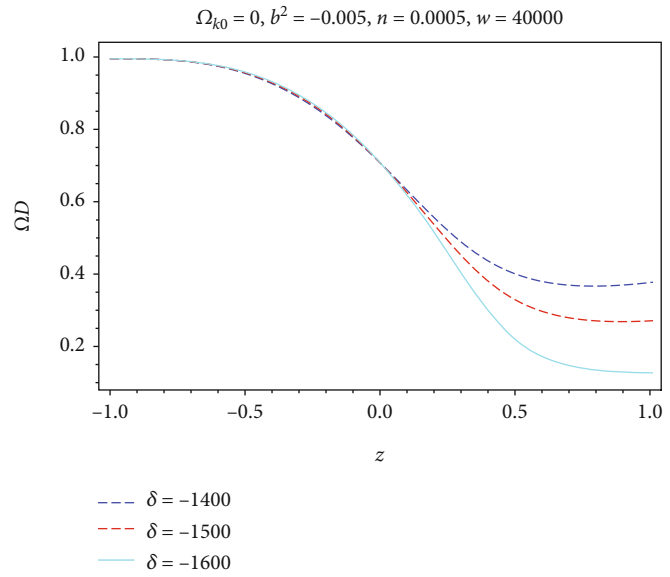

(a)

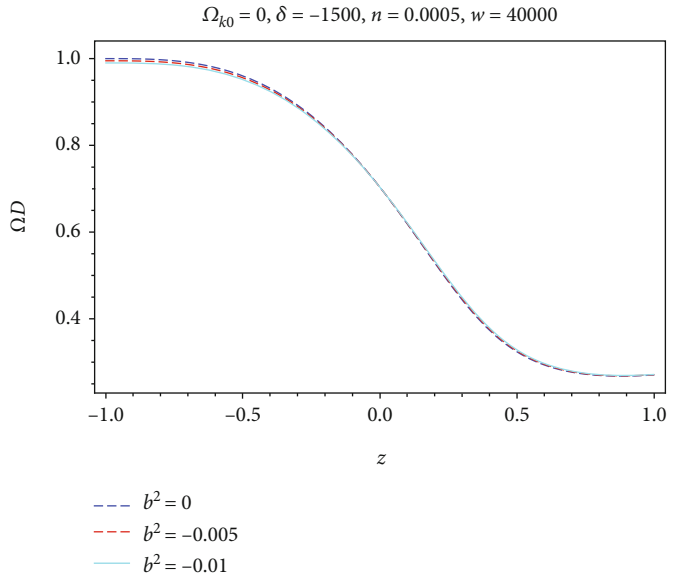

(b)

Figure 3: Continued.

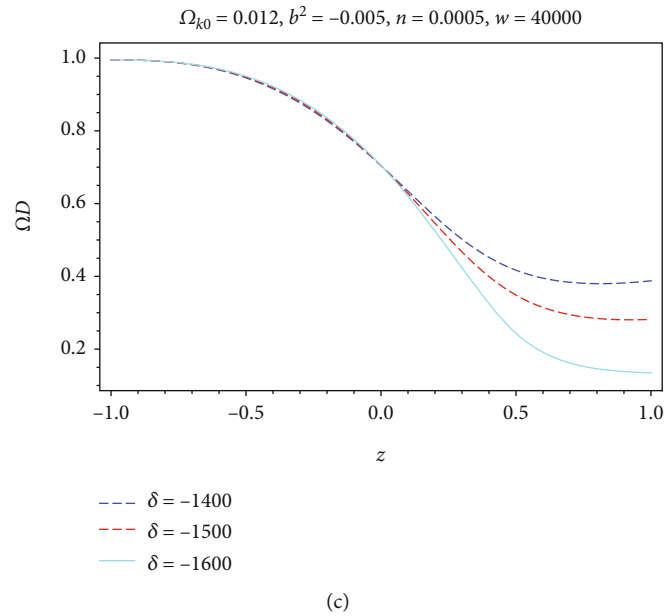

(c)

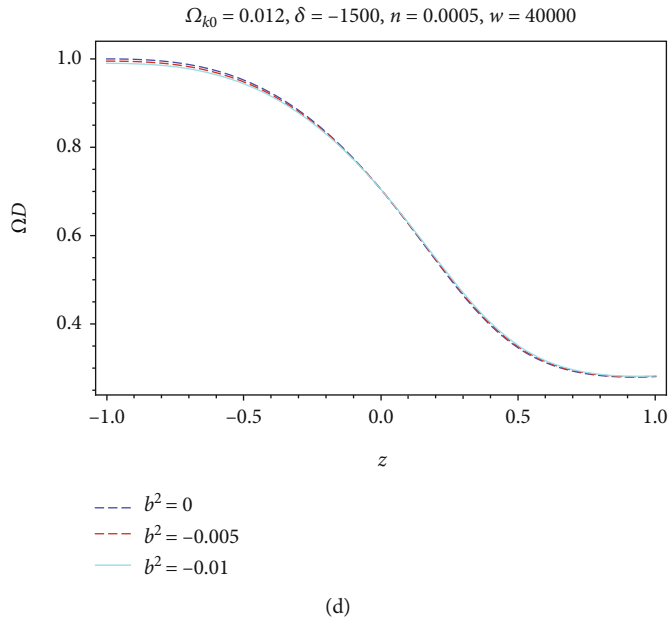

(d)

FIGURE 3: The evolutionary behavior of Ω_D against z for interacting RHDE for nonflat Universe (c, d) and flat Universe (a, b) for different values of δ and b^2. Here, $\Omega_{D0} = 0.704$ and $H_0 = 72.30$.

the Universe, in particular, the successive sequence of matter and DE era, can be observed from these figures for different values of δ and b^2 in both nonflat and flat Universes. We also observed that the RHDE density parameter is consistent with cosmological observations [7], and our results are consistent.

We have plotted the behavior of the Hubble parameter H of our derived interacting RHDE model for both the $\Omega_k = 0$ (two upper panels) and $\Omega_k = 0.012$, (two lower panels) cases, in Figure 4 for distinct values of parameter δ and coupling coefficient b^2. It depicts that the variation of δ affects the behavior of H, while different values of coupling coefficient b^2 do not affect it. The value of H decreases and approaches to a positive value near 70 in the far future.

3. Stability

In this section, we shall discuss the stability of the interacting RHDE model through the squared sound speed v_s^2 in both flat and nonflat Universes. The $v_s^2 \geq 0$ (the real value of speed), shows a regular propagating mode for a density perturbation. For $v_s^2 < 0$, the perturbation becomes an irregular wave equation. Hence the negative squared speed (imaginary value of speed) shows an exponentially growing mode for a density perturbation. That is, an increasing density

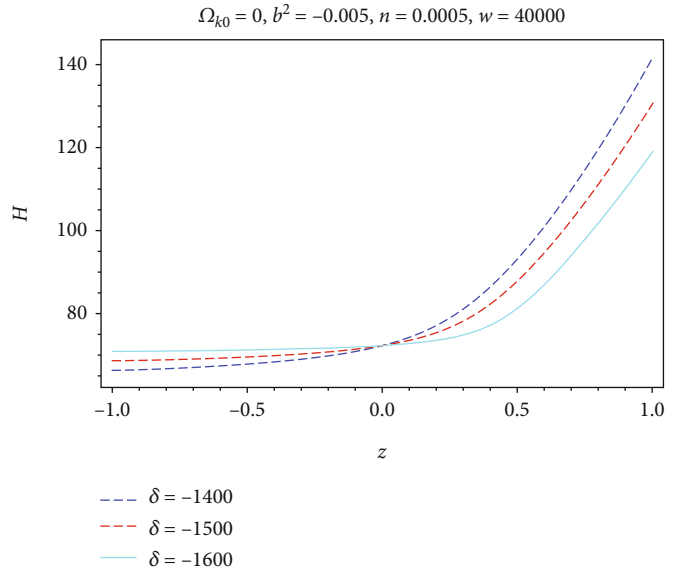

(a)

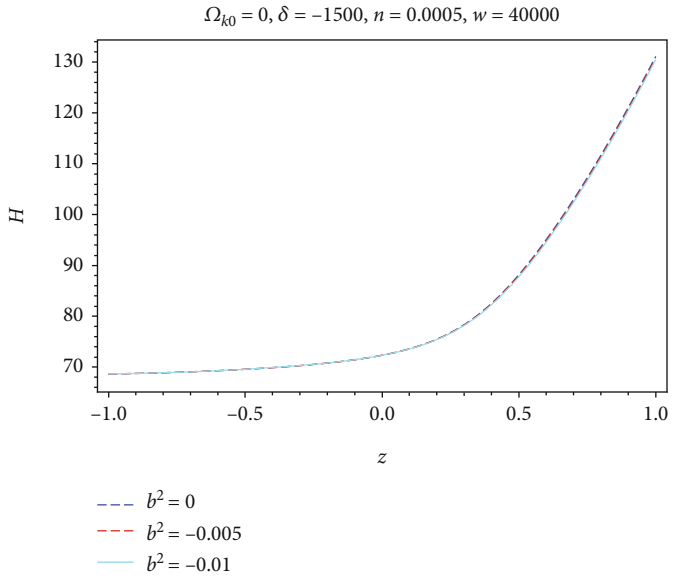

(b)

Figure 4: Continued.

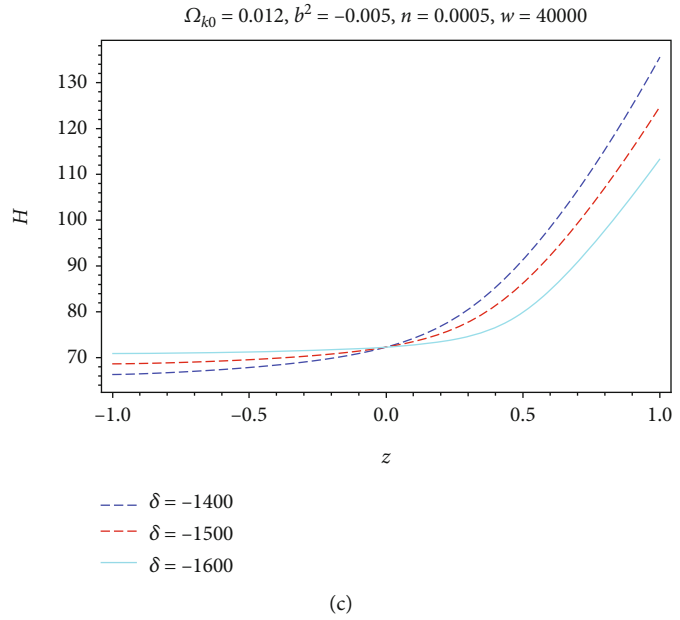

(c)

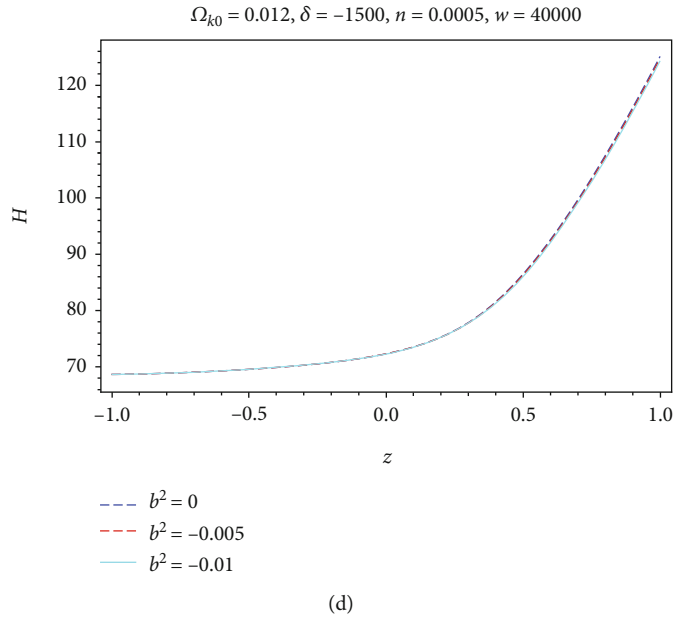

(d)

FIGURE 4: The Hubble parameter (H) evolutionary behavior versus redshift for nonflat Universe (c, d) and flat Universe (a, b) for distinct values of δ and b^2. Here, $H_0 = 72.30$ and $\Omega_{D0} = 0.704$.

perturbation induces a lowering pressure, supporting the emergence of instability [95].

The squared sound speed is given as [96, 97]

$$v_s^2 = \frac{dp_D}{d\rho_D} = \frac{\rho_D \dot{\omega}_D}{\dot{\rho}_D} + \omega_D. \quad (22)$$

Now, inserting the result of Equation (15) in Equation (22), we get

$$v_s^2 = \omega_D + \frac{\dot{\omega}_D}{2H\left(\left(\pi\delta/\left(\pi\delta + H^2\right) + 1\right)\left(\dot{H}/H^2\right) + \delta n\right)}. \quad (23)$$

We solve the Equation (23) numerically by using Mathematica package NDSolve and plotted the squared sound speed v_s^2 versus redshift z in Figure 5, for both $\Omega_k = 0$ (two upper panels) and $\Omega_k = 0.012$, (two lower panels) cases for distinct values of the parameter δ and coupling coefficient b^2.From Figure 5, we observe that the RHDE model is not stable initially by taking different values of δ and b^2 in both flat and nonflat Universes, while for $\delta = -1400$ in both flat and nonflat Universes, the value of the squared sound speed v_s^2 diverges. By taking different values of b^2 in both flat and nonflat Universes, the RHDE model becomes stable at the late time. By analyzing all these plots, we can say that values of δ and b^2 have qualitative effects on the nature of the

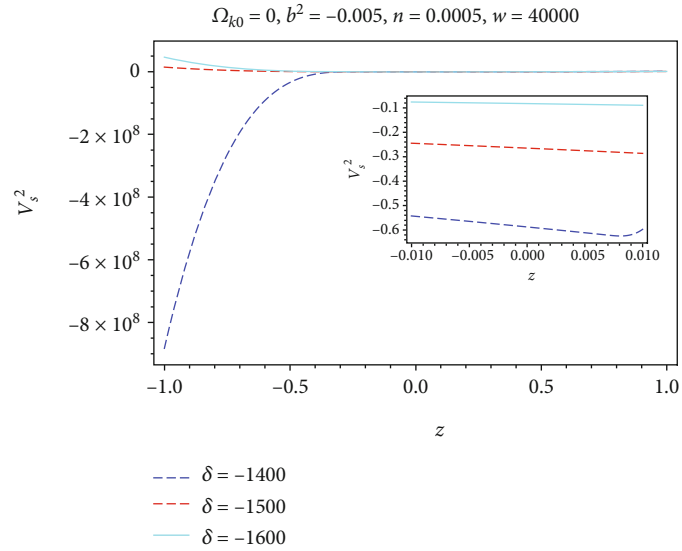

(a)

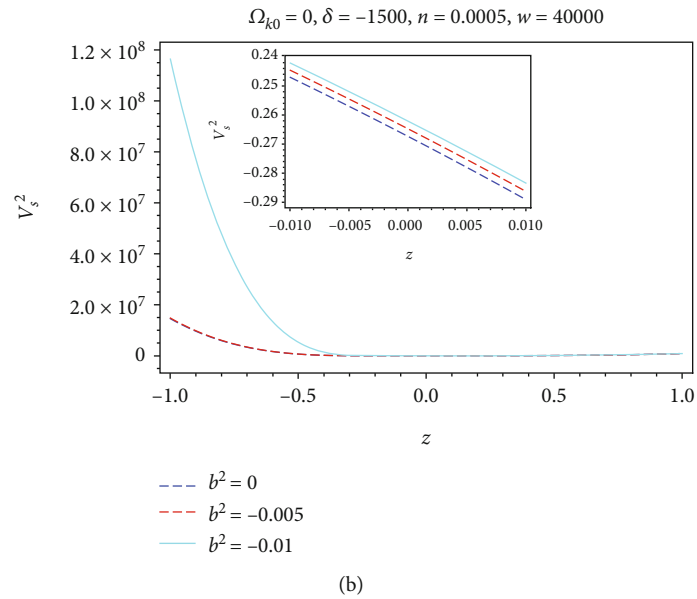

(b)

Figure 5: Continued.

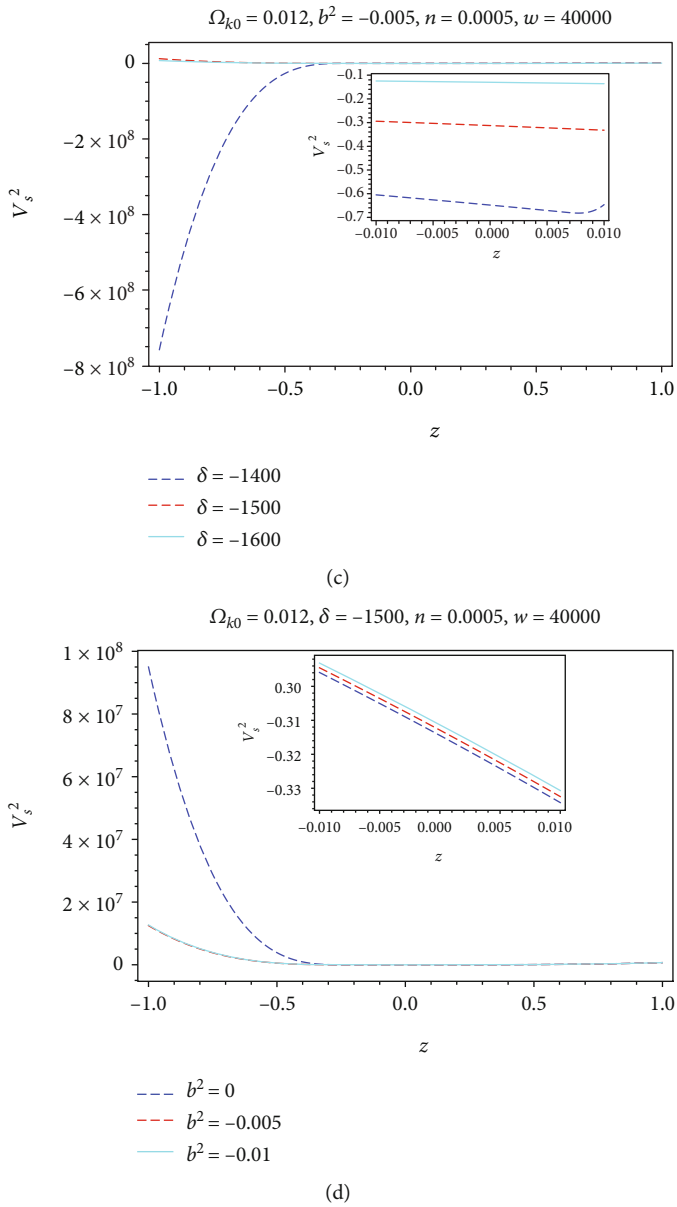

FIGURE 5: The behavior of v_s^2 against z for the interacting Rényi HDE for nonflat Universe (c, d) and flat Universe (a, b) for distinct values of δ and b^2. Here, $\Omega_{D0} = 0.704$ and $H_0 = 72.30$.

squared sound speed v_s^2 in both the nonflat and the flat cosmos. The inset plot of Figure 5 shows a close-up of the outer plot around $z = 0$ in which the difference can be seen. They are not exactly identical but the difference is very small.

4. Concluding Remarks

In this work, we explored the role of the interacting FLRW cosmos to model dark energy in the Brans-Dicke theory framework using RHDE by taking an infrared cut-off as the Hubble radius in both nonflat and flat Universes. The pressureless matter is assumed to interact with the RHDE through a sign-changeable interaction. In this analysis, we have used the initial values $\Omega_{D0} = 0.70$, $\Omega_{m0} = 0.30$, $H_0 = 72.30$, and $n = 0.005$ [77] for both flat Universe ($\Omega_k = 0$) and nonflat Universe ($\Omega_k = 0.012$). It has been found that for different values of the Rényi parameter δ and the coupling coefficient b^2, the interacting RHDE model produces the suitable behavior for the deceleration parameter (q), the EoS parameter (ω_D), the RHDE density parameter (Ω_D), and the Hubble parameter, in both the cases (see Figures 1–4). The effect of different values of δ and b^2 is only quantitative on these parameters.

As discussed earlier, the Brans-Dicke theory in the framework of HDE can explain the accelerated expansion if we choose the IR cut-off to be the event horizon. The theory also predicts no acceleration if we choose the IR cut-off to be the Hubble horizon. However, in our case, the deceleration

parameter q shows a smooth transition from the decelerated phase ($q > 0$) early to the accelerated phase ($q < 0$) at a later time. Hence, a remarkable feature of this model is that RHDE in the framework of the Brans-Dicke theory explains the accelerated expansion if we choose the IR cut-off to be the Hubble horizon. It has also been found that the EoS parameter ω_D varies from a quintessence ($\omega_D > -1$) to the phantom region ($\omega_D < -1$), and the RHDE model transits decelerating to an accelerating stage of the Universe and ω_D approach to -1 as $z \to -1$, which implies that the RHDE model imitates the cosmological constant at a far future. It is observed that the RHDE density parameter Ω_D becomes 1 as $z \to -1$. Moreover, it is observed that the variation of δ affects the behavior of the Hubble parameter H, while different values of b^2 do not affect it. Also, the value of H decreases and approaches to a value near 70 in the far future. Furthermore, we have investigated the classical stability of our model by analyzing the squared sound speed v_s^2. It has been found that the stability of our model crucially depends on the choices of the parameter δ in both flat and nonflat Universes (see Figure 5).

As we showed, the present model exhibits more interesting phenomenology comparing to the standard scenario, and hence, it can be a candidate for the description of nature. In a follow-up study, we would like to perform an observational analysis to constrain the parameter δ.

Data Availability

This manuscript has no associated data or the data will not be deposited. (Authors' comment: data sharing is not applicable to this article as no new data were created or analyzed in this study).

Conflicts of Interest

The authors declare that they have no conflicts of interest.

Acknowledgments

VCD and UKS are thankful to GLA University, India, for providing the support and help to carry out this research work.

References

[1] F. Zwicky, "Die Rotverschiebung von extragalaktischen Nebeln," *Helvetica physica acta*, vol. 6, p. 110, 1933.

[2] F. Zwicky, "On the masses of nebulae and of clusters of nebulae," *The Astrophysical Journal*, vol. 86, p. 217, 1937.

[3] V. C. Rubin and W. K. Ford Jr., "Rotation of the Andromeda Nebula from a spectroscopic survey of emission regions," *The Astrophysical Journal*, vol. 159, p. 379, 1970.

[4] A. G. Riess, A. V. Filippenko, P. Challis et al., "Observational evidence from supernovae for an accelerating universe and a cosmological constant," *The Astronomical Journal*, vol. 116, article 1009, 1998.

[5] S. Perlmutter, G. Aldering, G. Goldhaber et al., "Measurements of Ω and Λ from 42 high redshift supernovae," *The Astrophysical Journal*, vol. 517, p. 565, 1999.

[6] R. von Marttens, L. Lombriser, M. Kunz, V. Marra, L. Casarini, and J. Alcaniz, "Dark degeneracy I: dynamical or interacting dark energy?," *Physics of the Dark Universe*, vol. 28, p. 100490, 2020.

[7] N. Aghanim, Y. Akrami, M. Ashdown et al., "Planck 2018 results. VI. Cosmological parameters," *Astronomy and Astrophysics*, vol. 641, p. A6, 2020.

[8] S. Alam, M. Ata, S. Bailey et al., "The clustering of galaxies in the completed SDSS-III Baryon Oscillation Spectroscopic Survey: cosmological analysis of the DR12 galaxy sample," *Monthly Notices of the Royal Astronomical Society*, vol. 470, no. 3, pp. 2617–2652, 2017.

[9] M. A. Troxel, N. MacCrann, J. Zuntz et al., "Dark energy survey year 1 results: cosmological constraints from cosmic shear," *Physical Review D*, vol. 98, article 043528, 4 pages, 2018.

[10] T. Buchert, A. A. Coley, H. Kleinert, B. F. Roukema, and D. L. Wiltshire, "Observational challenges for the standard FLRW model," *International Journal of Modern Physics D*, vol. 25, no. 3, article 1630007, 2016.

[11] M. Li, "A model of holographic dark energy," *Physics Letters B*, vol. 603, no. 1-2, pp. 1–5, 2004.

[12] L. Susskind, "The world as a hologram," *Journal of Mathematical Physics*, vol. 36, no. 11, pp. 6377–6396, 1995.

[13] P. Horava and D. Minic, "Probable values of the cosmological constant in a holographic theory," *Physical Review Letters*, vol. 85, no. 8, pp. 1610–1613, 2000.

[14] S. D. Thomas, "Holography stabilizes the vacuum energy," *Physical Review Letters*, vol. 89, no. 8, article 081301, 2002.

[15] S. D. H. Hsu, "Entropy bounds and dark energy," *Physics Letters B*, vol. 594, no. 1-2, pp. 13–16, 2004.

[16] S. Wang, Y. Wang, and M. Li, "Holographic dark energy," *Physics reports*, vol. 696, pp. 1–57, 2017.

[17] A. G. Cohen, D. B. Kaplan, and A. E. Nelson, "Effective field theory, black holes, and the cosmological constant," *Physical Review Letters*, vol. 82, no. 25, pp. 4971–4974, 1999.

[18] B. Guberina, R. Horvat, and H. Nikolic, "Nonsaturated holographic dark energy," *Journal of Cosmology and Astroparticle Physics*, vol. 2007, article 012, 2007.

[19] S. Nojiri and S. D. Odintsov, "Unifying phantom inflation with late-time acceleration: scalar phantom-non-phantom transition model and generalized holographic dark energy," *General Relativity and Gravitation*, vol. 38, no. 8, pp. 1285–1304, 2006.

[20] S. Nojiri and S. D. Odintsov, "Covariant generalized holographic dark energy and accelerating universe," *The European Physical Journal C*, vol. 77, no. 8, p. 528, 2017.

[21] A. Rényi, *Proceedings of the 4th Berkely Symposium on Mathematics, Statistics and Probability (University California Press, Berkeley, CA, 1961)*, Probability Theory, North-Holland, Amsterdam, 1970.

[22] H. Moradpour, S. A. Moosavi, I. P. Lobo, J. M. Graça, A. Jawad, and I. G. Salako, "Thermodynamic approach to holographic dark energy and the Rényi entropy," *The European Physical Journal C*, vol. 78, no. 10, p. 829, 2018.

[23] H. Moradpour, A. Bonilla, E. M. C. Abreu, and J. A. Neto, "Accelerated cosmos in a nonextensive setup," *Physical Review D*, vol. 96, no. 12, article 123504, 2017.

[24] H. Moradpour, "Implications, consequences and interpretations of generalized entropy in the cosmological setups," *International Journal of Theoretical Physics*, vol. 55, no. 9, pp. 4176–4184, 2016.

[25] N. Komatsu, "Cosmological model from the holographic equipartition law with a modified Rényi entropy," *The European Physical Journal C*, vol. 77, no. 4, p. 229, 2017.

[26] S. Ghaffari, A. H. Ziaie, V. B. Bezerra, and H. Moradpour, "Inflation in the Rényi cosmology," *Modern Physics Letters A*, vol. 35, no. 1, article 1950341, 2019.

[27] S. Chunlen and P. Rangdee, "Exploring the Rényi holographic dark energy model with the future and the particle horizons as the infrared cut-off," 2020, https://arxiv.org/abs/2008.13730.

[28] U. Y. Divya Prasanthi and Y. Aditya, "Anisotropic Renyi holographic dark energy models in general relativity," *Results in Physics*, vol. 17, p. 103101, 2020.

[29] U. K. Sharma and V. C. Dubey, "Statefinder diagnostic for the Rényi holographic dark energy," *New Astronomy*, vol. 80, p. 101419, 2020.

[30] V. C. Dubey, A. K. Mishra, and U. K. Sharma, "Diagnosing the Rényi holographic dark energy model in a flat Universe," *Astrophysics and Space Science*, vol. 365, no. 7, p. 129, 2020.

[31] V. C. Dubey and U. K. Sharma, "Comparing the holographic principle inspired dark energy models," *New Astronomy*, vol. 86, Article ID 101586, 2021.

[32] G. Olivares, F. Atrio-Barandela, and D. Pavon, "Observational constraints on interacting quintessence models," *Physical Review D*, vol. 71, no. 6, article 063523, 2005.

[33] G. Olivares, F. Atrio-Barandela, and D. Pavon, "Matter density perturbations in interacting quintessence models," *Physical Review D*, vol. 74, no. 4, article 043521, 2006.

[34] S. Das, P. S. Corasaniti, and J. Khoury, "Superacceleration as the signature of a dark sector interaction," *Physical Review D*, vol. 73, no. 8, article 083509, 2006.

[35] L. Amendola, M. Gasperini, and F. Piazza, "Supernova legacy survey data are consistent with acceleration at $z \approx 3$," *Physical Review D*, vol. 74, no. 12, p. 127302, 2006.

[36] Z. K. Guo, N. Ohta, and S. Tsujikawa, "Probing the coupling between dark components of the universe," *Physical Review D*, vol. 76, no. 2, article 023508, 2007.

[37] W. Zimdahl and D. Pavon, "Letter: statefinder parameters for interacting dark energy," *General Relativity and Gravitation*, vol. 36, no. 6, pp. 1483–1491, 2004.

[38] R. R. Caldwell and M. Kamionkowski, "Expansion, geometry, and gravity," *Journal of Cosmology and Astroparticle Physics*, vol. 2004, 2004.

[39] W. Zimdahl and D. Pavon, "Interacting holographic dark energy," *Classical and Quantum Gravity*, vol. 24, no. 22, pp. 5461–5478, 2007.

[40] D. Pavon and W. Zimdahl, "Holographic dark energy and cosmic coincidence," *Physics Letters B*, vol. 628, no. 3-4, pp. 206–210, 2005.

[41] L. P. Chimento, "Linear and nonlinear interactions in the dark sector," *Physical Review D*, vol. 81, no. 4, article 043525, 2010.

[42] L. P. Chimento, M. I. Forte, and G. M. Kremer, "Cosmological model with interactions in the dark sector," *General Relativity and Gravitation*, vol. 41, no. 5, pp. 1125–1137, 2009.

[43] A. A. Mamon, A. H. Ziaie, and K. Bamba, "A generalized interacting Tsallis holographic dark energy model and its thermodynamic implications," *European Physical Journal C: Particles and Fields*, vol. 80, no. 10, p. 974, 2020.

[44] S. Das and A. A. Mamon, "An interacting model of dark energy in Brans-Dicke theory," *Astrophysics and Space Science*, vol. 351, no. 2, pp. 651–660, 2014.

[45] E. Di Valentino, A. Melchiorri, O. Mena, and S. Vagnozzi, "Interacting dark energy after the latest Planck, DES, and H_0 measurements: an excellent solution to the H_0 and cosmic shear tensions," 2019, https://arXiv.org/abs/1908.04281.

[46] J. Dutta, W. Khyllep, E. N. Saridakis, N. Tamanini, and S. Vagnozzi, "Cosmological dynamics of mimetic gravity," *Journal of Cosmology and Astroparticle Physics*, vol. 2018, 2018.

[47] A. A. Mamon, A. Paliathanasis, and S. Saha, "Dynamics of an interacting Barrow holographic dark energy model and its thermodynamic implications," *The European Physical Journal - Plus*, vol. 136, no. 1, p. 134, 2021.

[48] U. K. Sharma, G. Varshney, and V. C. Dubey, "Barrow agegraphic dark energy," *International Journal of Modern Physics D*, Article ID 2150021, 2021.

[49] A. Iqbal and A. Jawad, "Tsallis, Renyi and Sharma–Mittal holographic dark energy models in DGP brane-world," *Physics of the Dark Universe*, vol. 26, p. 100349, 2019.

[50] M. Younas, A. Jawad, S. Qummer, H. Moradpour, and S. Rani, "Cosmological implications of the generalized entropy based holographic dark energy models in dynamical Chern-Simons modified gravity," *Advances in High Energy Physics*, vol. 2019, Article ID 1287932, 9 pages, 2019.

[51] S. Rani, A. Jawad, K. Bamba, and I. U. Malik, "Cosmological consequences of new dark energy models in Einstein-Aether gravity," *Symmetry*, vol. 11, no. 4, p. 509, 2019.

[52] A. Jawad, K. Bamba, M. Younas, S. Qummer, and S. Rani, "Tsallis, Rényi and Sharma-Mittal holographic dark energy models in loop quantum cosmology," *Symmetry*, vol. 10, no. 11, p. 635, 2018.

[53] U. K. Sharma and V. C. Dubey, "Interacting Rényi holographic dark energy with parametrization on the interaction term," 2020, https://arXiv.org/abs/2001.02368.

[54] R. Gannouji, D. Polarski, A. Ranquet, and A. A. Starobinsky, "Scalar-tensor models of normal and phantom dark energy," *Journal of Cosmology and Astroparticle Physics*, vol. 2006, 2006.

[55] V. Faraoni, *Cosmology in scalar-tensor gravity*, vol. 139, Springer Science & Business Media, 2004.

[56] E. Elizalde, S. Nojiri, S. D. Odintsov, and P. Wang, "Dark energy: vacuum fluctuations, the effective phantom phase, and holography," *Physical Review D*, vol. 71, no. 10, p. 103504, 2005.

[57] C. Brans and R. H. Dicke, "Mach's principle and a relativistic theory of gravitation," *Physics Review*, vol. 124, no. 3, pp. 925–935, 1961.

[58] V. Acquaviva and L. Verde, "Observational signatures of Jordan-Brans-Dicke theories of gravity," *Journal of Cosmology and Astroparticle Physics*, vol. 2007, 2007.

[59] B. Bertotti, L. Iess, and P. Tortora, "A test of general relativity using radio links with the Cassini spacecraft," *Nature*, vol. 425, no. 6956, pp. 374–376, 2003.

[60] N. Banerjee and D. Pavon, "Cosmic acceleration without quintessence," *Physical Review D*, vol. 63, no. 4, article 043504, 2001.

[61] Y. G. Gong, "Holographic bound in Brans-Dicke cosmology," *Physical Review D*, vol. 61, article 043505, 2000.

[62] H. Kim, H. W. Lee, and Y. S. Myung, "Holographic energy density in the Brans-Dicke theory," 2005, https://arxiv.org/abs/hep-th/0501118.

[63] H. Kim, H. W. Lee, and Y. S. Myung, "Role of the Brans-Dicke scalar in the holographic description of dark energy," *Physics Letters B*, vol. 628, no. 1-2, pp. 11–17, 2005.

[64] L. Xu, W. Li, and J. Lu, "Holographic dark energy in Brans-Dicke theory," *European Physical Journal C: Particles and Fields*, vol. 60, no. 1, pp. 135–140, 2009.

[65] Y. G. Gong, "Extended holographic dark energy," *Physical Review D*, vol. 70, article 064029, 2004.

[66] B. Nayak and L. P. Singh, "Present acceleration of universe, holographic dark energy and Brans-Dicke theory," *Modern Physics Letters A*, vol. 24, p. 1785, 2011.

[67] M. R. Setare, "The holographic dark energy in non-flat Brans-Dicke cosmology," *Physics Letters B*, vol. 644, no. 2-3, pp. 99–103, 2007.

[68] N. Banerjee and D. Pavon, "Holographic dark energy in Brans-Dicke theory," *Physics Letters B*, vol. 647, no. 5-6, pp. 477–481, 2007.

[69] M. Jamil, K. Karami, A. Sheykhi, E. Kazemi, and Z. Azarmi, "Holographic dark energy in Brans-Dicke cosmology with Granda-Oliveros cut-off," *International Journal of Theoretical Physics*, vol. 51, no. 2, pp. 604–611, 2012.

[70] A. Khodam-Mohammadi, E. Karimkhani, and A. Sheykhi, "Best values of parameters for interacting HDE with GO IR-cutoff in Brans-Dicke cosmology," *International Journal of Modern Physics D*, vol. 23, no. 10, article 1450081, 2014.

[71] U. K. Sharma, G. K. Goswami, and A. Pradhan, "Bianchi type-I dust-filled accelerating Brans-Dicke cosmology," *Gravitation and Cosmology*, vol. 24, no. 2, p. 191, 2018.

[72] B. J. Barros, L. Amendola, T. Barreiro, and N. J. Nunes, "Coupled quintessence with a ΛCDM background: removing the σ_8 tension," *Journal of Cosmology and Astroparticle Physics*, vol. 2019, 2019.

[73] J. Valiviita, R. Maartens, and E. Majerotto, "Observational constraints on an interacting dark energy model," *Monthly Notices of the Royal Astronomical Society*, vol. 402, no. 4, pp. 2355–2368, 2010.

[74] H. Wei, "Cosmological evolution of quintessence and phantom with a new type of interaction in dark sector," *Nuclear Physics B*, vol. 845, no. 3, pp. 381–392, 2011.

[75] A. Jawad, A. Aslam, and S. Rani, "Cosmological implications of Tsallis dark energy in modified Brans-Dicke theory," *International Journal of Modern Physics D*, vol. 28, no. 11, article 1950146, 2019.

[76] Y. Aditya, S. Mandal, P. K. Sahoo, and D. R. K. Reddy, "Observational constraint on interacting Tsallis holographic dark energy in logarithmic Brans-Dicke theory," *The European Physical Journal C*, vol. 79, no. 12, p. 1020, 2019.

[77] S. Ghaffari, H. Moradpour, I. P. Lobo, J. M. Graça, and V. B. Bezerra, "Tsallis holographic dark energy in the Brans-Dicke cosmology," *The European Physical Journal C*, vol. 78, no. 9, p. 706, 2018.

[78] U. K. Sharma and V. C. Dubey, "Rényi holographic dark energy in the Brans–Dicke cosmology," *Modern Physics Letters A*, vol. 35, no. 34, article 2050281, 2020.

[79] N. Banerjee and D. Pavon, "A quintessence scalar field in Brans-Dicke theory," *Classical and Quantum Gravity*, vol. 18, no. 4, pp. 593–599, 2001.

[80] H. Moradpour, A. H. Ziaie, and M. Kord Zangeneh, "Generalized entropies and corresponding holographic dark energy models," *The European Physical Journal C*, vol. 80, p. 732, 2020.

[81] H. Moradpour, A. Sheykhi, C. Corda, and I. G. Salako, "Implications of the generalized entropy formalisms on the Newtonian gravity and dynamics," *Physics Letters B*, vol. 783, pp. 82–85, 2018.

[82] S. Abe, "General pseudoadditivity of composable entropy prescribed by the existence of equilibrium," *Physical Review E*, vol. 63, no. 6, article 061105, 2001.

[83] A. Majhi, "Non-extensive statistical mechanics and black hole entropy from quantum geometry," *Physics Letters B*, vol. 775, pp. 32–36, 2017.

[84] T. S. Biró and V. G. Czinner, "A q-parameter bound for particle spectra based on black hole thermodynamics with Rényi entropy," *Physics Letters B*, vol. 726, p. 861, 2013.

[85] V. G. Czinner and H. Iguchi, "Rényi entropy and the thermodynamic stability of black holes," *Physics Letters B*, vol. 752, pp. 306–310, 2016.

[86] C. Tsallis, "Possible generalization of Boltzmann-Gibbs statistics," *Journal of Statistical Physics*, vol. 52, no. 1-2, pp. 479–487, 1988.

[87] C. Tsallis, "The nonadditive entropy S_q and its applications in physics and elsewhere: some remarks," *Entropy*, vol. 13, article 1765, 2011.

[88] K. Abbasi and S. Gharaati, "Tsallisian gravity and cosmology," *Advances in High Energy Physics*, vol. 2020, Article ID 9362575, 6 pages, 2020.

[89] H. Moradpour, C. Corda, and A. H. Ziaie, "Tsallis uncertainty," 2020, https://arxiv.org/abs/2012.08316.

[90] E. M. Barboza Jr., R. D. Nunes, E. M. C. Abreu, and J. A. Neto, "Dark energy models through nonextensive Tsallis' statistics," *Physica A*, vol. 436, pp. 301–310, 2015.

[91] R. C. Nunes, E. M. Barboza Jr., E. M. C. Abreu, and J. A. Neto, "Probing the cosmological viability of non-Gaussian statistics," *Journal of Cosmology and Astroparticle Physics*, vol. 2016, 2016.

[92] G. K. Goswami, "Cosmological parameters for spatially flat dust filled Universe in Brans-Dicke theory," *Research in Astronomy and Astrophysics*, vol. 17, no. 3, p. 27, 2017.

[93] G. Hinshaw, D. Larson, E. Komatsu et al., "Nine-year Wilkinson Microwave Anisotropy Probe (WMAP) observations: cosmological parameter results," *The Astrophysical Journal Supplement Series*, vol. 208, p. 19, 2013.

[94] R. G. Cai, L. M. Cao, and Y. P. Hu, "Hawking radiation of an apparent horizon in a FRW universe," *Classical and Quantum Gravity*, vol. 26, no. 15, p. 155018, 2009.

[95] H. Kim, "Brans-Dicke theory as a unified model for dark matter-dark energy," *Monthly Notices of the Royal Astronomical Society*, vol. 364, no. 3, pp. 813–822, 2005.

[96] E. Calabrese, R. de Putter, D. Huterer, E. V. Linder, and A. Melchiorri, "Future CMB constraints on early, cold, or stressed dark energy," *Physical Review D*, vol. 83, no. 2, article 023011, 2011.

[97] S. Vagnozzi, L. Visinelli, O. Mena, and D. F. Mota, "Do we have any hope of detecting scattering between dark energy and baryons through cosmology?," *Monthly Notices of the Royal Astronomical Society*, vol. 493, no. 1, pp. 1139–1152, 2020.

Hindawi
Advances in High Energy Physics
Volume 2021, Article ID 6638827, 7 pages
https://doi.org/10.1155/2021/6638827

Research Article

Gravitational Collapse and Singularity Removal in Rastall Theory

Ehsan Dorrani

Department of Physics, Kahnooj Branch, Islamic Azad University, Kahnooj, Iran

Correspondence should be addressed to Ehsan Dorrani; ehsandorrani@gmail.com

Received 10 October 2020; Revised 22 November 2020; Accepted 12 February 2021; Published 28 February 2021

Academic Editor: Hooman Moradpour

In the present work, we study spherically symmetric gravitational collapse of a homogeneous fluid in the framework of Rastall gravity. Considering a nonlinear equation of state (EoS) for the fluid profiles, we search for a class of nonsingular collapse solutions and the possibility of singularity removal. We find that depending on the model parameters, the collapse scenario halts at a minimum value of the scale factor at which a bounce occurs. The collapse process then enters an expanding phase in the postbounce regime, and consequently the formation of a spacetime singularity is prevented. We also find that, in comparison to the singular case where the apparent horizon forms to cover the singularity, the formation of apparent horizon can be delayed allowing thus the bounce to be causally connected to the external universe. The nonsingular solutions we obtain satisfy the weak energy condition (WEC) which is crucial for physical validity of the model.

1. Introduction

The process of gravitational collapse of a massive object and its final outcome is one of the central questions in relativistic astrophysics and gravitation theory. In the framework of general relativity (GR), the Hawking and Penrose singularity theorems predict that under physically reasonable conditions, a continual collapse process leads to the formation of a spacetime singularity, that is, a spacetime event where densities and spacetime curvatures grow limitlessly and diverge [1]. During the last years, much attempts have been directed towards exploring different aspects of the gravitational collapse process and the studies along this line of research indicate that the spacetime singularity that forms as the collapse end product could be dressed by a spacetime event horizon (black hole formation) or visible by the observers in the universe (naked singularity formation) [2]. Usually, formation of a naked singularity as the collapse outcome is considered the violation of the cosmic censorship conjecture [3–5]. This conjecture states that singularities that form as the collapse final state will always be hidden by the event horizon of a black hole and cannot be visible to the observers in the universe [6] (see [7] for a recent review on this conjecture). However, during the past decades, many examples of naked singularity formation as possible counterexamples to the cosmic censorship conjecture have been reported in the literature, among which we can quote gravitational collapse of dust, perfect fluids, and radiation shells [8, 9]. Such a study has been extended to gravitational collapse in the presence of a cosmological constant term [10], higher dimensional collapse models [11–14], higher-order gravity theories [15], scalar field collapse [16–20], and self-similar collapse [21–23] (see also [2] for a recent review). Also, in the context of modified gravity theories, it is shown that naked singularities could form depending on different aspects of the theory (see, e.g., [24–30]).

Despite the fact that the formation of naked singularities may provide us a useful observational testbed for detecting high energy phenomena, these objects seem unpleasant as classical GR breaks down at the spacetime singularity. However, it is generally believed that such a singularity that forms in a classical regime can be avoided once quantum gravity corrections are taken into account. In this regard, a great amount of work has been devoted to investigate nonsingular collapse models, for example, corrections that may arise in the strong field regime, as obtained in the framework of some Loop Quantum Gravity (LQG) models [31–36]. Work along this line has been also extended to modified gravity models, e.g., singularity avoidance in Eddington-inspired

Born-Infeld theory [37], modified Gauss-Bonnet gravity [38, 39], Horava-Lifshitz gravity [40], nonminimal coupling of classical gravity with fermions [41], and other modified gravity theories [42].

In the light of the above considerations, one may be motivated to study modified gravity theories in the context of which the collapse scenario leads to a nontrivial outcome, different to singular collapse settings that have been studied in GR [9]. In this regard, one can generalize the standard GR to include a nonminimal coupling between geometry and matter fields. As we know, in most of the modified gravity theories, the energy-momentum source is characterized by a divergence-free tensor field which couples to the geometry in a minimal way [43, 44]. However, such a property of the energy-momentum tensor (EMT) which leads to the energy-momentum conservation law is not obeyed by the particle production process [45–48]. Hence, it seems reasonable to assume a nonvanishing divergence for EMT and seek for a modified gravitational theory whose geometrical degrees of freedom (not present in GR) may affect the final fate of the collapse. In this regard, one may relax the condition on EMT conservation law; i.e., mathematically the relation $\nabla_\mu T^\mu{}_\nu = 0$ is not valid anymore [49–55]. This idea was firstly put forward by Peter Rastall [54] who proposed a gravitational model in which the divergence of $T^\mu{}_\nu$ is proportional to the gradient of the Ricci scalar, i.e., $\nabla_\mu T^\mu{}_\nu \propto \nabla_\nu R$, so that the usual conservation law is recovered in the flat spacetime. This kind of modified gravity model has attracted a great deal of attention recently and is in good agreement with various observational data and theoretical expectations [56]. In the present article, we are motivated to investigate a simple model for gravitational collapse of an isotropic and homogeneous matter distribution with nonlinear EoS in Rastall gravity. We therefore proceed with considering the field equations in Rastall gravity in Section 2 and search for nonsingular collapse solutions in Section 3. Our conclusions are drawn in Section 4.

2. Field Equations of Rastall Gravity

According to the original idea of Rastall [54], the vanishing of covariant divergence of the matter energy-momentum tensor is no longer valid and this vector field is proportional to the covariant derivative of the Ricci curvature scalar as

$$\nabla_a T^a_b = \lambda \nabla_b \mathscr{R}, \tag{1}$$

where λ is the Rastall parameter. The Rastall field equations are then given by [54, 57]

$$G_{ab} + \gamma g_{ab} \mathscr{R} = \kappa T_{ab}, \tag{2}$$

where $\gamma = \kappa\lambda$ is the Rastall dimensionless parameter and κ is the Rastall gravitational coupling constant. The above equation can be rewritten in an equivalent form as

$$G_{ab} = \kappa T^{\text{eff}}_{ab}, \tag{3}$$

where

$$T^{\text{eff}}_{ab} = T_{ab} - \frac{\gamma T}{4\gamma - 1} g_{ab} \tag{4}$$

is the effective energy-momentum tensor whose components are given by [58, 59]

$$T^{\text{eff}\,0}_0 \equiv -\rho^{\text{eff}} = -\frac{(3\gamma - 1)\rho + \gamma(p_r + 2p_t)}{4\gamma - 1}, \tag{5}$$

$$T^{\text{eff}\,1}_1 \equiv p^{\text{eff}}_r = \frac{(3\gamma - 1)p_r + \gamma(\rho - 2p_t)}{4\gamma - 1}, \tag{6}$$

$$T^{\text{eff}\,2}_2 = T^{\text{eff}\,3}_3 \equiv p^{\text{eff}}_t = \frac{(2\gamma - 1)p_t + \gamma(\rho - p_r)}{4\gamma - 1}. \tag{7}$$

It is noteworthy that in the limit of $\lambda \to 0$, the standard GR is recovered. Moreover, for an electromagnetic field source, we get $T^{\text{eff}}_{ab} = T_{ab}$ leading to $G_{ab} = \kappa T_{ab}$. Therefore, the GR solutions for $T = 0$, or equivalently $R = 0$, are also valid (the Rastall gravity) [57, 60].

3. Solutions to the Field Equations

In the framework of classical GR, the continual gravitational collapse of a massive body under its own weight was investigated for the first time by Oppenheimer, Snyder, and Datt (OSD) [61, 62]. They considered the evolution of a spherically symmetric homogeneous dust cloud which starts from rest. The interior spacetime of such a collapse setting can be described by the Friedman-Robertson-Walker metric given by

$$ds^2 = -dt^2 + \frac{a^2(t)}{1 - kr^2} dr^2 + R^2(t, r) d\Omega^2, \tag{8}$$

where k determines the spatial curvature, $R(t, r) = ra(t)$ is the physical radius of the collapsing object, with $a(t)$ being the scale factor, and $d\Omega^2$ is the standard line element on the unit 2-sphere. The EMT of a pressureless matter is simply given by $T^a_b = \text{diag}\,(-\rho, 0, 0, 0)$, from which one can find the Einstein field equations as

$$\frac{3k}{a^2} + 3\frac{\dot{a}^2}{a^2} = 2\kappa_G \rho, \tag{9}$$

$$\frac{k}{a^2} + \frac{\dot{a}^2}{a^2} + 2\frac{\ddot{a}}{a} = 0, \tag{10}$$

where $\kappa_G = 4\pi G$. Also, the conservation of EMT ($\nabla_\alpha T^\alpha_\beta = 0$) gives $\rho = C/a^3$, where C is a constant. Substituting them for energy density into equation (9) along with defining the conformal time $d\eta = dt/a$, we arrive at the following solution for the scale factor:

$$a(\eta) = \frac{a_i}{2}(1 + \cos(\eta)), t(\eta) = \frac{a_i}{2}(\eta + \sin(\eta)), \tag{11}$$

where $0 \le \eta \le \pi$. The above solution describes the collapse process of a homogeneous dust fluid for which the scale factor starts from the finite value a_i at $(\tau, \eta) = (0, 0)$ and becomes zero at $(\tau, \eta) = (\pi a_i/2, \pi)$. The vanishing of the scale factor at a finite time signals the formation of a spacetime singularity, i.e., a spacetime event at which the energy density and curvature get arbitrary large values and diverge. It can be shown that the singularity in the OSD model is necessarily hidden by an event horizon and thus a black hole is formed as the end state of a homogeneous dust collapse (see, e.g., [63] for a review on the OSD model).

In the present section, we seek for a class of homogeneous collapse solutions for which the formation of spacetime singularity is avoided. We shall see that this is possible in case we generalize the OSD model from GR to Rastall gravity along with assuming a nonlinear EoS for the fluid pressure. To this aim, we begin with a homogeneous and isotropic interior line element representing a spatially nonflat FLRW geometry. The field equations for an isotropic source $(T^a_b = \text{diag}\,(-\rho, p, p, p))$ then read

$$3\frac{\dot{a}^2}{a^2} + \frac{3\mathrm{k}}{a^2} = \kappa\rho_{\text{eff}} = \frac{2\kappa_G}{6\gamma - 1}[(3\gamma - 1)\rho + 3\gamma p], \tag{12}$$

$$2\frac{\ddot{a}}{a} + \frac{\dot{a}^2}{a^2} + \frac{k}{a^2} = -\kappa p_{\text{eff}} = \frac{2\kappa_G}{6\gamma - 1}[(1 - \gamma)p - \gamma\rho]. \tag{13}$$

Applying the Bianchi identity on equation (3) leaves us with the following continuity equation in Rastall gravity as

$$\left(\frac{3\gamma - 1}{4\gamma - 1}\right)\dot{\rho} + \left(\frac{3\gamma}{4\gamma - 1}\right)\dot{p} + 3H(\rho + p) = 0. \tag{14}$$

Next, we proceed to build and study collapse scenarios assuming a polytropic EoS $p = \alpha\rho^\beta$, where α and β are constants. Equation (14) can be solved for this EoS, and the solution reads

$$\ln(a) + \ln\left(\rho^{\beta(a_1+a_2)/3(\beta-1)}\left(\rho + \alpha\rho^\beta\right)^{-(a_1+\beta a_2)/3(\beta-1)}\right) + C_0 = 0, \tag{15}$$

where C_0 is an integration constant and

$$a_1 = \frac{1 - 3\gamma}{1 - 4\gamma}, a_2 = \frac{3\gamma}{1 - 4\gamma}, \beta \neq 1. \tag{16}$$

In order to find an explicit expression for energy density, we set $a_1 = -\beta a_2$ within equation (15). This gives

$$\rho(a) = \rho_i\left(\frac{a}{a_i}\right)^{3(4\gamma-1)/(3\gamma-1)}, \tag{17}$$

where $\rho_i = \rho(t_i)$ and $a_i = a(t_i)$ are the initial values of energy density and scale factor, respectively, and $t = t_i$ is the initial time at which the collapse begins. Equations (12) and (13) can then be rewritten as (we set the units so that $2\kappa_G = 1$)

$$3\frac{\dot{a}^2}{a^2} + \frac{3k}{a^2} = \frac{6\alpha\gamma\rho_i^{(3\gamma-1)/3\gamma}}{6\gamma - 1}\left(\frac{a_i}{a}\right)^{(4\gamma-1)/\gamma} + \rho_i\left(\frac{a_i}{a}\right)^{3(4\gamma-1)/(3\gamma-1)}, \tag{18}$$

$$2\frac{\ddot{a}}{a} + \frac{\dot{a}^2}{a^2} + \frac{k}{a^2} = \frac{2(1 - \gamma)}{6\gamma - 1}\rho_i^{(3\gamma-1)/3\gamma}\left(\frac{a_i}{a}\right)^{(4\gamma-1)/\gamma} - \frac{2\gamma}{6\gamma - 1}\rho_i\left(\frac{a_i}{a}\right)^{3(4\gamma-1)/(3\gamma-1)}. \tag{19}$$

Next, we proceed to study the collapse dynamics using numerical methods in order to solve equation (19). We further employ equation (18) to find the initial condition on the speed of collapse which is given by

$$\dot{a}(t_i) = -\left[\frac{3ka_i^2(1 - 6\gamma) + 2\rho_i a_i^4\left(3\gamma\left(1 + \alpha\rho_i^{-1/3\gamma}\right) - 1\right)}{3a_i^2(6\gamma - 1)}\right]^{1/2}. \tag{20}$$

Figure 1(a) shows the numerical solution to equation (19) for a closed geometry ($k = 1$) and different values of the Rastall parameter. As we observe, the collapse starts its evolution by a finite velocity, i.e., $\dot{a}_i < 0$ and continues through a contracting regime until the bounce time $t = t_b$ is reached. At this time, the collapse process halts at a nonzero minimum value of the scale factor so that we have $a_{\min} = a(t_b)$ and $\dot{a}(t_b) = 0$ (see also Figure 1(b)). This minimum value of the scale factor can be obtained through equation (18) as

$$\frac{2\rho_i}{6\gamma - 1}\left(\frac{a_i}{a_{\min}}\right)^4\left[\left(\frac{a_i}{a_{\min}}\right)^{1/(3\gamma-1)}(3\gamma - 1) + 3\left(\frac{a_i}{a_{\min}}\right)^{-1/\gamma}\alpha\gamma\rho_i^{-1/3\gamma}\right] - 3a_{\min}^{-2} = 0. \tag{21}$$

From Figure 1(a), we also note that the Rastall parameter could change the minimum value of the scale factor and the bounce time in such a way that the larger the values of the γ parameter, the greater the value of $a_{\min}$ and the sooner the bounce occurs. For $t > t_b$, the contracting regime switches to an expanding regime and the collapsing body disperses as the time passes. We also observe that the case of $\gamma = 0$ corresponds to the GR limit of the theory where the gravitational collapse process leads to singularity formation (see the dashed curve). Figure 1(c) shows the behavior of collapse acceleration. We therefore observe that the collapse experiences four phases during its dynamical evolution. (i) During the time interval at which $\dot{a} < 0$ and $\ddot{a} < 0$, the collapse undergoes an accelerated contracting regime. (ii) As time goes by, the collapse enters a decelerated contracting regime where $\dot{a} < 0$ and $\ddot{a} > 0$. (iii) After the bounce time, the collapse turns into an accelerated expanding phase for which $\dot{a} > 0$ and $\ddot{a} > 0$. (iv) Finally, at later times, the collapse enters a decelerated expanding regime where $\dot{a} > 0$ and $\ddot{a} < 0$.

For the sake of physical reasonability, we require that the weak energy condition (WEC) be satisfied. According to this condition, the energy density as measured by any local observer must be positive. Hence, for the energy-

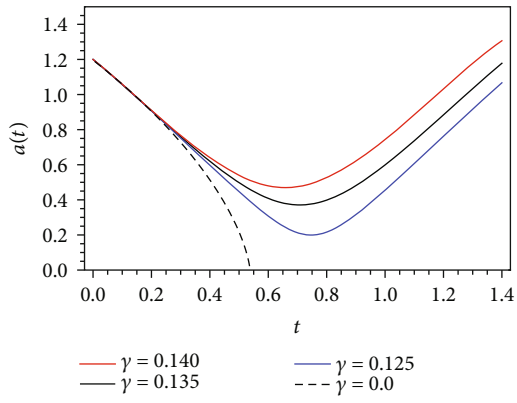

(a)

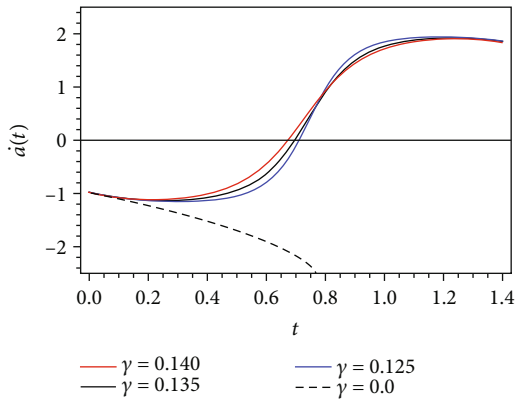

(b)

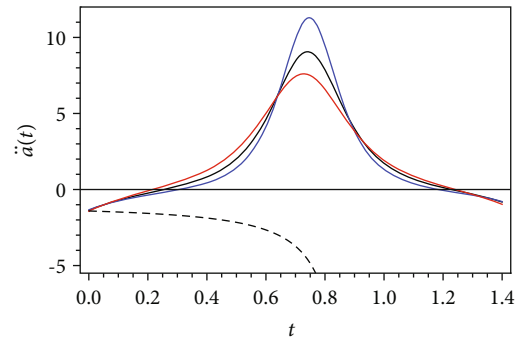

(c)

FIGURE 1: (a) The behavior of the scale factor over time for $a_i = 1.2$, $\rho_i = 2.0$, and $\alpha = 4.24$. (b) The behavior of speed of collapse for the same values of the parameters as chosen above. (c) The behavior of acceleration of collapse for the same values of the parameters as chosen above.

momentum tensor of ordinary matter and the effective fluid, the conditions

$$\rho \geq 0, \rho + p \geq 0, \tag{22}$$

$$\rho_{\text{eff}} \geq 0, \rho_{\text{eff}} + p_{\text{eff}} \geq 0 \tag{23}$$

must be satisfied along any nonspacelike vector field. In Figure 2(a), we have plotted for energy density the WEC

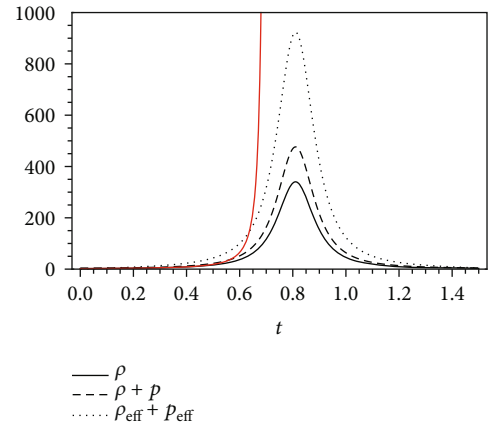

(a)

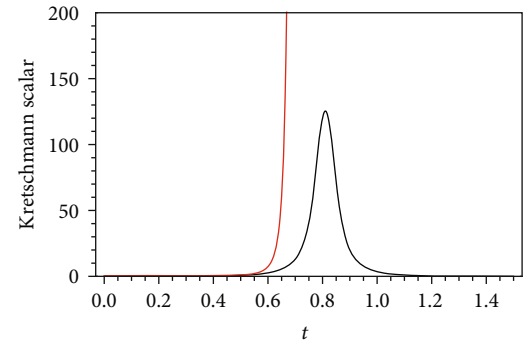

(b)

FIGURE 2: (a) The behavior of energy density over time for $a_i = 1.2$, $\rho_i = 2.0$, $\alpha = 4.24$, and $\gamma = 0.14$. The red curve stands for the case with $\gamma = 0$. (b) The behavior of the Kretschmann scalar for the same values of the parameters as chosen above.

for ordinary EMT and the WEC for effective EMT. We also observe that in the limit where $\gamma \to 0$, the energy density diverges signaling the occurrence of a spacetime singularity (see the red curve). Another quantity that the divergence of which implies singularity formation is the Kretschmann scalar defined as

$$\mathcal{K} = \mathcal{R}_{\alpha\beta\delta\varepsilon}\mathcal{R}^{\alpha\beta\delta\varepsilon} = \dot{H}^2 + 2H^4 + 2H^2\dot{H} = \frac{4\ell(1 - 3\gamma(+w))^2}{81(1+w)^4(1-4\gamma)^4(t-t_s)^4}. \tag{24}$$

In Figure 2(a), we have plotted for the behavior of this quantity where we observe that the Kretschmann scalar behaves regularly and is finite throughout the collapse process (black solid curve), while, for $\gamma = 0$ (red curve), this quantity grows unboundedly and diverges at the singularity. We also note that for $\beta = 0$ the results of [64] will be recovered.

An important issue that needs to be examined in each collapse setting is the study of dynamics of apparent horizon and causal structure of spacetime during the evolution of the collapse process. The apparent horizon is the outermost boundary of the trapped region, and the condition for its

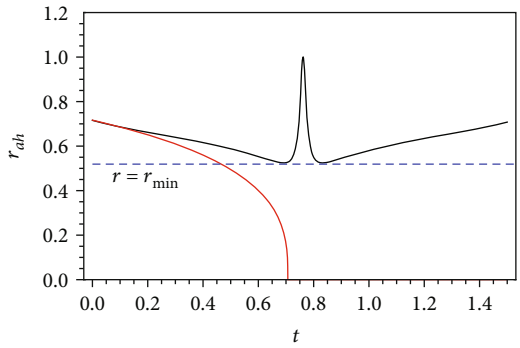

FIGURE 3: The behavior of the apparent horizon curve over time for $a_i = 1.2$, $\rho_i = 2.0$, $\alpha = 4.24$, and $\gamma = 0.14$. The red curve stands for the case with $\gamma = 0$.

formation is provided by the requirement that the surface with $R(t, r) = \text{Constant}$ is lightlike or in other words $g^{\mu\nu}\partial_\mu R\,\partial_\nu R = 0$ [9]. This condition for our model reduces to $\dot{R}^2 + r^2 = 1$ from which we can find the radius of the apparent horizon as

$$r_{ah} = \frac{1}{\sqrt{\dot{a}^2 + 1}}. \tag{25}$$

In Figure 3, we have plotted for the radius of the apparent horizon and compared the cases with $\gamma = 0.14$ and $\gamma = 0$. In the former (black solid curve), we observe that during the collapse process, the apparent horizon radius decreases to the minimum value $r = r_{\min}$ and then reaches a maximum value at the bounce time. It then converges to the same minimum radius in the postbounce regime. The apparent horizon curve will never vanish; i.e., it will never hit the singularity at $R = 0$, in contrast to the case with $\gamma = 0$ where the apparent horizon covers the singularity at a finite amount of time, leading to black hole formation (see the red curve).

4. Concluding Remarks

In this work, we studied the process of gravitational collapse of an isotropic homogeneous fluid which obeys a nonlinear EoS, i.e., $p = \alpha\rho^\beta$, between energy density and pressure profile. We found that, depending on the model parameters, nonsingular collapse solutions can be obtained in such a way that the collapse starts from regular initial data, proceeds for a while, and halts at a bounce time at which the scale factor reaches its minimum value. Then, after the bounce time is passed, the collapse scenario turns into an expanding phase. We further observed that the energy density and Kretschmann scalar behave regularly and are finite throughout the contracting and expanding regimes. In this regard, the spacetime singularity which is present in the OSD collapse model is avoided. Also, for the singular model, the apparent horizon necessarily forms to cover the singularity whereas in the model described herein, the initial radius of the collapsing matter $(R(t_i, r) = r)$ can be chosen as $r < r_{\min}$. In this case, the horizon formation is prevented, and thus, the bounce can be visible to faraway observers in the universe. As the Rastall parameter is a measure of ability of matter and curvature to interact with each other, we therefore conclude that such an ability can provide a setting in which the formation of spacetime singularities is avoided in a gravitational collapse process.

As the final remarks, it is noteworthy that the present collapse scenario can be compared to other collapse settings such as gravitational collapse of a homogeneous Weyssenhoff fluid in the framework of Einstein-Cartan gravity [65]. The Weyssenhoff fluid is a generalization of a perfect fluid in GR to include the intrinsic angular momentum (spin) of the fermionic matter field. Comparing equations (18) and (19) with the corresponding equations given in [65], we observe that for $\gamma = -1/2$, the collapse dynamics presented in this work mimics that of a Weyssenhoff fluid with EoS $w = 1/5$. Although a more detailed and in-depth analysis is needed in order to understand the correspondence between the two theories, one may intuitively imagine a possible relation between matter-curvature coupling in Rastall theory and spacetime torsion in Einstein-Cartan gravity. It is also worth mentioning that the exterior spacetime of the collapsing body can be obtained by matching the interior spacetime through a timelike hypersurface to an exterior Vaidya spacetime [66–68], using Israel-Darmois junction conditions [69]. By doing so, one can show that in the framework of the present study, the exterior region of the collapsing object is a Schwarzschild spacetime with dynamical boundary [64, 65].

Data Availability

The data used to support the findings of this study are available from the corresponding author upon request.

Conflicts of Interest

The author declares that he has no conflicts of interest.

References

[1] S. W. Hawking and G. F. R. Ellis, *The Large Scale Structure of Space-Time*, Cambridge University Press, 1973.

[2] P. S. Joshi and D. Malafarina, "Recent developments in gravitational collapse and spacetime singularities," *International Journal of Modern Physics D: Gravitation; Astrophysics and Cosmology*, vol. 20, no. 14, pp. 2641–2729, 2011.

[3] R. Penrose, "Gravitational collapse: the role of general relativity," *Nuovo Cimento Rivista Serie*, vol. 1, p. 252, 1969.

[4] R. Penrose, ""Golden Oldie": gravitational collapse: the role of general relativity," *General Relativity and Gravitation*, vol. 34, no. 7, pp. 1141–1165, 2002.

[5] R. M. Wald, *Black holes and relativistic stars*, University of Chicago Press, 1998.

[6] P. S. Joshi, "Spacetime singularities," in *Springer Handbook of Spacetime*, p. 409, Springer Berlin Heidelberg, Germany, 2014.

[7] Y. C. Ong, "Space–time singularities and cosmic censorship conjecture: a review with some thoughts," *International Journal of Modern Physics A: Particles and Fields; Gravitation; Cosmology; Nuclear Physics*, vol. 35, no. 14, article 2030007, 2020.

[8] P. S. Joshi, *Global Aspects in Gravitation and Cosmology*, Oxford University Press, Oxford, 1993.

[9] P. S. Joshi, *Gravitational Collapse and Space-Time Singularities*, Cambridge University Press, Cambridge, 2007.

[10] S. S. Deshingkar, S. Jhingan, A. Chamorro, and P. S. Joshi, "Gravitational collapse and the cosmological constant," *Physical Review D*, vol. 63, no. 12, article 124005, 2001.

[11] U. Miyamoto, H. Nemoto, and M. Shimano, "Naked singularity explosion in higher dimensions," *Physical Review D*, vol. 84, no. 6, article 064045, 2011.

[12] N. Dadhich, S. G. Ghosh, and S. Jhingan, "Gravitational collapse in pure Lovelock gravity in higher dimensions," *Physical Review D*, vol. 88, no. 8, article 084024, 2013.

[13] M. Shimano and U. Miyamoto, "Naked singularity explosion in higher-dimensional dust collapse," *Classical and Quantum Gravity*, vol. 31, no. 4, article 045002, 2014.

[14] S. G. Ghosh and A. Beesham, "Naked singularities in higher dimensional inhomogeneous dust collapse," *Classical and Quantum Gravity*, vol. 17, no. 24, pp. 4959–4965, 2000.

[15] R. Giambo, "Gravitational collapse of homogeneous perfect fluids in higher order gravity theories," *Journal of Mathematical Physics*, vol. 50, no. 1, article 012501, 2009.

[16] M. D. Roberts, "Scalar field counterexamples to the cosmic censorship hypothesis," *General relativity and gravitation*, vol. 21, no. 9, pp. 907–939, 1989.

[17] P. R. Brady, "Self-similar scalar field collapse: naked singularities and critical behavior," *Physical Review D*, vol. 51, no. 8, pp. 4168–4176, 1995.

[18] M. W. Choptuik, "Universality and scaling in gravitational collapse of a massless scalar field," *Physical Review Letters*, vol. 70, no. 1, pp. 9–12, 1993.

[19] V. Husain, E. A. Martinez, and D. Nunez, "Exact solution for scalar field collapse," *Physical Review D*, vol. 50, no. 6, pp. 3783–3786, 1994.

[20] K. Ganguly and N. Banerjee, "Pramana," *Journal de Physique*, vol. 80, no. 3, pp. 439–448, 2013.

[21] P. S. Joshi and I. H. Dwivedi, "The structure of naked singularity in self-similar gravitational collapse," *Communications in Mathematical Physics*, vol. 146, no. 2, pp. 333–342, 1992.

[22] C. F. C. Brandt, R. Chan, M. F. A. Da Silva, and J. F. Villas da Rocha, "Gravitational collapse of an anisotropic fluid with self-similarity of the second kind," *International Journal of Modern Physics D: Gravitation; Astrophysics and Cosmology*, vol. 15, no. 9, pp. 1407–1417, 2006.

[23] C. F. C. Brandt, L.-M. Lin, J. F. Villas da Rocha, and A. Z. Wang, "Gravitational collapse of spherically symmetric perfect fluid with kinematic self-similarity," *International Journal of Modern Physics D: Gravitation; Astrophysics and Cosmology*, vol. 11, no. 2, pp. 155–186, 2002.

[24] R. Garattini, "Naked singularity in modified gravity theory," *Journal of Physics Conference Series*, vol. 174, article 012066, 2009.

[25] A. H. Ziaie, K. Atazadeh, and Y. Tavakoli, "Naked singularity formation in Brans–Dicke theory," *Classical and quantum gravity*, vol. 27, no. 7, article 075016, 2010.

[26] A. H. Ziaie, K. Atazadeh, and S. M. M. Rasouli, "Naked singularity formation in $f(\mathscr{R})$ gravity," *General Relativity and Gravitation*, vol. 43, no. 11, pp. 2943–2963, 2011.

[27] S. G. Ghosh and S. D. Maharaj, "Gravitational collapse of null dust inf(R)gravity," *Physical Review D*, vol. 85, no. 12, p. 124064, 2012.

[28] A. H. Ziaie, A. Ranjbar, and H. R. Sepangi, "Trapped surfaces and the nature of singularity in Lyra's geometry," *Classical and Quantum Gravity*, vol. 32, no. 2, article 025010, 2015.

[29] G. Abbas and M. Tahir, "Gravitational perfect fluid collapse in Gauss–Bonnet gravity," *European Physical Journal C: Particles and Fields*, vol. 77, no. 8, p. 537, 2017.

[30] R. Shaikh and P. S. Joshi, "Gravitational collapse in (2+1)-dimensional Eddington-inspired Born-Infeld gravity," *Physical Review D*, vol. 98, no. 2, article 024033, 2018.

[31] C. Bambi, D. Malafarina, and L. Modesto, "Non-singular quantum-inspired gravitational collapse," *Physical Review D*, vol. 88, no. 4, article 044009, 2013.

[32] M. Bojowald, R. Goswami, R. Maartens, and P. Singh, "Black hole mass threshold from nonsingular quantum gravitational collapse," *Physical Review Letters*, vol. 95, no. 9, article 091302, 2005.

[33] R. Goswami, P. S. Joshi, and P. Singh, "Quantum evaporation of a naked singularity," *Physical Review Letters*, vol. 96, no. 3, article 031302, 2006.

[34] Y. Tavakoli, J. Marto, and A. Dapor, "Semiclassical dynamics of horizons in spherically symmetric collapse," *International Journal of Modern Physics D: Gravitation; Astrophysics and Cosmology*, vol. 23, no. 7, article 1450061, 2014.

[35] C. Bambi, D. Malafarina, and L. Modesto, "Terminating black holes in asymptotically free quantum gravity," *European Physical Journal C: Particles and Fields*, vol. 74, no. 2, p. 2767, 2014.

[36] C. Barcelo, S. Liberati, S. Sonego, and M. Visser, "Fate of gravitational collapse in semiclassical gravity," *Physical Review D*, vol. 77, no. 4, article 044032, 2008.

[37] Y. Tavakoli, C. Escamilla-Rivera, and J. C. Fabris, "The final state of gravitational collapse in Eddington-inspired Born-Infeld theory," *Annalen der Physik*, vol. 529, no. 5, article 1600415, 2017.

[38] K. Bamba, S. D. Odintsov, L. Sebastiani, and S. Zerbini, "Finite-time future singularities in modified Gauss–Bonnet and $\mathscr{F}$(R,G) gravity and singularity avoidance," *European Physical Journal C: Particles and Fields*, vol. 67, no. 1-2, pp. 295–310, 2010.

[39] O. Gorbunova and L. Sebastiani, "Viscous fluids and Gauss–Bonnet modified gravity," *General Relativity and Gravitation*, vol. 42, no. 12, pp. 2873–2890, 2010.

[40] Y. Misonoh, M. Fukushima, and S. Miyashita, "Stability of singularity-free cosmological solutions in Hořava-Lifshitz gravity," *Physical Review D*, vol. 95, no. 4, article 044044, 2017.

[41] C. Bambi, D. Malafarina, A. Marciano, and L. Modesto, "Singularity avoidance in classical gravity from four-fermion interaction," *Physics Letters B*, vol. 734, pp. 27–30, 2014.

[42] R. Myrzakulov, L. Sebastiani, and S. Zerbini, "Some aspects of generalized modified gravity models," *International Journal of Modern Physics D: Gravitation; Astrophysics and Cosmology*, vol. 22, no. 8, article 1330017, 2013.

[43] F. S. N. Lobo, "Beyond Einstein's general relativity," *Journal of Physics Conference Series*, vol. 600, article 012006, 2015.

[44] V. Faraoni, S. Capozziello, S. Capozziello, and V. Faraoni, "The landscape beyond Einstein gravity," in *Beyond Einstein Gravity*, pp. 59–106, Springer, Dordrecht, 2011.

[45] N. D. Birrell and P. C. W. Davies, *Quantum Fields in Curved Space*, Cambridge University Press, Cambridge, 1982.

[46] G. W. Gibbons and S. W. Hawking, "Cosmological event horizons, thermodynamics, and particle creation," *Physical Review D*, vol. 15, no. 10, pp. 2738–2751, 1977.

[47] L. Parker, "Quantized fields and particle creation in expanding universes. II," *Physical Review D*, vol. 3, no. 2, pp. 346–356, 1971.

[48] L. H. Ford, "Gravitational particle creation and inflation," *Physical Review D*, vol. 35, no. 10, pp. 2955–2960, 1987.

[49] S. Nojiri and S. D. Odintsov, "Gravity assisted dark energy dominance and cosmic acceleration," *Physics Letters B*, vol. 599, no. 3-4, pp. 137–142, 2004.

[50] G. Allemandi, A. Borowiec, M. Francaviglia, and S. D. Odintsov, "Dark energy dominance and cosmic acceleration in first-order formalism," *Physical Review D*, vol. 72, no. 6, article 063505, 2005.

[51] T. Koivisto, "A note on covariant conservation of energy–momentum in modified gravities," *Classical and Quantum Gravity*, vol. 23, no. 12, pp. 4289–4296, 2006.

[52] O. Bertolami, C. G. Böhmer, T. Harko, and F. S. N. Lobo, "Extra force in f(R) modified theories of gravity," *Physical Review D*, vol. 75, no. 10, article 104016, 2007.

[53] T. Harko and F. S. N. Lobo, "Generalized curvature-matter couplings in modified gravity," *Galaxies*, vol. 2, no. 3, pp. 410–465, 2014.

[54] P. Rastall, "Generalization of the Einstein theory," *Physical Review D*, vol. 6, no. 12, pp. 3357–3359, 1972.

[55] H. Moradpour, Y. Heydarzade, F. Darabi, and I. G. Salako, "A generalization to the Rastall theory and cosmic eras," *European Physical Journal C: Particles and Fields*, vol. 77, no. 4, p. 259, 2017.

[56] F. Darabi, H. Moradpour, I. Licata, Y. Heydarzade, and C. Corda, "Einstein and Rastall theories of gravitation in comparison," *The European Physical Journal C*, vol. 78, no. 1, 2018.

[57] A. S. Al-Rawaf and M. O. Taha, "A resolution of the cosmological age puzzle," *Physics Letters B*, vol. 366, no. 1-4, pp. 69–71, 1996.

[58] A. S. Al-Rawaf and M. O. Taha, "Cosmology of general relativity without energy-momentum conservation," *General Relativity and Gravitation*, vol. 28, no. 8, pp. 935–952, 1996.

[59] H. Moradpour, N. Sadeghnezhad, and S. H. Hendi, "Traversable asymptotically flat wormholes in Rastall gravity," *Canadian Journal of Physics*, vol. 95, no. 12, pp. 1257–1266, 2017.

[60] K. A. Bronnikov, J. C. Fabris, O. F. Piattella, and E. C. Santos, "Static, spherically symmetric solutions with a scalar field in Rastall gravity," *General Relativity and Gravitation*, vol. 48, no. 12, p. 162, 2016.

[61] J. R. Oppenheimer and H. Snyder, "On continued gravitational contraction," *Physics Review*, vol. 56, no. 5, pp. 455–459, 1939.

[62] S. Datt, "Über eine klasse von Lösungen der gravitationsgleichungen der relativität," *Zeitschrift für Physik*, vol. 108, no. 5-6, pp. 314–321, 1938.

[63] T. W. Baumgarte and S. L. Shapiro, *Numerical relativity: solving Einstein's equations on the computer*, Cambridge University Press, Cambridge, 2010.

[64] A. H. Ziaie, H. Moradpour, and S. Ghaffari, "Gravitational collapse in Rastall gravity," *Physics Letters B*, vol. 793, pp. 276–280, 2019.

[65] M. Hashemi, S. Jalalzadeh, and A. H. Ziaie, "Collapse and dispersal of a homogeneous spin fluid in Einstein–Cartan theory," *European Physical Journal C: Particles and Fields*, vol. 75, no. 2, p. 53, 2015.

[66] P. C. Vaidya, "The gravitational field of a radiating star," *Proceedings of the Indian Academy of Sciences-Section A*, vol. 33, no. 5, p. 264, 1951.

[67] N. O. Santos, "Non-adiabatic radiating collapse," *Monthly Notices of the Royal Astronomical Society*, vol. 216, no. 2, pp. 403–410, 1985.

[68] W. B. Bonnor, A. K. G. de Oliveira, and N. O. Santos, "Radiating spherical collapse," *Physics Reports*, vol. 181, no. 5, pp. 269–326, 1989.

[69] W. Israel, "Singular hypersurfaces and thin shells in general relativity," *Il Nuovo Cimento B (1965-1970)*, vol. 44, no. 1, pp. 1–14, 1966.

Hindawi
Advances in High Energy Physics
Volume 2020, Article ID 9362575, 6 pages
https://doi.org/10.1155/2020/9362575

Research Article

Tsallisian Gravity and Cosmology

Kavoos Abbasi and Shirvan Gharaati

Department of Physics, College of Sciences, Yasouj University, Yasouj 75918-74831, Iran

Correspondence should be addressed to Kavoos Abbasi; kabbasi@yu.ac.ir

Received 4 August 2020; Revised 9 September 2020; Accepted 25 September 2020; Published 7 October 2020

Academic Editor: Hooman Moradpour

In this paper, we adopt the Verlinde hypothesis on the origin of gravity as the consequence of the tendency of systems to increase their entropy and employ the Tsallis statistics. Thereinafter, modifications to the Newtonian second law of motion, its gravity, and radial velocity profile are studied. In addition, and in a classical framework, the corresponding cosmology and also its ability in describing the inflationary phases are investigated.

1. Introduction

The study of the relation between thermodynamics and gravity has a long history [1–7]. On the one hand, Gibbs shows that gravitational systems are not extensive [1], a conclusion in agreement with the Bekenstein entropy of black holes [2], which is a nonextensive entropy. On the other, it seems that all gravitational systems satisfy the Bekenstein entropy bound expressed as [8]

$$S_{BE} = \frac{Ac^3}{4G\hbar}, \tag{1}$$

where $A = 4\pi R^2$ and R denote the area of the system boundary and its radius, respectively, and k_B (Boltzmann constant). Using this entropy and Clausius relation, one can show that the Einstein gravitational field is in fact a thermodynamic equation of state [9]. This amazing result is valid in various gravitational and cosmological setups which lead to notable predictions about the behavior of cosmos and gravitational systems [10–30]. Motivated by the Gibbs work [1], the nonextensivity of the Bekenstein entropy, and based on the long-range nature of gravity [31], recently, the use of nonextensive statistical mechanics (based on possible generalizations of Gibbs entropy) has been proposed to model and study some phenomena such as the cosmic evolution [32–39], black holes [40–49], and Jeans mass [50, 51].

In order to find the probable thermodynamic aspects of gravity, Verlinde describes it as the implication of the tendency of systems to increase their entropy [52], an astonishing approach which attracts investigators to itself [53–65]. In the framework of generalized entropies, the Verlinde hypothesis leads to significant implications on the cosmic evolution [35, 66–68], Newtonian gravity [69], Jeans mass (as a stability criterion) [70], and also gravitational systems [71–76]. Indeed, the differences between generalized entropies and the Bekenstein entropy, originated from the nonextensive viewpoint, can (i) describe the universe inflationary phases [32–34, 39], (ii) relate Padmanabhan emergent gravity scenario to the Verlinde hypothesis [32], and (iii) propose an origin for the MOND theory [69].

Based on the Verlinde hypothesis [52], the entropy change of a system increases as

$$\Delta S = 2\pi \frac{mc}{\hbar} \Delta x, \tag{2}$$

when the test mass m has distance $\Delta x = \hbar/mc \equiv \lambda_c$ (reduced Compton wavelength) with respect to the holographic screen (boundary of system). This screen consists of N degrees of freedom calculated by

$$N = \frac{Ac^3}{G\hbar}, \tag{3}$$

in agreement with Eq.(1) and thus $S_{BE} = N/4$ [2]. Following [55, 56], we assume $\Delta x = \eta\lambda_c$ from now, and use the Unruh temperature [7]

$$T = \frac{1}{2\pi}\frac{\hbar a}{c}, \tag{4}$$

to get [55, 56]

$$F = T\frac{\Delta S}{\Delta x} = T\frac{dS}{dA}\frac{\Delta A}{\Delta x} = ma, \tag{5}$$

as the net force that source M applies to particle m, which finally brings it acceleration a. Indeed, this result is available if $\eta = 1/8\pi$ leading to $\Delta x = \lambda_c/8\pi$, to get Eq. (5). Now, combining $A = 4\pi R^2$ and Eq. (3) with

$$E = \frac{1}{2}NT = Mc^2, \tag{6}$$

and using Eq. (5), one easily reaches at Newtonian gravity

$$a = G\frac{M}{R^2}. \tag{7}$$

It is also useful to mention that it seems there is a deep connection between generalized entropies and quantum gravity scenarios, and indeed, quantum aspects of gravity may also be considered as another motivation for considering generalized entropies [77, 78]. Tsallis entropy is one of the generalized entropy measures which leads to acceptable results in the cosmological and gravitational setups [32, 36, 40, 47, 49]. In fact, there are two Tsallis entropies [40, 47, 49]. One of them has been proposed by Tsallis and Cirto [40] which is confirmed by the multifractal structure of horizon in quantum gravity [78] and modifies Eq. (1) as $S \sim A^{\delta}$ (δ is a free unknown parameter [77]).

The second one has recently been calculated in [49] by relying on statistical properties of degrees of freedom distributed on the holographic screen. The result is compatible with a detailed study in the framework of quantum gravity [47]. This case proposes an exponential relation between the horizon entropy and its surface, and we will focus on it in this paper. In the next section, modifications to the Newtonian second law of motion and also Newtonian gravity is derived by using the Tsallis entropy. Its implications on the radial velocity are also addressed. In the third section, after evaluating the Tsallis modification to the gravitational potential, we adopt the approach of paper [79] and find out the corresponding Friedmann first equation in a classical way in which a test mass is located on the edge of the universe, namely apparent horizon [79]. The possibility of obtaining an accelerated universe is also debated in this section. A summary of the work is presented in the last section.

2. Tsallis Gravity and Dynamics

Employing the Tsallis statistics, it has been recently shown that Eq. (1) is modified as [49]

$$S_q^T = \frac{1}{1-q}\left[\exp\left((1-q)S_{BE}\right) - 1\right], \tag{8}$$

in full agreement with quantum gravity calculations [47]. Here, q is a free parameter evaluated from other parts of physics and also observations, and Eq. (1) is recovered when $q = 1$ [31, 47, 49]. In the nonextensive scenarios, Eq. (6) takes the form [35, 80]

$$E = \frac{1}{5-3q}NT = Mc^2, \tag{9}$$

which approaches Eq. (1) at the appropriate limit of $q = 1$.

Now, following the recipe which led to Eq. (5), one can use Eq. (8) to find

$$F^T = T\frac{dS_q^T}{dA}\frac{\Delta A}{\Delta x} = ma\ \exp\left(\delta\frac{(2+3\delta)Mc^3\pi}{2\hbar a}\right), \tag{10}$$

where $\delta = 1 - q$ is the Tsallis second law of motion. Clearly, Eq. (5) is recovered whenever $\delta = 0$, and therefore, this approach claims the net force F^T that source M applies to m depends on M. In order to obtain the above result, we used $S_{BE} = N/4$ [2], and $N = ((5-3q)Mc^2)/T$. Of course, since the relation $F = ma$ works very well (classical regime), one can deduce that δ is very close to 0 meaning that the exponential factor may have nonsensible effects in the classical regime.

The modified form of Eq. (7), called Tsallis gravity, is also obtained as

$$a^T = G_q\frac{M}{R^2}\ \exp\left(\delta\frac{R_0^2}{R^2}\right), \tag{11}$$

where $R_0^2 \equiv G\hbar/c^3\pi = l_P^2/\pi$, l_P denotes the Planck length, and $G_q \equiv ((5-3q)/2)G$ in full agreement with [35]. In order to have a comparison between the Tsallis second law of motion and also the Tsallis gravity and those of Newton, let us write

$$\begin{aligned}\frac{F^T}{F} &= \exp\left(\frac{d}{a}\right),\\ \frac{a^T}{a} &= (5-3q)\exp\left(\frac{l}{R^2}\right),\end{aligned} \tag{12}$$

where $d \equiv \delta((2+3\delta)Mc^3\pi)/2\hbar$ and $l = \delta R_0^2$. As a crucial point, one should note that, for an event, the sign of a and a^T should be the same (the predictions of different theories about the value of accelerations should address the same motion meaning that both of a^T and a should have the same sign). It leads to this limitation $q < 5/3$ meaning that $\delta > -2/5$. Thus, l and d can be negative.

Now, let us compare Eq. (11) with the results of [55] and [56] where authors employ different entropies in the

framework of the Verlinde theory and address two modifications for the Newtonian gravity. Unlike Eq. (11) of [11], the modified gravity obtained in [55] (Eq. (17)) diverges at large distances ($R \gg 1$). Of course, both of them claim that the gravitational force between the source M and test particle m can vanish for some points on their interface line, a property incompatible with the Newtonian gravity and experience. From Eq. (11), one can easily see that the obtained gravitational force does not diverge at large distances where it will be ignorable. Thus, it seems that this equation is a more reliable modification to the Newtonian gravity compared with those of [55, 56].

2.1. Velocity Profile. For a circular motion at radius r with velocity v, and thus acceleration $(v^2/r)(\equiv a^T)$ obeying Eq. (11), one reaches

$$v = \sqrt{\frac{G_q M}{r}} \exp\left(\frac{l}{2r^2}\right), \tag{13}$$

which implies that we should have $q < 5/3$ to get real values of velocity.

On the other hand, if one assumes the mass m in the gravitational field of source M feels the force GMm/r^2, then using (10), we can write

$$GMm/r^2 = F^T, \tag{14}$$

yields

$$GM/r = v^2 \exp\left(\frac{dr}{v^2}\right), \tag{15}$$

for $a \equiv (v^2/r)$, finally leading to

$$v^2 \cong \frac{Gm}{r} - dr \tag{16}$$

if we expand $\exp(dr/v^2)$ as $1 + (dr/v^2)$. For a constant d, this approximation is valid when radial acceleration (v^2/r) is small. Indeed, in this manner, the dr term leads to an increase in the velocity of particle m, compared with the Newtonian case for which $v^2 \cong (Gm/r)$, if $d < 0$.

3. A Tsallis Cosmology

In order to find the Friedmann first equation corresponding to the obtained Tsallis gravity, we follow the classical viewpoint fully described in [79]. The series expansion $\exp(l/r^2) = \sum_{n=0}^{\infty} l^n/n!r^{2n}$ leads to

$$\int \frac{\exp\left(l/r^2\right)}{r^2} dr = \sum_{n=0}^{\infty} \int \frac{l^n}{n!r^{2n+2}} dr = -\frac{1}{r} \sum_{n=0}^{\infty} \frac{l^n}{n!(2n+1)r^{2n}}, \tag{17}$$

combined with Eq. (11) to help us in calculating Tsallis gravitational potential as

$$\phi(r) = -\frac{G_q M}{r} \sum_{n=0}^{\infty} \frac{l^n}{n!(2n+1)r^{2n}}. \tag{18}$$

Considering a test particle on the edge of a flat FRW universe, and following the recipe of [79], this equation leads to

$$H^2 = \frac{8\pi G_q}{3} \rho \sum_{n=0}^{\infty} \frac{l^n H^{2n}}{n!(2n+1)}, \tag{19}$$

in which ρ is the cosmic fluid density and H denotes the Hubble parameter, and we used the fact that the apparent horizon is located at $r = 1/H$. Moreover, the standard Friedmann first equation [79] is recovered at the desired limit of $q = 1$ (or equally, $\delta = 0(\|l = 0)$).

3.1. Accelerated Universe. Bearing the fact that the Hubble parameter decreases during the cosmic evolution in mind, rewriting Eq. (19) as

$$\frac{H^2}{\sum_{n=0}^{\infty}\left(\left(l^n H^{2n}\right)/(n!(2n+1))\right)} = \frac{8\pi G_q}{3}\rho \tag{20}$$

and keeping terms up to the H^4 term in LHS (the first corrective term to the standard cosmology ($H^2 = (8\pi G_q/3)\rho$) due to Tsallis gravitational potential), one easily reaches at

$$H^2 \simeq \frac{3}{2l}\left(1 \pm \sqrt{1 - \frac{32\pi G_q l}{9}\rho}\right). \tag{21}$$

In order to have real solutions for H^2, this equation claims that there is a maximum bound on the density of cosmic fluid as $\rho_{\max} = 9/32\pi G_q l$ at which the universe feels a de-Sitter phase with $H = \sqrt{3/2l}$ when $l > 0$. As the universe expands, ρ decreases, and when $\rho = 0$, the positive branch experiences again the primary de-Sitter phase ($H = \sqrt{3/l}$ for $l > 0$), but forever, while the universe expansion rate vanishes for the negative solution. In fact, the vacuum solution ($\rho = 0$) of the above Friedmann first equation is an inflationary universe for the positive branch and a Minkowski universe for the negative branch.

4. Summary

In the framework of the Verlinde hypothesis on the origin of gravity, we employed the recently proposed Tsallis entropy [47, 49] to find its implications on the Newtonian dynamics (second law of motion) and gravity. The velocity profile in a circular motion has also been analyzed. Finally, adopting the classical approach to get the Friedmann first equation described in [79], the corresponding cosmology was achieved after finding the Tsallis gravitational potential. The obtained modified Friedmann first equation (20) includes a complex function of H.

Since the Hubble parameter decreases during the cosmic evolution, and because the standard Friedmann first equation $(H^2 = (8\pi G/3)\rho)$ has notable achievements, we only focused on the first corrective term due to the Tsallis gravitational potential (i.e., we only hold terms up to H^4 in writing Eq. (21)). We saw that, in some situations and depending on the value of δ, the resulting equation addresses the (anti) de-Sitter universes with $H = \sqrt{3\pi/2\delta l_P^2}$ and $H = \sqrt{3\pi/\delta l_P^2}$, depending on ρ. It also admits an upper bound on the energy density of cosmic fluid of order of $((l_P^{-2}G^{-1})/((2+3\delta)\delta)) \sim ((10^{81})/((2+3\delta)\delta))$. We also obtained that there are two branches for the assumed approximation. Whenever $\rho = 0$, the positive branch, depending on the value of δ, guides us to an eternal (anti) de-Sitter phase, and the negative branch addresses a Minkowskian fate for the universe.

Data Availability

There is no data used in this paper.

Conflicts of Interest

The authors declare that there are no conflicts of interest regarding the publication of this paper.

Acknowledgments

We are grateful to the anonymous reviewer for worthy hints and constructive comments.

References

[1] J. W. Gibbs, *Statistical Mechanics, Mathematical Physics*, Charles Scribner's Sons, New York, NY, 1902.

[2] J. D. Bekenstein, "Black holes and entropy," *Physical Review D*, vol. 7, no. 8, pp. 2333–2346, 1973.

[3] S. W. Hawking, "Particle creation by black holes," *Communications In Mathematical Physics*, vol. 43, no. 3, pp. 199–220, 1975.

[4] S. W. Hawking, "Black hole explosions?," *Nature*, vol. 248, no. 5443, pp. 30-31, 1974.

[5] J. M. Bardeen, B. Carter, and S. W. Hawking, "The four laws of black hole mechanics," *Communications in Mathematical Physics*, vol. 31, no. 2, pp. 161–170, 1973.

[6] P. C. W. Davies, "Scalar production in Schwarzschild and Rindler metrics," *Journal of Physics A: Mathematical and General*, vol. 8, no. 4, pp. 609–616, 1975.

[7] W. G. Unruh, "Notes on black-hole evaporation," *Physical Review D*, vol. 14, no. 4, pp. 870–892, 1976.

[8] M. Srednicki, "Entropy and area," *Physical Review Letters*, vol. 71, no. 5, pp. 666–669, 1993.

[9] T. Jacobson, "Thermodynamics of Spacetime: the Einstein equation of state," *Physical Review Letters*, vol. 75, no. 7, pp. 1260–1263, 1995.

[10] T. Padmanabhan, "Classical and quantum thermodynamics of horizons in spherically symmetric spacetimes," *Classical and Quantum Gravity*, vol. 19, no. 21, pp. 5387–5408, 2002.

[11] T. Padmanabhan, "Gravity and the thermodynamics of horizons," *Physics Reports*, vol. 406, no. 2, pp. 49–125, 2005.

[12] C. Eling, R. Guedens, and T. Jacobson, "Nonequilibrium thermodynamics of spacetime," *Physical Review Letters*, vol. 96, no. 12, p. 121301, 2006.

[13] M. Akbar and R. G. Cai, "Friedmann equations of FRW universe in scalar–tensor gravity, f(R) gravity and first law of thermodynamics," *Physics Letters B*, vol. 635, no. 1, pp. 7–10, 2006.

[14] M. Akbar and R. G. Cai, "Thermodynamic behavior of field equations for f(R) gravity," *Physics Letters B*, vol. 648, no. 2-3, pp. 243–248, 2007.

[15] M. Akbar and R. G. Cai, "Thermodynamic behavior of the Friedmann equation at the apparent horizon of the FRW universe," *Physical Review D*, vol. 75, no. 8, 2007.

[16] R. G. Cai and L. M. Cao, "Unified first law and the thermodynamics of the apparent horizon in the FRW universe," *Physical Review D*, vol. 75, no. 6, 2007.

[17] R. G. Cai and L. M. Cao, "Thermodynamics of apparent horizon in brane world scenario," *Nuclear Physics B*, vol. 785, no. 1-2, pp. 135–148, 2007.

[18] A. Sheykhi, B. Wang, and R. G. Cai, "Thermodynamical properties of apparent horizon in warped DGP braneworld," *Nuclear Physics B*, vol. 779, no. 1-2, pp. 1–12, 2007.

[19] A. Sheykhi, B. Wang, and R. G. Cai, "Deep connection between thermodynamics and gravity in Gauss-Bonnet braneworlds," *Physical Review D*, vol. 76, no. 2, 2007.

[20] T. Padmanabhan, "Thermodynamical aspects of gravity: new insights," *Reports on Progress in Physics*, vol. 73, no. 4, 2010.

[21] H. Moradpour, A. Sheykhi, N. Riazi, and B. Wang, "Necessity of Dark Energy from Thermodynamic Arguments," *Advances in High Energy Physics*, vol. 2014, Article ID 718583, 9 pages, 2014.

[22] H. Moradpour and N. Riazi, "Thermodynamic equilibrium and rise of complexity in an accelerated universe," *International Journal of Theoretical Physics*, vol. 55, no. 1, pp. 268–277, 2016.

[23] H. Moradpour and R. Dehghani, "Thermodynamical Study of FRW Universe in Quasi-Topological Theory," *Advances in High Energy Physics*, vol. 2016, 7248510 pages, 2016.

[24] H. Moradpour and I. G. Salako, "Thermodynamic Analysis of the Static Spherically Symmetric Field Equations in Rastall Theory," *Advances in High Energy Physics*, vol. 2016, Article ID 3492796, 5 pages, 2016.

[25] H. Moradpour and S. Nasirimoghadam, "Thermodynamic Motivations of Spherically Symmetric Static Metrics," *Romanian Journal of Physics*, vol. 61, no. 9-10, p. 1453, 2016.

[26] H. Moradpour, N. Sadeghnezhad, S. Ghaffari, and A. Jahan, "Thermodynamic Analysis of Gravitational Field Equations in Lyra Manifold," *Advances in High Energy Physics*, vol. 2017, Article ID 9687976, 6 pages, 2017.

[27] H. Moradpour, R. C. Nunes, E. M. C. Abreu, and J. A. Neto, "A note on the relations between thermodynamics, energy definitions and Friedmann equations," *Modern Physics Letters A*, vol. 32, no. 13, p. 1750078, 2017.

[28] H. Moradpour, J. P. M. Graça, I. P. Lobo, and I. G. Salako, "Energy Definition and Dark Energy: A Thermodynamic Analysis," *Advances in High Energy Physics*, vol. 2018, 8 pages, 2018.

[29] K. Bamba, A. Jawad, S. Rafique, and H. Moradpour, "Thermodynamics in Rastall gravity with entropy corrections," *European Physical Journal C: Particles and Fields*, vol. 78, no. 12, 2018.

[30] H. Moradpour and M. Valipour, "Generalized Misner–Sharp energy in generalized Rastall theory," *Journal de Physique*, vol. 98, no. 9, pp. 853–856, 2020.

[31] M. Masi, "A step beyond Tsallis and Rényi entropies," *Physics Letters A*, vol. 338, no. 3-5, pp. 217–224, 2005.

[32] H. Moradpour, "Implications, consequences and interpretations of generalized entropy in the cosmological setups," *International Journal of Theoretical Physics*, vol. 55, no. 9, pp. 4176–4184, 2016.

[33] N. Komatsu, "Cosmological model from the holographic equipartition law with a modified Rényi entropy," *European Physical Journal C: Particles and Fields*, vol. 77, no. 4, p. 229, 2017.

[34] H. Moradpour, A. Bonilla, E. M. C. Abreu, and J. A. Neto, "Accelerated cosmos in a nonextensive setup," *Physical Review D*, vol. 96, no. 12, p. 123504, 2017.

[35] E. M. C. Abreu, J. A. Neto, A. C. R. Mendes, A. Bonilla, and R. M. de Paula, "Tsallis' entropy, modified Newtonian accelerations and the Tully-Fisher relation," *EPL*, vol. 124, no. 3, p. 30005, 2018.

[36] M. Tavayef, A. Sheykhi, K. Bamba, and H. Moradpour, "Tsallis holographic dark energy," *Physics Letters B*, vol. 781, pp. 195–200, 2018.

[37] A. Sayahian Jahromi, S. A. Moosavi, H. Moradpour et al., "Generalized entropy formalism and a new holographic dark energy model," *Physics Letters B*, vol. 780, pp. 21–24, 2018.

[38] H. Moradpour, S. A. Moosavi, I. P. Lobo, J. P. M. Graça, A. Jawad, and I. G. Salako, "Thermodynamic approach to holographic dark energy and the Rényi entropy," *European Physical Journal C: Particles and Fields*, vol. 78, no. 10, p. 829, 2018.

[39] S. Ghaffari, A. H. Ziaie, V. B. Bezerra, and H. Moradpour, "Inflation in the Rényi cosmology," *Modern Physics Letters A*, vol. 35, no. 1, 2020.

[40] C. Tsallis and L. J. L. Cirto, "Black hole thermodynamical entropy," *European Physical Journal C: Particles and Fields*, vol. 73, no. 7, p. 2487, 2013.

[41] T. S. Biró and V. G. Czinner, "A q-parameter bound for particle spectra based on black hole thermodynamics with Rényi entropy," *Physics Letters B*, vol. 726, no. 4-5, pp. 861–865, 2013.

[42] A. Belin, A. Maloney, and S. Matsuura, "Holographic phases of Renyi entropies," *Journal of High Energy Physics*, vol. 2013, no. 12, 2013http://arxiv.org/abs/1306.2640.

[43] G. Czinnera and H. Iguchia, "Rényi entropy and the thermodynamic stability of black holes," *Physics Letters B*, vol. 752, pp. 306–310, 2016.

[44] V. G. Czinnera and H. Iguchia, "Thermodynamics, stability and Hawking–Page transition of Kerr black holes from Rényi statistics," *European Physical Journal C: Particles and Fields*, vol. 77, no. 12, p. 892, 2017.

[45] A. Bialas and W. Czyz, "Renyi entropies of a black hole from Hawking radiation," *EPL (Europhysics Letters)*, vol. 83, 2008.

[46] S. Ghaffari, A. H. Ziaie, H. Moradpour, F. Asghariyan, F. Feleppa, and M. Tavayef, "Black hole thermodynamics in Sharma–Mittal generalized entropy formalism," *General Relativity and Gravitation*, vol. 51, no. 7, 2019.

[47] K. Mejrhit and S. E. Ennadifi, "Thermodynamics, stability and Hawking–Page transition of black holes from non-extensive statistical mechanics in quantum geometry," *Physics Letters B*, vol. 794, pp. 45–49, 2019.

[48] E. Abreu, J. A. Neto, E. M. Barboza Jr., A. C. Mendes, and B. B. Soares, "On the equipartition theorem and black holes non-gaussian entropies," 2020, http://arxiv.org/abs/2002.02435.

[49] H. Moradpour, A. H. Ziaie, and M. Kord Zangeneh, "Generalized entropies and corresponding holographic dark energy models," *European Physical Journal C*, vol. 80, p. 732, 2020, http://arxiv.org/abs/2005.06271.

[50] K. Ourabah, E. M. Barboza, E. M. C. Abreu, and J. A. Neto, "Superstatistics: Consequences on gravitation and cosmology," *Physical Review D*, vol. 100, no. 10, p. 103516, 2019.

[51] K. Ourabah, "Jeans instability in dark matter halos," *Physica Scripta*, vol. 95, no. 5, 2020.

[52] E. Verlinde, "On the origin of gravity and the laws of Newton," *JHEP*, vol. 4, p. 29, 2011.

[53] T. PADMANABHAN, "EQUIPARTITION OF ENERGY IN THE HORIZON DEGREES OF FREEDOM AND THE EMERGENCE OF GRAVITY," *Modern Physics Letters A*, vol. 25, no. 14, pp. 1129–1136, 2011.

[54] R. G. Cai, L. M. Cao, and N. Ohta, "Friedmann equations from entropic force," *Physical Review D*, vol. 81, no. 6, 2010.

[55] L. Modesto and A. Randono, "Entropic corrections to Newton's law," 2010, http://arxiv.org/abs/1003.1998.

[56] A. Sheykhi, "Entropic corrections to Friedmann equations," *Physical Review D*, vol. 81, no. 10, p. 104011, 2010.

[57] A. Kobakhidze, "Gravity is not an entropic force," *Physical Review D*, vol. 83, no. 2, 2011.

[58] S. Gao, "Is gravity an entropic force?," *Entropy*, vol. 13, no. 5, pp. 936–948, 2011.

[59] M. Chaichian, M. Oksanen, and A. Tureanu, "On gravity as an entropic force," *Physics Letters B*, vol. 702, no. 5, pp. 419–421, 2011.

[60] M. Visser, "Conservative entropic forces," *Journal of High Energy Physics*, vol. 2011, no. 10, p. 140, 2011.

[61] J. W. Lee, "On the origin of entropic gravity and inertia," *Foundations of Physics*, vol. 42, no. 9, pp. 1153–1164, 2012.

[62] M. Chaichian, M. Oksanen, and A. Tureanu, "On entropic gravity: the entropy postulate, entropy content of screens and relation to quantum mechanics," *Physics Letters B*, vol. 712, no. 3, pp. 272–278, 2012.

[63] E. M. C. Abreu and J. A. Neto, "Considerations on gravity as an entropic force and entangled states," *Physics Letters B*, vol. 727, no. 4-5, pp. 524–526, 2013.

[64] A. Sheykhi, H. Moradpour, and N. Riazi, "Lovelock gravity from entropic force," *General Relativity and Gravitation*, vol. 45, no. 5, pp. 1033–1049, 2013.

[65] H. Moradpour and A. Sheykhi, "From the Komar mass and entropic force scenarios to the Einstein field equations on the Ads brane," *International Journal of Theoretical Physics*, vol. 55, no. 2, pp. 1145–1155, 2016.

[66] R. C. Nunes, E. M. Barboza Jr., E. M. C. Abreu, and J. A. Neto, "Probing the cosmological viability of non-gaussian statistics," *Journal of Cosmology and Astroparticle Physics*, vol. 2016, no. 8, p. 51, 2016.

[67] R. C. Nunes, H. Moradpour, E. M. Barboza Jr., E. M. Abreu, and J. A. Neto, "Entropic gravity from noncommutative black holes," *International Journal of Geometric Methods in Modern Physics*, vol. 15, 2018.

[68] H. Moradpour, A. Amiri, and A. Sheykhi, "Implications of maximum acceleration on dynamics," *Iranian Journal of Science and Technology, Transactions A: Science*, vol. 43, no. 3, pp. 1295–1301, 2019.

[69] H. Moradpour, A. Sheykhi, C. Corda, and I. G. Salako, "Implications of the generalized entropy formalisms on the Newtonian gravity and dynamics," *Physics Letters B*, vol. 783, pp. 82–85, 2018.

[70] H. Moradpour, A. H. Ziaie, S. Ghaffari, and F. Feleppa, "The generalized and extended uncertainty principles and their implications on the Jeans mass," *Monthly Notices of the Royal Astronomical Society: Letters*, vol. 488, no. 1, pp. L69–L74, 2019.

[71] J. A. Neto, "Nonhomogeneous cooling, entropic gravity and MOND theory," *International Journal of Theoretical Physics*, vol. 50, no. 11, pp. 3552–3559, 2011.

[72] E. Dil, "q-Deformed Einstein equations," *Canadian Journal of Physics*, vol. 93, no. 11, pp. 1274–1278, 2015.

[73] E. Dil, "Can quantum black holes be (q, p)-fermions?," *International Journal of Modern Physics A: Particles and Fields; Gravitation; Cosmology; Nuclear Physics*, vol. 32, no. 15, p. 1750080, 2017.

[74] E. M. C. Abreu, J. A. Neto, A. C. R. Mendes, A. Bonilla, and R. M. de Paula, "Cosmological considerations in Kaniadakis statistics," *EPL*, vol. 124, no. 3, p. 30003, 2018.

[75] M. Senay and S. Kibaroğlu, "q-deformed Einstein equations from entropic force," *International Journal of Modern Physics A*, vol. 33, no. 36, 2018.

[76] S. Kibaroğlu and M. Senay, "Effects of bosonic and fermionicq-deformation on the entropic gravity," *Modern Physics Letters A*, vol. 34, no. 31, 2019.

[77] H. Moradpour, C. Corda, A. H. Ziaie, and S. Ghaffari, "The extended uncertainty principle inspires the Rényi entropy," *EPL*, vol. 127, no. 6, p. 60006, 2019.

[78] J. D. Barrow, "The Area of a Rough Black Hole," 2020, http://arxiv.org/abs/2004.09444.

[79] M. K. Zangeneh, H. Moradpour, and N. Sadeghnezhad, "A note on cosmological features of modified Newtonian potentials," *Modern Physics Letters A*, vol. 34, no. 21, 2019.

[80] A. R. Plastino and J. A. S. Lima, "Equipartition and virial theorems within general thermostatistical formalisms," *Physics Letters A*, vol. 260, no. 1-2, pp. 46–54, 1999.